A functional study on novel genes involved in regulating aldosterone secretion in normal human zona glomerulosa and in aldosterone-producing adenomas

Carmela Maniero
Gonville and Caius College
Department of Medicine

Dissertation for the degree of Doctor of Philosophy

Declaration

This dissertation is the result of my own work and includes nothing that is the outcome of work done in collaboration except as declared in the Preface and specified in the text. It is not substantially the same as any that I have submitted, or, is being concurrently submitted for a degree or diploma or other qualification at the University of Cambridge or any other University or similar institution except as declared in the Preface and specified in the text. The text in this dissertation does not contain more than 60,000 words, excluding figures, tables, and bibliography.

Contents

Thesis Summary

Primary aldosteronism (PA) is the most common secondary cause of hypertension with a prevalence of about 10%. About half of PA cases are caused by aldosterone-producing adenomas (APA).

Two APA subtypes, ZG-like and ZF-like APAs, have been described, according to the histological resemblance to normal adrenocortical zona glomerulosa (ZG) and zona fasciculata (ZF), underlying somatic mutations (*KCNJ5* commonly found in ZF-like, *CACN1AD, ATP1A1, ATP2B3, CTNNB1* in ZG-like APAs), and transcriptome profile. It is unknown if the process of tumorigenesis differs between ZG- and ZF-like APAs. In order to define ZG-specific genes, we have compared the transcriptome of APAs and their adjacent adrenal glands by microarray assay. RNA was isolated by laser capture microdissection (LCM) from adjacent ZG, ZF and APAs from 14 patients with Conn's and 7 patients with phaeocromocytoma. Two top hit genes from the comparison of ZG vs ZF were functionally studied, *ANO4* and *NEFM*.

NEFM, encoding neurofilament medium, was the fourth most up-regulated gene in ZG vs ZF, showing 14.8-fold-fold higher expression levels ($p=9.16^{-12}$) in ZG than ZF. NEFM was also one of the most down-regulated genes in ZF-like vs ZG-like APAs. Immunohistochemistry (IHC) confirmed selective high expression of NEFM in ZG and ZG-like APAs.

Silencing *NEFM* in H295R cells increased aldosterone secretion and cell proliferation. In addition, it increased stimulation and inhibition, respectively, of aldosterone secretion from H295R cells by the dopamine receptor D1R agonist fenoldopam and antagonist SCH23390.

IHC showed predominantly intracellular staining for D1R in NEFM-rich ZG-like APAs, but membranous staining in NEFM-poor ZF-like APAs. Aldosterone secretion in response to fenoldopam in primary cells from ZG-like APAs was lower than in cells from ZF-like APAs. NEFM expression levels directly

correlate with *KCNJ5* phenotype: *KCNJ5* mutations down-regulate *NEFM* mRNA and protein levels in H295R cells and in primary cells from ZG-like APAs.

ANO4, encoding a Ca^{2+}-activated chloride channel family member, was the third most upregulated gene, showing 19.9-fold higher expression levels ($p=6.6x10^{-24}$) in ZG than ZF. IHC confirmed ZG selectivity of ANO4 protein in the adrenal cortex. The staining was mainly cytoplasmic. Unlike NEFM, there was no difference in expression of *ANO4* between ZG- and ZF-like APAs, the levels being mid-way between those of ZF and ZG.

Overexpression of *ANO4* in H295R cells caused an increase in *CYP11B2* and *NR4A2* gene expression levels but basal aldosterone secretion was unchanged. In the presence of calcium agonists and aldosterone secretagogues, *ANO4* reduced aldosterone secretion. ANO4 subcellular localisation was confirmed as cytoplasmic by immunofluorescence microscopy of transfected cells. When exposed to calcium ionophores, ANO4 generated only small chloride currents as detected by YFP assay.

In summary, the comparison of whole transcriptome of ZG with their paired ZF found unexpected up-regulated genes. Most of the highly up regulated genes in human ZG, including *NEFM* and *ANO4*, inhibit either basal or stimulated aldosterone secretion, and this may reflect an adaptive response to chronic high salt intake.

No clear-cut correspondence was found between transcriptome of APAs and their resembling zone of adrenal cortex. The down-regulation of NEFM following transfection of mutant *KCNJ5* suggests that ZF-like properties may be a consequence of mutation, rather than tissue of origin.

Acknowledgements of help and support

First of all, I would like to take this opportunity to thank my first supervisor, Professor Morris J. Brown for his outstanding supervision and continuous support throughout my research adventure. His great enthusiasm for work, rigorous attitude towards research and warm encouragements to our exploration on science has always been the best guidance for my research.

I would also like to sincerely thank Dr Mark Gurnell, who became my supervisor in February 2016. His support and interest in the wellbeing and scientific stimulation of us PhD students in transition times has been precious.

I would like to thank Dr Elena A. B. Azizan, Dr Junhua Zhou and Dr Lalarukh Haris for providing help to the very first stages of my PhD.

Many thanks to my colleagues and the staff of the research group, both past and present, for their generous help and invaluable friendship. Special thanks goes out to Dr Yasmin and Ms Sarah Cleary.

I would like to thank my parents, my brother and my large Italian family, my old and new friends for their love and support.

My PhD is funded by the British Heart Foundation clinical research fellowship. My research is also supported by grants awarded by Gonville and Caius College, University of Cambridge.

Acknowledgements of specific contributions

I would like to acknowledge the following individuals for their specific contributions to my research and thesis:

Professor Morris J. Brown contributed to the project design and statistical analyses.

Dr Elena A. B. Azizan and Dr Junhua Zhou performed genotyping and laser capture microdissection.

Dr Sudeshna G. Neogi, Dr Brian Lam and Professor Ian McFarlane performed the microarray and analysis for microarray data.

Dr Wanfeng Zhao performed immunohistochemistry on paraffin-embedded sections for ANO4, NEFM and D1R. Dr Celso E Gomez-Sanchez provided the *CYP11B2* antibody for immunohistochemistry.

Professor Felder, Professor Wang, Professor Laureano Asico from Washington University (USA) for the D1R antibody gift.

Mrs Sumedha Garg helped me on the shRNA design and discussion of the experiments in the last year of PhD. Timothy Isaac Johnson helped me with the proliferation assays.

Dr Luis Galietta and Dr Paolo Scudieri helped me with *ANO4* project, providing the anoctamin plasmids, performing YFP assay and IF on their cell lines.

For the Cambridge cohort, the Human Research Tissue Bank supported by the NIHR Cambridge Biomedical Research Centre (Addenbrookes Hospital, Cambridge) helped with collecting patient samples. All the PhD students of Professor Morris J. Brown involved in the collection of adrenal samples.

List of Abbreviations

AAG	Adjacent adrenal glands (normal adrenal adjacent to the lesion-either APA or phaeocromocytoma)
ACTH	The adrenocorticotropic hormone
Ang II	Angiotensin II
APA	Aldosterone-producing adenoma
APCC	Aldosterone producing cell cluster
ARR	Aldosterone/renin ratio
ATP1A1	ATPase, Na+/K+ Transporting, Alpha 1 Polypeptide
AVS	Adrenal vein sampling
BAH	Bilateral adrenal hyperplasia
BP	Blood pressure
Ca	Calcium
$[Ca^{2+}]_i$	Intracellular calcium
CaMKs	Ca2+/calmodulin-dependent protein kinases
cAMP	Cyclic adenosine monophosphate
cDNA	Complementary DNA
CT-scan	Computed tomography-scanning
CYP11A1	Cholesterol side-chain cleavage enzyme/ Cytochrome P450, Family 11, Subfamily A, Polypeptide 1
CYP21A	The 21α-hydroxylase
DAG	Diacylglycerol
E. coli	Escherichia coli
eGFR	Estimated Glomerular Filtration Rate
FC	Fold of change
gDNA	Genomic DNA

GIRK4/*KCNJ5*	G protein-activated inward rectifier potassium channel 4
G-protein	Guanine nucleotide binding proteins
h	hour
HT	Hypertension
125I	125Iodine
IHC	Immunohistochemistry
IP3	Inositol 1,4,5-trisphosphate
K+	Potassium
LCM	Laser capture microdissection
M	mol/L
min	minutes
MR	Mineralocorticoid receptor
MRI	Magnetic resonance imaging
mRNA	messenger ribonucleic acid
Na+	Sodium
OR	Odds ratio
PET	Positron emission tomography
PA	Primary aldosteronism
Phaeo	Phaeocromocytoma
PCR	Polymerase chain reaction
qPCR	quantitative polymerase chain reaction
RAS	Renin-angiotensin-system
StAR	Steroidogenic acute regulatory protein
sec	second
WT	Wild-type
ZF	Zona fasciculata
ZF-like APA	Aldosterone-producing adenoma with≤50% compact cells
ZG	Zona glomerulosa
ZG-like APA	Aldosterone-producing adenoma with

	>50% compact cells
ZR	Zona reticularis
ΔCT	The difference of cycle threshold between the target gene and the house-keeping gene

Chapter 1 – Introduction

1.1 Primary aldosteronism: a clinical overview

Primary aldosteronism (PA) is the most common curable cause of arterial hypertension (HT). This condition is defined as a state of increased secretion of aldosterone, autonomous of the renin–angiotensin system. Dr. Jerome W. Conn described PA in 1955 (Conn 1955; Conn & Louis 1956).

PA causes sodium and water retention and potassium loss eventually causing HT and hypokalaemia, but also cardiovascular and renal damage.
It was Jerome Conn himself who, 10 years after describing the firs PA case, reported a series of PA cases in which PA with normokalaemia was the most frequent presentation, while severe cases with prolonged exposure to aldosterone excess had HT and low serum potassium levels.

Despite these early reports, in most of the studies from the 1970s to early 1990s PA was screened exclusively in hypokalemic patients, and this strategy consequently affected its prevalence estimation. Most of the studies performed before the introduction of the aldosterone-to-renin-ratio (ARR) in 1981 as a screening tool for PA reported a low prevalence (<1%) (Hiramatsu et al. 1981). In the following years, the PA screening strategy based on the ARR in hypertensive patients (independently from potassium levels) has been used in several studies that, although showing different prevalence because of the use of different diagnostic criteria, found that PA is the commonest treatable cause of HT.

The first prospective study, the Primary Aldosteronism Prevalence in Hypertensives (PAPY) study, was published only in 2006. The PAPY Study showed that PA was present in about 11% of newly diagnosed consecutive HT patients referred to a third level HT centre. About half of them, 4.8% of the overall studied patients, had a surgically treatable subtype, i.e. aldosterone producing adenomas (APAs) (Rossi et al. 2006).

The subtype differentiation is fundamental in PA diagnostic work-up, as patients could receive a specific treatment (adrenalectomy for the unilateral subtypes, mineralocorticoid receptor (MR) antagonists for those patients who are not suitable of surgery or with bilateral aldosterone excess).

The high prevalence of PA in hypertensive populations represents a challenge in terms of planning a strategy of investigation and selection of patients in different public health systems. Some centres prefer to screen all referred patients despite the costs, taking into consideration both the high prevalence of PA and its high rate of cardiovascular complications, while other centres address to the diagnostic work-up for PA only those subgroups of patients with an increased pre-test probability of having PA (resistant HT, significant target organ damage, young age, hypokalemia, early onset of stroke or HT, HT plus adrenal mass, family history of PA).

Of note, the ARR, used as a screening test for PA, is affected by several factors, in primis most of the first-line anti-hypertensive medications, such as MR antagonists, beta-blockers, ACE Inhibitors, sartans, diuretics and dihydropyridinic calcium channel blockers. According to the Endocrine Society guidelines, these medications should be stopped for at least four weeks and replaced by alpha-blockers and/or verapamil to control HT, but this is not always feasible in clinical practice. Nevertheless, other noncardiovascular medications (as instance some anti-depressants) can influence both aldosterone and renin levels. Some physiological factors should also be considered when interpreting the ARR, such as age and race (both afro caribbean and elderly patients are known to have low renin levels), orthostatism, water and salt intake, or different phases of menstrual cycle in women (Funder et al. 2016).

1.1.1 PA Subtypes, differentiation and diagnosis

Once the biochemical diagnosis of PA has been confirmed, the next steps and tests in the diagnostic workup aim at differentiating the PA subtypes.

As mentioned before, the purpose of subtype differentiation is mainly therapeutic and discriminates unilateral from bilateral adrenal aldosterone producing lesions, while excluding rare malignant and genetic forms.

If the autonomous aldosterone production is unilateral, indication is given to homolateral adrenalectomy, which provides biochemical cure of PA in 100% of patients (if the pre-surgery diagnosis of unilateral disease was correct) and can either cure (in 40–80% of cases) or improve BP control in most of patients.

Bilateral PA forms are treated medically with aldosterone antagonists as first choice (mainly spironolactone, eplerenone as MR antagonist and amiloride as epithelial sodium channel blocker). Medical treatment does not affect the number of medications needed to achieve BP control target in most of patients.

According to the Endocrine Society guidelines, MRI, CT or both should be performed in patients with PA with the main purpose of excluding an aldosterone-producing carcinoma and to study the anatomy of the adrenal veins in view of performing an adrenal vein sampling (AVS).
A CT scan with 2–3 mm cuts is currently the best technique available for the detection of adrenal nodules, but here are some important caveats about adrenal imaging in PA: a high percentage (about 40%) of APAs are <6 mm in diameter and hardly visible even with CT or MRI scan. Moreover, not secreting adrenal nodules (or incidentalomas) are quite frequent in general population (especially over 40 years), and this obviously affects the sensitivity and specificity of adrenal imaging in the diagnosing unilateral PA.
Even the discrimination of unilateral vs bilateral PA subtypes cannot rely on conventional adrenal imaging: a review found that, when compared to AVS as gold standard for the diagnosis, CT scans are misleading in about 50% of patients, giving false positive and false negative in 25% of the cases (Kempers et al. 2009).

In view of these evidences, the indication to adrenalectomy should not be decided on the basis of the imaging findings, but only after solid evidence of lateralisation of the aldosterone excess.

AVS, as defined in the Endocrine Society guidelines, is instead the gold standard test to differentiate unilateral and bilateral causes.
AVS is an invasive and expensive test, and patients should be prepared to in terms of modifications of antihypertensive therapy and correction of hypokalemia. Moreover AVS has a considerable percentage of failure in selectivity due to difficulties in cannulising the right adrenal vein for its anatomy, even in the hands of an expert radiologist.
Therefore, AVS should be performed only in patients with confirmed and unequivocal PA biochemical diagnosis, willing to have adrenalectomy and with no contraindications to general anesthesia. All the likely, not surgically treatable causes of PA potentially diagnosable at this stage (such as familial PA type I) should be excluded before the patient undergoes AVS.

1.1.2 PA treatment according to the subtypes

In 100% of patients with unilateral PA adrenalectomy normalizes the biochemical pattern of PA (aldosterone-to renin ratio and potassium levels), improves BP control and target organ damage, reduces the number of anti hypertensive medications, but HT is cured in only 40% of cases. Prediction of the surgical cure of HT has been HT with several clinical factors, as instance young age, shorter duration of HT, higher preoperative blood pressure; preoperative normal renal function, but none of the possible “scores” had been conventionally accepted in clinical practice (Rossi, 2011).
PA patients with bilateral aldosterone overproduction or not willing to or unelegible to surgery, should be receive as first line medications that specifically inhibit aldosterone action.
Side effects from overtreatment or high doses are volume depletion, pre-renal kidney failure, increased creatinine, and potentially severe hyperkalemia.

These drugs should therefore be used carefully, at minimum doses and with strict monitoring of potassemia and creatinine in patients with known renal failure, or taking other drugs affecting kidney function.
Spironolactone blocks mineralocorticoid receptor as an agonist competitor. This drug has also inhibitory activity at the testosterone receptor and agonist activity at the progesterone receptor, therefore it can cause sex-steroid-related adverse effects, such as gynecomastia, loss of libido, menstrual irregularities, in a dose-dependent manner. Eplerenone is a more selective MR antagonist with less action on sex-steroid receptors and consequently less side effects. It is also indicated in children and pregnancy for the same reasons. Other potassium sparing diuretics such as amiloride, can be associated to MR antagonists to achieve BP and hypokalemia control (Delyani, 2000).

Alongside these specific medications, PA patients may need other anti-hypertensives belonging to other classes for which no absolute contraindication exists. Figure 1 summarizes the raccomandations given by the Endocrine Society in the last guidelines.

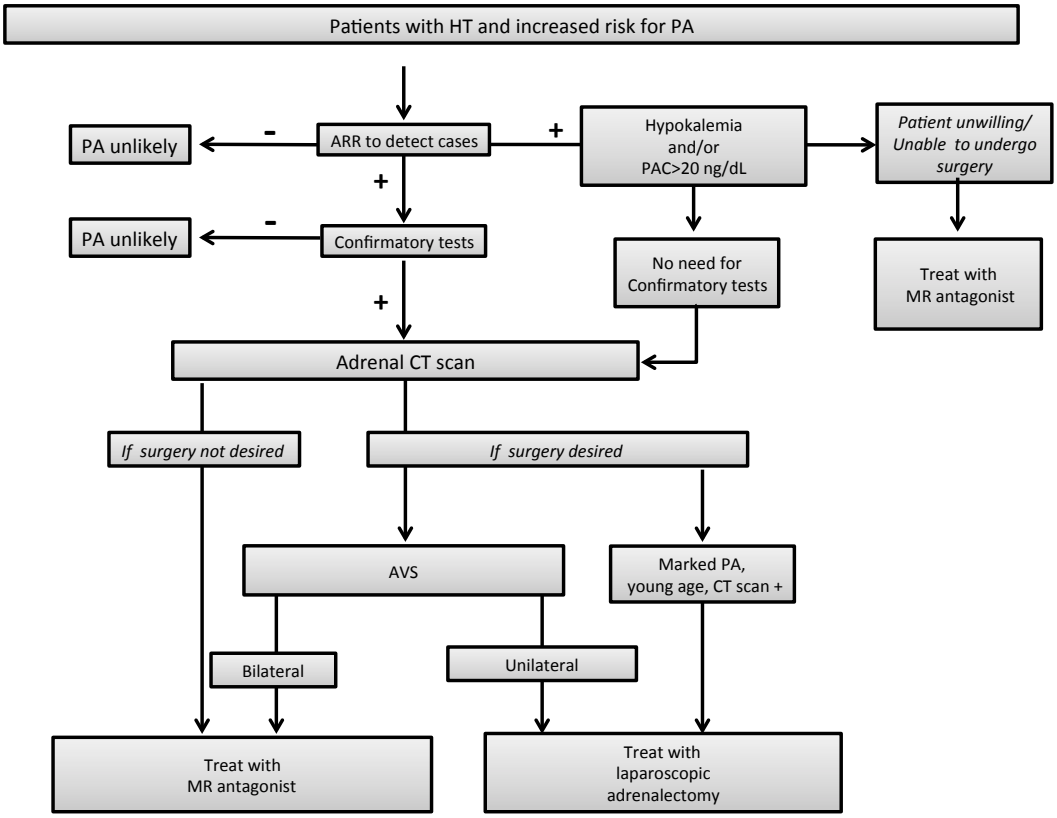

Figure 1.1: Diagnostic and therapeutic alghoritm for PA as elaborated from the Endocrine Society guidelines (Funder et al. 2016).

1.2. The adrenal gland: Histology and functional zonation

The adrenal gland is composed of two well distinguished parts: the adrenal cortex and the medulla. The adrenal cortex can be further divided into three different zones: the zona glomerulosa (ZG), the zona fasciculata (ZF), and the zona reticularis (ZR) (Figure 2). The outer layer under the capsule is the ZG. It is the primary site for the production of mineralocorticoids (mainly aldosterone in humans). The ZG cells are characterized by a low cytoplasm to nucleus ratio and are arranged in an arched or arcuate pattern. The ZF produces glucocorticoids and is the thickest zone (about 70%) of the cortex. It is composed of columns of clear cells with high cytoplasm to nucleus ratio, separated by capillaries. The ZR cells are polyhedral too, but arranged as nests. They produce sex hormones, mainly androgens. The medulla mainly

consists of chromaffin cells located in clusters and in trabeculae, and produce cathecolamines.

1.2.1 Synthesis of aldosterone

Aldosterone precursor is cholesterol, as for any other steroid hormone. In humans it is synthesized almost exclusively in the ZG, through the action of three cytochrome P-450 enzymes and one hydroxysteroid dehydrogenase.

The first step consists of transport of cholesterol from the outer to the inner mitochondrial membrane by steroidogenic acute regulatory (StAR) protein. Cholesterol is then converted to pregnenolone by the CYP11A1 (or cholesterol side chain cleavage enzyme). The reaction continues in the endoplasmic reticulum where pregnenolone is converted to progesterone by HSD3B2 and progesterone is hydroxylated to deoxycorticosterone by 21-hydroxylase (also named *CYP21*).

The final three steps happen in the mitochondria and are mediated by a single enzyme, the aldosterone synthase (or *CYP11B2*), which catalyses 11-hydroxylation, 18-hydroxylation, and 18-oxidation of deoxycorticosterone.

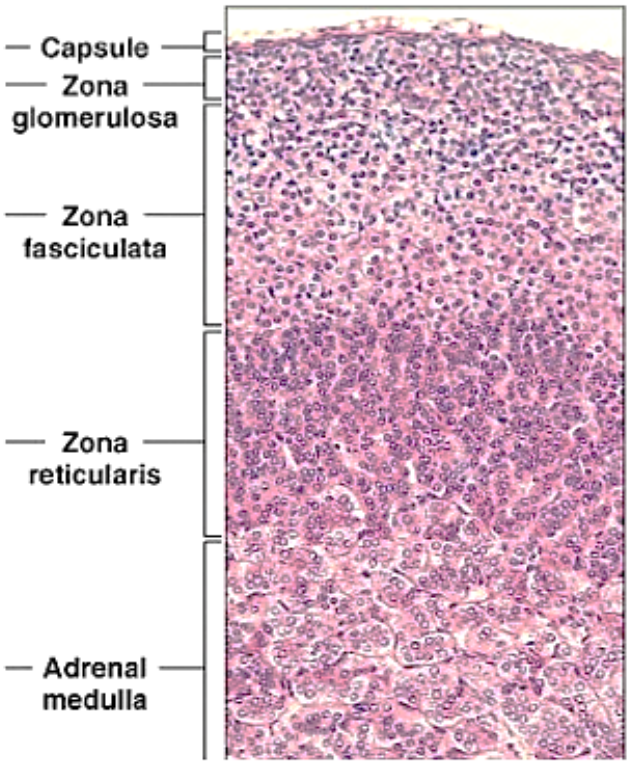

Figure 1.2: Haematoxylin and eosin staining of the human adrenal gland (low amplification). Zona glomerulosa cells are compact with low cytoplasm to nucleus ratio; zona fasciculata cells are clear, large, and lipid-laden with high cytoplasm to nucleus ratio.

Cortisol steroidogenesis, confined into the ZF, overlaps aldosterone synthesis pathway until the first two reactions and the conversion of cholesterol to pregnenolone. CYP17 (or 17alpha-hydroxylase) is necessary for pregnenolone or progesterone hydroxylation. The last three steps are mediated by 3βHSD (HSD3B2), 21OHase (CYP21) and 11βOHase (*CYP11B1*).

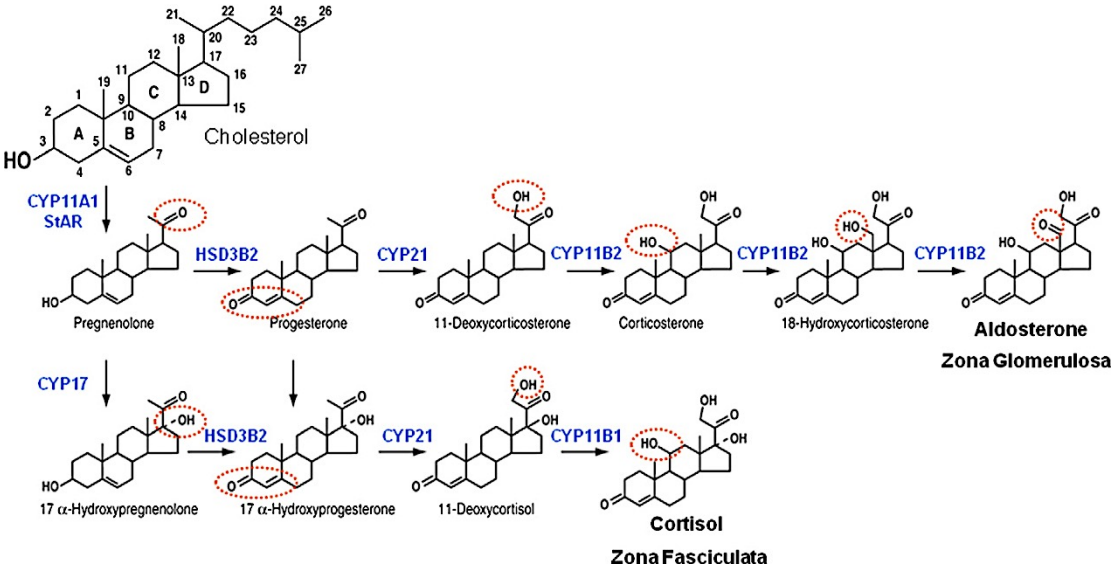

Figure 1.3: Adrenal cortex steroidogenesis (figure modified from Hattangady et al. 2012).

The anatomical separation of these biochemical events in the adrenal cortex layers, in other words the exclusive synthesis of aldosterone in ZG and of cortisol in ZF, is called “functional zonation”.

Three phenomena maintain it: a) the exclusive ZG expression of *CYP11B2*, b) the exclusive ZF and ZR expression of *CYP17A1* and *CYP11B1* and c) absence of HSD3B2 expression, necessary for aldosterone and cortisol synthesis, in ZR.

Additionally, the centripetal blood flow in the adrenal cortex avoids the precursors of aldosterone synthesized in the ZF from coming into contact with *CYP11B2* specifically and exclusively expressed in the ZG, thus contributing to the functional separation of the adrenocortical zones.

1.2.2 Regulation of aldosterone

Aldosterone synthesis is strictly regulated both acutely (within minutes from stimulus) and chronically (hours to days).
The renin-angiotensin system, via the final mediator angiotensin II (AngII), represents the main regulator of aldosterone synthesis and secretion.
There are two AngII receptors in the human adrenal, AT1 and AT2. The latter constitutes the main fetal adrenal receptor, whereas AT1 is the principal binding site for AngII in the adults.

Acute increases of AngII trigger several pathways and activate several ion transporters through it:
1) The activation of phosphoinositide-specific phospholipase C (PLC) which generates diacylglycerol (DAG) and inositol 1,4,5-trisphosphate (IP_3) from phosphatidylinositol 4,5-bisphosphate (PIP_2);
2) Activation of phospholipase D (PLD), which generates DAG precursor phosphatidylcholine (PC).
IP_3 activates its endoplasmic reticulum (ER) receptor thus triggering the release of calcium into the cytosol.

DAG inhibits TWIK-related acid sensitive (TASK or “leak”) potassium channels that maintain the resting membrane potential thus inducing depolarization. Additionally, AngII induces depolarization of ZG cell due to the activation of the voltage-gated L-and T-type calcium channels, which mediate calcium influx and contribute to increase intracellular calcium concentration, and activation of calcium/calmodulin-dependent protein kinases I/II (CaMK), as well as PKC.

CaMK and PKC regulate StAR phosphorylation and expression by activating cAMP-response element binding protein (CREB). DAG metabolite 12-hydroxyeicosatetraenoic acid (12-HETE) also positively acts on the phosphorylation (and activation) of CREB.

Similar to AngII, small increases in extracellular potassium levels also stimulate calcium influx, via depolarization of the glomerulosa cell plasma membrane and activation of the voltage dependent calcium channels, transient T-type and long-lasting L type.

ACTH can stimulate aldosterone production only acutely. Acute stimulation involves the binding of ACTH to its receptor, the melanocortin type 2 receptor (MC2R), activation of the adenylate cyclase (AC), and increased production of cAMP. This second messenger activates protein kinase A (PKA), which increases both expression and activation of StAR. Activated PKA also increases calcium influx through L-type calcium channels. These mechanisms are represented in figure 1.4

Chronic regulation of aldosterone is mainly mediated by the induction of *CYP11B2* expression in the ZG. AngII can also up-regulate its own receptor. The signaling cascades involved in chronic AngII stimulation are the ones involved in acute. PKD signaling is involved too, but one of the best characterized is the PLC-mediated generation of DAG and IP_3, which increases intracellular calcium activating CaMK. Calcium signaling appears to be the primary regulator of *CYP11B2* transcription.

DAG-activated PKC inhibits the expression of *CYP17A1*. AngII stimulates *CYP11B2* expression through the activation of its transcription. AngII stimulates different transcription factors such as CREB and nuclear receptor related 1 protein encoded by *NURR1* (also known as nuclear receptor subfamily 4, group A, member 2, *NR4A2*). It also up-regulates the expression of LDL and HDL receptors to provide the ZG cells of cholesterol. Moreover, it induces ZG hypertrophy and hyperplasia.

Chronic exposure to potassium in either animal models or in vitro models such as H295R induces an up-regulation of *CYP11B2*. Potassium signaling in ZG cells finally causes activation T- and L-type calcium channels causing

depolarization of the cells and increased calcium influx. Calcium binds calmodulin (CaM) and the complex activates several enzymes and ZG specific kinases, many of which are expressed in a tissue-specific manner, such as CaM kinases (CaMK) types IV and I. These mechanisms are represented in figure 1.5.

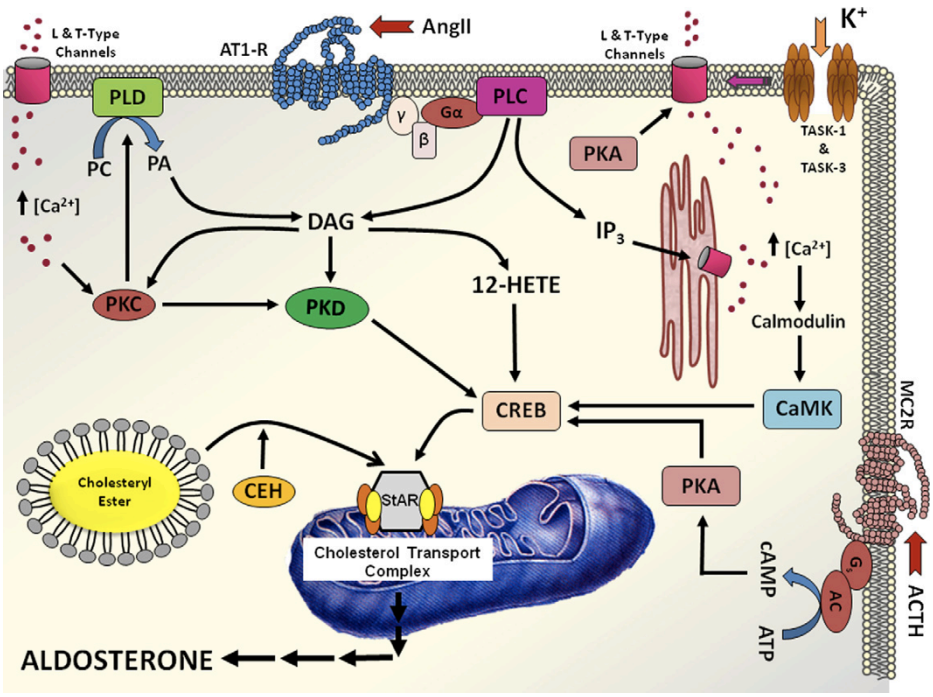

Figure 1.4: Acute actions of AngII, K+ and ACTH on adrenal glomerulosa cell aldosterone production (from Hattangady et al. 2012).

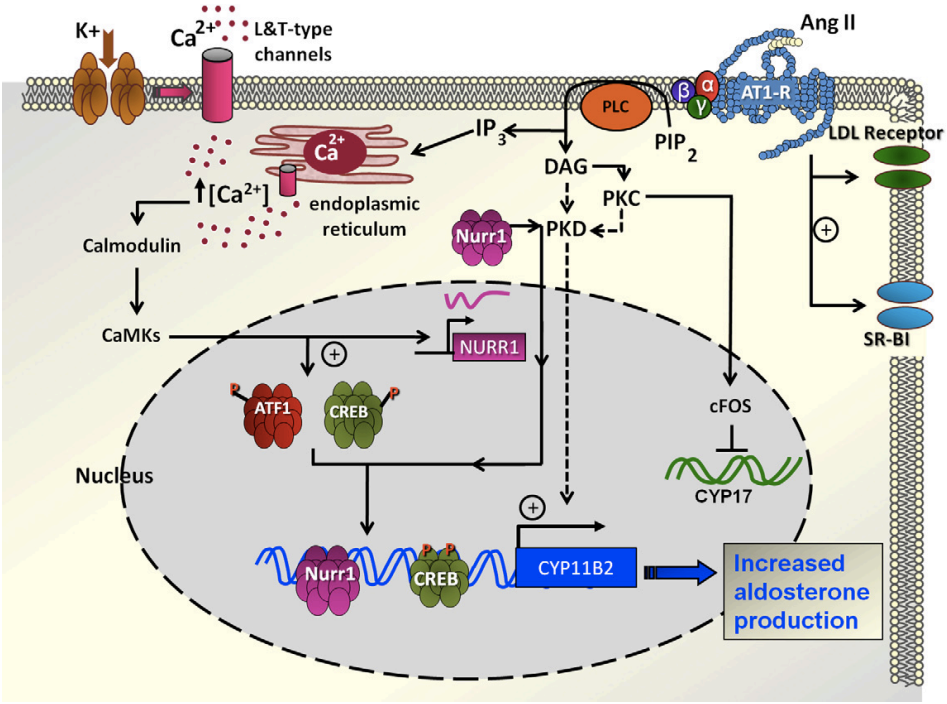

Figure 1.5: Regulation of the chronic production of aldosterone by AngII and potassium (K+) (from Hattangady et al. 2012).

1.2.3. Intracellular Ca^{2+}, depolarization and cation channels: a functional union.

The two most important aldosterone secretagogues (ANG II and K^+) cause ZG cell depolarization, the principal mechanism driving to an increase of $[Ca^{2+}]_i$.

The membrane potential of ZG cells is determined by the distribution of diffusible ions and their selective conductance through plasma membrane.

The Na^+-K^+ and Ca^{2+} pumps are responsible for the asymmetrical distribution of the major cations, and are modulated by AngII. The Na^+-K^+-ATPase (also called sodium pump) greatly contributes in maintaining the rest membrane potential hyperpolarized by exchanging three cytoplasmic Na^+ for two extracellular K^+. ANG II inhibits its activity, thus dissipating the K^+ gradient and resulting in depolarization.

The ZG membrane potential is close to the predicted equilibrium potential of K^+ (-70/-90 mV), therefore other K^+ conductances are also of great significance in setting it. Several voltage gated K^+ channels had been identified in ZG cells, as instance outward rectifier, Ca^{2+}-dependent and maxi-K^+ channels, some of which slowly voltage activating/voltage inactivating or noninactivating, but most of them are inactive at the negative resting membrane voltages and, although inhibited by ANG II in experimental conditions, they cannot induce the required depolarization for aldosterone secretion. Between the K^+ channels active in ZG cells (leak and inward rectifiers), only leak K^+ currents have been recorded at both single channel and macroscopic levels. Nevertheless both leak and inward rectifier K^+ channels had been described to be involved in the physiopathology of PA, as described below.

1.2.4 K2P channels and leak K currents

The leak currents recorded in adrenal ZG share all leak K^+ channels features, i.e the apparent rectification in physiological solutions is caused exclusively by unequal K^+ concentrations on the two sides of the plasma membrane. Their role in ZG cells is to stabilize the negative resting membrane potential and counterbalance depolarization.

The most highly expressed K^+ channels in the ZG are the TASK (TWIK [tandem of P domains in a weak inward rectifying K channel]-like, acid-sensitive K^+ channel) channels, in particular TASK1 and TASK3, which belong to the two pore domain K^+ (K2P) channel family. In recent years, single or combined knock out mouse models had highlighted their functional role. TASK-$1^{-/-}$ mice have hypertension, low plasma renin and a sexually dimorphic hyperaldosteronism independent of salt intake; the phenotype is correlated to sex and sexual hormones.

TASK$3^{-/-}$ mice have only mild hyperaldosteronism resembling low-renin salt-sensitive hypertension, with suppressed plasma renin activity, nonsuppressible aldosterone with salt, increased aldosterone/renin ratio, hypersensitivity to ANG II. The adrenal cells from this model were also

profoundly depolarized. The adrenal phenotype of the TASK-3$^{-/-}$ mice is severe in neonatal mice and becomes milder in the adult (Davies et al., 2008).

The TASK-1$^{-/-}$/TASK-3$^{-/-}$ double knockout mice exhibited no TASK-like currents, resulting in an approximately 20-mV baseline membrane depolarization and markedly increased (+400%) aldosterone production. Plasma aldosterone was increased by a low-sodium diet but again not suppressible by high salt intake. Candesartan, an ANG II receptor blocker, partially suppressed aldosterone increase, revealing that regulation of its production in this double knockout is at least partially preserved, probably because other potassium channels compensate for the loss of TASK-1 and TASK-3. (Guagliardo et al., 2012)
In humans, a possible influence of genetic variants (single-nucleotide polymorphisms (SNPs)) in KCNK9 (coding for TASK3) on BP and aldosterone levels had been recently described in a study on healthy subjects, while no associations were found with KCNK3 (coding for TASK1). (Jung et al., 2012)

1.2.5 Mechanisms of action of aldosterone

The main function of aldosterone as mineralocorticoid is to maintain the extracellular volume and blood pressure and to control potassium homeostasis by its effects of increasing sodium retention and potassium and hydrogen ions secretion in the distal nephron, the distal colon and sweat glands. Aldosterone activates the MR, which is located in the cytosol of the target cells when inactive and moves to the nucleus when binds aldosterone. MR has similar binding affinity for aldosterone and cortisol, but cortisol is inactivated to cortisone by 11beta-hydroxysteroid dehydrogenase type 2, thus preventing MR activation in conditions of increased cortisol levels.

Aldosterone has both genomic and non-genomic effects. Activated MR when localized into the nucleus can affect gene expression acting as a transcription factor.

The target gene mediating the classic mineralocorticoid effects of aldosterone in the distal nephron is the epithelial sodium channel (ENaC). Activated MR stimulates the expression of its alpha subunit, and prevents its degradation by increasing the expression of the sgk kinase, which inactivates by phosphorylation Nedd4-2, a regulator of ENaC ubiquitylation.

Aldosterone also increases the expression of ROMK in the distal convoluted and collecting duct cells, thereby enhancing the tubular capacity to excrete potassium, but only if potassium is elevated and extracellular volumes are normal.

MR is expressed in several other non-epithelial cells where its activation can contribute to the control of blood pressure, and consequently to HT when aldosterone secretion is excessive.

Faster non-genomic effects of aldosterone do not affect gene expression and are not prevented by MR blockers such as spironolactone. They are mediated by the interactions of aldosterone with MR or other receptors in the cell membrane, and are due to the activation of several signaling pathways, transporters and channels.

1.2.6. Consequences of aldosterone excess

Aldosterone excess, relatively to the extracellular volume homeostasis, causes sodium retention and volume expansion, and its eventual clinical manifestation is HT. Urinary potassium is also not retained in the distal tubule, with consequent hypokalemia. The augmented urinary excretion of hydrogen ions can cause metabolic alkalosis.

In addition to these effects, HT and cardiovascular complications due to aldosterone excess are also mediated by MR activation in tissues other than epithelia. Aldosterone excess in fact causes endothelial dysfunction and vascular remodeling, enhance sympathetic outflow, and impair baroreflex

function, and in PA these may be additional mechanisms contributing to developing HT and cardiovascular damage.

From a clinical standpoint, it is known from several studies that aldosterone excess causes inflammation, remodeling, and fibrosis in cardiovascular tissues, and this is independent from its BP effects and from the severity of HT. This has been shown both in animal models and in clinical studies that have confirmed the increased cardiovascular damage in PA patients in comparison to essential HT subjects matched for HT degree. Several markers and predictors of cardiovascular events are in fact more severe in PA patients, such as left ventricular hypertrophy, fibrosis, carotid intima-media thickness and femoral pulse wave velocity. This increased amount of damage would translate in increased rates of cardiovascular events (stroke, coronary syndromes, arrhythmias) and mortality.

Aldosterone damage on kidney, independent on HT and its action on extracellular volume and potassium homeostasis, is due to MR mediated fibrosis and vascular and tubular inflammation. Clinically, PA patients have higher urinary albumin excretion, higher creatinine clearance (both due to glomerular hyperfiltration) and increased intrarenal vascular resistance than matched essential hypertensives. The resolution of glomerular hyperfiltration by specific PA treatment can unmask the real kidney function impairment by prolonged aldosterone excess with decline of the eGFR.

1.2.7 Metabolic effects of aldosterone excess

In recent years, there has been compelling evidence that PA is associated to the “metabolic syndrome”. Body mass index correlates positively with aldosterone levels in normal subjects and hypertensives, and different studies have reported that hyperglicemia, metabolic sindrome and insuline resistance are more prevalent in PA patients and their biochemical indexes improved after specific treatment in APAs, although the studies reported small number of cases. These effects on glucose metabolism could be due to both direct

aldosterone effects or to hypokalemia (Fallo et al., 2006; Giacchetti et al., 2007).

1.2.8 Psychological effects of aldosterone excess

PA reported also to cause an impairment quality about adverse psychological effects and is associated to depression, anxiety lethargy, fatigue. Moreover they may find some resolution after specific medical teatment or adrenalectomy (Ahmed et al., 2011).

1.3. Aldosterone producing adenomas and genetic abnormalities

Recent advances in genome sequencing techniques helped researchers to discover part of the genetic abnormalities involved the development and pathophysiology of sporadic and familial hyperaldosteronism.

Genes encoding for ion channels (*KCNJ5* and *CACNA1D*, *ATP1A1* and *ATP2B3*) involved in intracellular ionic homeostasis and cell membrane potential regulation have been identified as mutated in sporadic APAs.

Germline mutations of *KCNJ5* are responsible for familial hyperaldosteronism type 3; germline *CACNA1D* mutations have been identified in two patients with PA and neurological symptoms. These mutations are present in about 50% of all tumors.

1.3.1. Familial Hyperaldosteronism- introduction

So far, four types of familial hyperaldosteronism have been described. Their prevalence is quite low: type I accounts for <1% of PA cases, type II has been reported to have a prevalence of about 7% in one series of patients, type III and IV are extremely rare.

1.3.2. Familial Hyperaldosteronism Type I

The first familial form of PA described is the autosomal dominant,

glucocorticoid-remediable PA, also known as Familial Hyperaldosteronism Type I (FH-I).

The underlying genetic abnormality is the presence of a “chimaera gene” mutation, made of *CYP11B1* sequences at 5’ end and *CYP11B2* sequences at its 3’ end. The encoded enzyme is able to synthesize aldosterone but is under the regulation of ACTH and not the RAS (Lifton et al., 1992).

Therapeutically, aldosterone overproduction and the consequent biochemical pattern of PA and HT are controlled by small doses of glucocorticoids that down-regulate the expression of the hybrid gene.

In the adrenal cortex of these patients, the normal zonation is abolished and aldosterone synthesis occurs in both ZG and ZF. Moreover, hybrid steroids 18 hydroxy- and 18 oxo-cortisol are highly synthesized.

The clinical phenotype of FH-I is variable in terms of onset and severity of HT. The most severe cases present resistant HT and cerebrovascular complications such as hemorrhagic stroke. However, the resolution of HT and PA is prompt and rapid with small doses of corticosteroids even in patients with severe manifestations.

FH-I should be suspected in patients with familiarity for PA, early age diagnosis, history of haemorrhagic stroke and suppression of aldosterone after a dexamethasone suppression test. Long-PCR test should be performed to confirm the diagnosis.

1.3.3 Familial Hyperaldosteronism Type II

FH-II is diagnosed when not glucocorticoid-suppressible PA occurs in families in an autosomal dominant way and FH-I or FH-III is definitely excluded. Its clinical, biochemical and radiological presentation are very close to non-familial, sporadic PA.

Patients with FH-II features are not significantly different from those with apparently non-familial PA. Affected members from the same family can have different PA subtypes and phenotype in terms of AngII responsiveness and cellular composition of the APAs.

The real prevalence of FH-II is unknown because ARR-based screening for

PA is not routinely and extensively performed in relatives of PA patients.
The genetic abnormality underlying FH-II is still unknown. So far, linkage studies only identified a locus at chromosome 7p22, but no mutation has been found (Carss et al. 2011).
Other forms of FH are described in the following paragraph as they are closely connected with the recent discovery of somatic mutations in sporadic APAs.

1.3.4 KNCJ5 mutations, sporadic APA, and Familial Hyperaldosteronism-III

Recent applications of next-generation sequencing (NGS) in APA research have enlightened novel genetic abnormalities in both sporadic and familial forms of PA.
KCNJ5 encodes the G-protein activated potassium inwardly rectifying channel Kir3.4, which is made of 419 amino acids and is expressed in several tissues and cell types. In the adrenal cortex, KCNJ5 is localized mainly in the ZG and the outer part of ZF (Figure 1.6).
The channel has two membrane- spanning domains, cytoplasmic NH2 and COOH termini, and the channel's ion selectivity filter is localized in an extracellular pore-forming loop. Its function in physiological conditions is to let potassium ions cross the pore and enter the cytoplasm while preventing the entrance of sodium ions.
Choi et al. discovered, by using whole exome sequencing, germline and somatic mutations in *KCNJ5* in samples from patients with either the familial or sporadic form of APA (Choi et al. 2011).
Two hot spot somatic mutations were at G151R and L168R, situated on the conserved glycine–tyrosine–glycine (GYG) motif of the selective filter and the second transmembrane (TM) domain of KCNJ5, respectively. G151R and L168R, associated with sporadic APAs, and in following confirmation studies resulted to be the most common mutations in *KCNJ5* mutant sporadic APAs.
The mutations cause the loss of the K+ selectivity of the channel, which leads to higher Na+ conductance and depolarization of the cell, followed by the

opening of the voltage-gated Ca^{2+} channels, increased influx of Ca^{2+} and increased aldosterone production.

The first family affected by FH-III was described as a severe form of PA, with important hypokalemia, resistant HT, and enlarged adrenals on both sites (Geller et al. 2008). In this family, a germline mutation (T158A) was identified in the *KCNJ5* gene as responsible for the syndrome (Choi et al. 2011) .

Following the first description, six more families and three germline *KCNJ5* mutations (G151R, G151E, p157S) were described (Mulatero et al. 2012; Scholl et al. 2012; Charmandari et al. 2012). In vitro all the mutations causes the same changes described before.

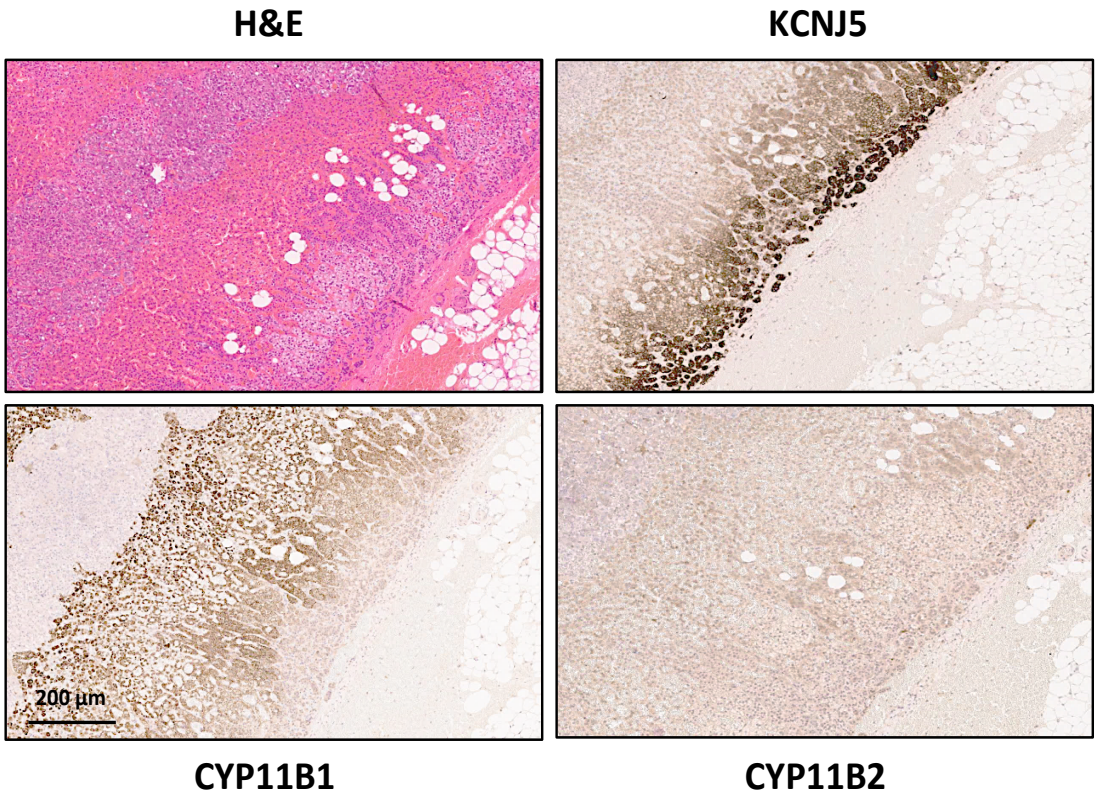

Figure 1.6: From the top left quadrant in a clockwise sense: Haematoxylin & Eosin staining of normal adrenal cortex; IHC of *KCNJ5* encoded potassium channel Kir3.4.; IHC of *CYP11B1* encoding for cortisol synthase; iv) IHC of *CYP11B2* encoding aldosterone synthase Of note, Kir3.4 is localized mainly in the ZG and the outer part of ZF.

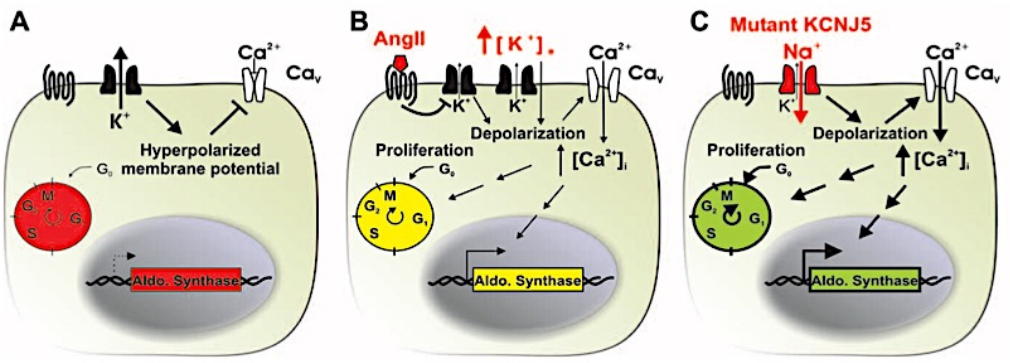

Figure 1.7: Role of *KCNJ5* and its mutation in the regulation of aldosterone synthesis. (A) Adrenal glomerulosa cells have a high resting K^+ conductance and hyperpolarized membrane potential (B) Membrane depolarization activates voltage-gated Ca^{2+} channels, increasing intracellular Ca^{2+} and stimulation of aldosterone synthase expression and cell proliferation. (C) *KCNJ5* mutant channels conduct Na^+, resulting in Na^+ entry, chronic depolarization, constitutive aldosterone production, and cell proliferation. (Modified from Choi et al. 2011).

1.3.5 CACNA1D mutations

The 2013 exome sequencing studies on sporadic and familial APAs led to discovery of new mutations in CACNA1D (Azizan et al. 2013; Scholl et al. 2013). In particular, our group studied 10 APAs with ZG-like phenotype, KCNJ5 wild-type and reported that 9 over 10 have mutations in either ATP1A1 or in CACNA1D.

CACNA1D encodes the pore-forming a1D subunit of a voltage-gated L-type calcium channel (Cav1.3) which is composed of further b, a2d, and g auxiliary subunits. a1D's four homologous repeats (I–IV) have six transmembrane segments (S1–S6).

Unlike KCNJ5, ATP1A1, and ATP2B3, the 21 somatic CACNA1D mutations reported so far are not localized in hotspot(s) but occur throughout the gene, around transmembrane segments S4, S5, and S6, which play a role as with

the channel's activation gate and voltage sensing, and the cytoplasmic S4–S5 linker coupling the voltage-sensing domain to the pore.
Patch clamping showed that the gain-of-function CACNA1D mutations increase intracellular calcium concentration through few different effects on the channel activity and status: shifting voltage dependent activation of the channel to more negative potentials, slowing inactivation, and/or increasing currents through a higher open channel probability.

Scholl et al. also reported two cases of early-onset HT and PA with germline mutations in CACNA1D. The first case had HT at birth, with PA and hypokalemia, biventricular hypertrophy, a ventricular septal defect, pulmonary hypertension, and second-degree heart block. Treatment with a calcium channel blocks normalized blood pressure and biventricular hypertrophy. Neurological symptoms included seizures, apparent cerebral palsy, cortical blindness, and complex neuromuscular abnormalities. The second case was born with cerebral palsy, spastic quadriplegia, severe intellectual disability, and seizures. At age 5 years, she had HT, polydipsia, hypokalemia and metabolic alkalosis and PA with no adrenal masses (Scholl et al., 2013).

1.3.6 *ATP1A1* and *ATP2B3* mutations

After the initial identification of *KCNJ5* mutations in 2011, two further NGS studies were performed in *KCNJ5* wild-type APAs (Azizan et al. 2013; Beuschlein et al. 2013) and led to the discovery of gain-of-function mutations in two P-type ATPase pumps, *ATP1A1* and *ATP2B3*. *ATP1A1* corresponds to the catalytic alpha1 subunit of the Na/K-ATPase. The pump exchanges three cytoplasmic Na+ ions for two extracellular K ions against their concentration gradient, regulating the resting cell membrane potential.
ATP2B3 encodes the plasma membrane Ca2+-ATPase isoform 3, a regulator of intracellular calcium homeostasis that pumps calcium ions out of the cell against gradient.

The L104 residue in transmembrane helix M1 and the V332 in M4 are in close

approximation to residue E334 crucial for K^+ binding and gating. The mutant L104R has impaired ion binding, and no Na+/K+- ATPase pump activity. The Na^+-dependent phosphorylation is also reduced. Electrophysiologically, cells carrying *ATP1A1* mutations are more depolarized. Removal of extracellular Na+ exaggerated the expected hyperpolarization, supporting the hypothesis that the mutations did not involve higher Na^+ conductance causing depolarization, but caused disturbed intracellular ion composition.

Beleuschlein et al. concluded from these results that aldosterone overproduction is due to the loss of functional *ATP1A1* pump activity as a consequence of the haploinsufficiency.

Our group discovered at the same time the same *ATP1A1* mutations in ZG-like APAs, and we have suggested that gain-of-function occurs.

The wild type pump generates a current at positive membrane potentials stimulated by extracellular K^+. L104R and del100_104 and V332G mutants pumping activity was not sensitive to K^+, however at physiological membrane potentials they were marked ouabain-sensitive, producing a voltage-dependent inward current partially inhibited by K^+.

Moreover, while removal of extracellular Na+ had little effect on the reversal potential, a change in pH of 1 changed the reversal potential by about 20 mV, suggesting that protons were the main carrier of the current in the L104R mutant enzyme.

Reversely Na^+ was the main carrier of current in del100_104 mutant as its removal shifted the reversal potential while changes in pH did not. Rearrangements of the M1 helix caused a broader opening responsible of Na leak.

Transfection of the H295R with the rat ouabain-insensitive wild type and rat mutant L104R cDNA showed an increased in aldosterone secretion and expression of the *CYP11B2* mRNA when incubated with ouabain or angiotensin II.

The *ATP2B3* mutations stimulate aldosterone production by losing the physiological pump function and reducing Ca^{2+}outward currents, alongside

opening of depolarization-activated Ca^{2+}channels and Ca^{2+} leak through the mutated pump thus increasing calcium influx.

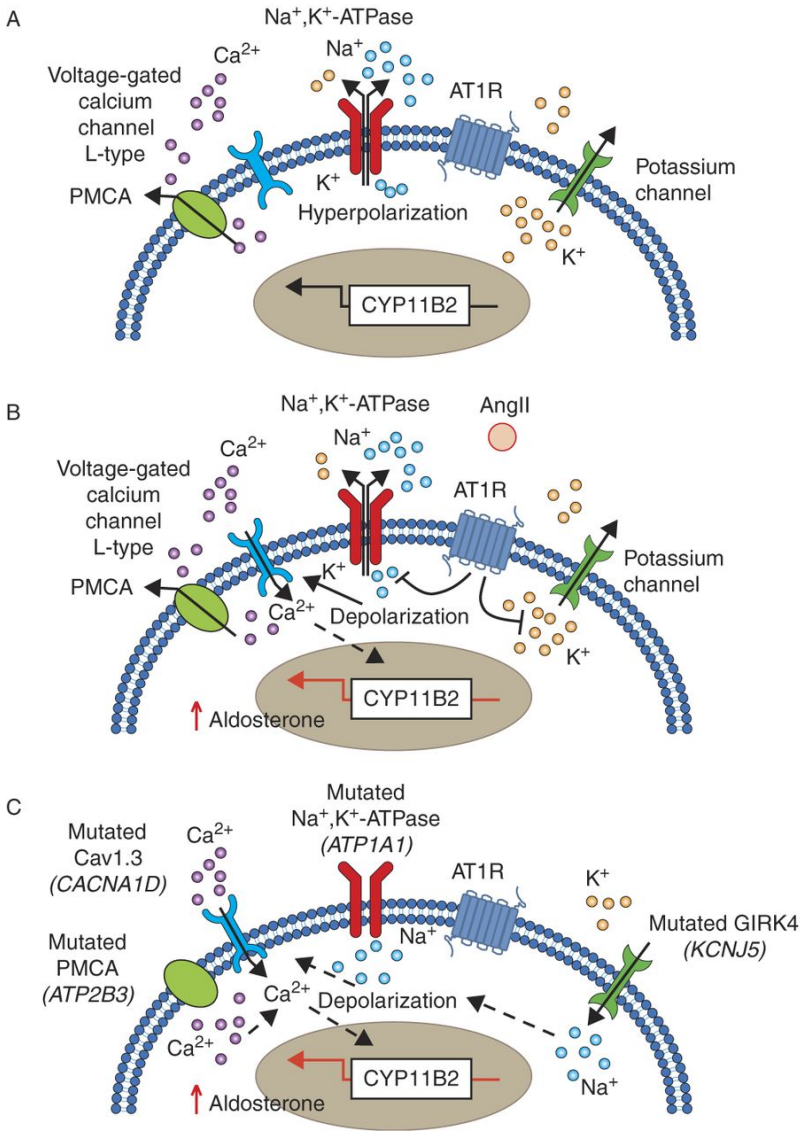

Figure 1.8: Proposed model of changes in the electrical properties of APA cells carrying mutations in the ion channels discovered so far (from Zennaro et al. 2015).

1.3.7 *CTNNB1* mutations

CTNNB1 mutations were reported in two exome sequencing studies, then reported in a Swedish cohort(A. E. D. Teo et al. 2015; Åkerström et al. 2016). Of interest, *CTNNB1* mutated APAs occurred almost exclusively in female patients. In three female patients the diagnosis was unmasked by pregnancy or menopause (A. E. Teo et al. 2015).

The reported mutations (S33C, G34R, A39Efs_3, T41A, S45P, and S45F) involve serine/threonine residues in exon 3 that, if phosphorylated, address beta-catenin to degradation. When a mutation occurs, beta-catenin is not phosphorylated nor degraded, thus causing constitutive activation of the Wnt signaling and high *CYP11B2* expression.

These mutations also cause adrenocortical cells de-differentiation toward the adrenal-gonadal precursor cell type, with high expression of gonadal receptors LHCGR and GNRHR, which would explain the clinical phenotype of the three cases.

Both the adrenal cortex and the ovaries originate from a common progenitor-cell population, and gene expression regulating the differentiation and cell fate is SF1-dependent and regulated by the Wnt signaling pathway. Transfection of primary ZG-like adenoma cells with mutant *CTNNB1* led to expression of LHCGR and GATA4, markers of gonadal differentiation normally unexpressed in adrenal cells.

Previous studies showed that GNRH activation of transfected GNRHR stimulates *CYP11B2* expression and aldosterone synthesis in H295R. Therefore, aldosterone synthesis is likely to increase during pregnancy when these aberrant gonadal receptors are stimulated.

1.3.8 Prevalence of Somatic Mutations and Genotype/Phenotype Correlations

As mentioned previously, *KCNJ5* mutations are the most common genetic abnormalities in sporadic APAs. Since the first study, there have been

several prevalence studies from different research groups worldwide (Boulkroun et al. 2012; Taguchi et al. 2012; Åkerström et al. 2012; Williams et al. 2014; Azizan et al. 2012). The prevalence of *KCNJ5* mutations varies between 30–65% in different cohorts, with a higher prevalence in the Asian population and among females (~70%). G151R and L168R are the most frequent, but overall 15 different mutations have been reported, also near or within the selectivity filter.

After *KCNJ5*, mutations in the *CACNA1D* are the second most frequent in sporadic APAs, reported to be up to 11% (Scholl et al. 2013). *ATP1A1* and *ATP2B3* are rarer, below 10% (Fernandes-Rosa et al. 2014).
beta catenin mutations have a similar mutation rate, between 2 and 5% (Akerstrom et al., 2016; Wu et al., 2017).
Fascinatingly, the clinical and biochemical parameters of patients with a somatic *CACNA1D* mutant APA differed from those with a somatic *KCNJ5* mutant APA.
Although patients with wild-type and *KCNJ5* mutant APAs did not show any difference in terms of clinical BP and serum potassium levels, patients with *KCNJ5* mutant APAs have higher aldosterone levels.
Moreover, they are more frequently female, had larger adenomas, and were treated by adrenalectomy at a younger age. One studied reported that they also have higher lateralization ratios at AVS thus explaining the earlier diagnosis and treatment, alongside the fact that these adenomas have bigger dimensions and are also easy to be detected at the conventional imaging (Seccia et al., 2012).
One study by Williams et al. found that specific somatic mutations in APAs present with distinct steroid profiles in the lateralization side and in peripheral blood plasma.
APA carrying a *KCNJ5* mutation have in fact higher concentrations of hybrid steroids 18-hydroxycortisol, and 18-oxocortisol, which can be explained by the phenotypical differences found in comparison to *KCNJ5* wild-type APAs (Williams et al. 2016).

Histologically, these tumors are mainly composed of large, lipid-rich, zona fasciculata-like cells whereas APAs carrying *CACNA1D* mutations have histological resemblance to small and compact ZG-like cells.
Transcriptome analysis found that *CYP17A1A1* and *CYP11B1*, encoding the steroidogenic enzymes involved in cortisol synthesis, were highly expressed in ZF-like, *KCNJ5* mutant APAs when compared to the ZG-like, *KCNJ5* wild-type APAs (Azizan et al. 2012). Thus, 11-deoxycortisol is highly synthesized and becomes substrate for *CYP11B2* converting it to 18-hydroxycortisol and 18-oxocortisol.

1.3.9 APCCs and new hypothesis about the cellular origin of APA

The progression from normal adrenal to APA is still not well understood.
Of interest, aldosterone synthesis is suppressed and zona glomerulosa does not express *CYP11B2* encoding aldosterone synthase thoroughly but this enzyme shows a patchy expression pattern at IHC. *CYP11B2* positive cells clusters (APCCs) are the only areas in adrenal cortex expressing aldosterone synthase and are located below the adrenal capsule, extending into ZF. Mixed cell composition in APCCs includes both ZG like and ZF like cells that often show a zonation pattern recalling the normal zonation of adrenal cortex, although ZF-like cells in APCCs express *CYP11B2*.

This phenomenon is likely to be connected to high salt intake with the western diet, which abolishes the need of high aldosterone production to save salt and water. Moreover, APCCs are also present in normal adrenal glomerulosa adjacent to APA despite the low renin levels, thus suggesting that aldosterone synthesis in these cells differ from other ZG cells in terms of independence from the RAS.

Nishimoto et al. have found that, in normal adrenals from donors, APCCs are a common finding and have performed sequencing and microarray analysis and found that APCCs cells have APA-related somatic mutations. These mutations are localized in known ion channels/pumps (*ATP1A1* and

CACNA1D (Nishimoto et al. 2015). These findings may suggest that APCCs are pre-adenomatous lesions leading to ZG-like APAs.
Of interest *KCNJ5* mutations have not been found in APCCs although mutations in this gene are the commonest in sporadic APAs. If *KCNJ5* mutations arise in ZG cells and stimulate *CYP11B2* expression, *KCNJ5* mutant APCCs are not detected probably because of a rapid evolution in APAs or because a second hit mutation is necessary.

1.3.10 Study Hypothesis

Cells composing APAs present different histological phenotypes: there are ZF-like cells (cells morphologically similar to normal ZF cells with a high cytoplasm to nucleus ratio and cytoplasm occupied by lipid vacuoles), ZG-like cells (compact cells similar to normal ZG cells with a low cytoplasm to nucleus ratio and no or little lipid droplets), and intermediated cells with a 'hybrid' characteristics of both.
APAs could be classified according to the percentage of ZG-like and ZF-like cells in two subtypes, ZG-like and ZF-like APAs that differ not only histologically but biochemically and genotypically. The latter usually have *KCNJ5* mutations; the small ZG-like APAs are *KCNJ5* wild type.

The finding of common gain-of-function mutations in a distinct group of ZG-like APAs led to the question whether these tumours arise from normal adrenal ZG cells, and if ZG- and ZF-like APAs differ in terms of tumorigenesis.

We have undertaken a microarray analysis comparing normal adrenocortical ZG with ZF using LCM (figure 1.9) to define ZG-specific genes. We have then compared the transcriptome of 5 ZG-like APAs with mutations in *CACNA1D* or *ATP1A1*, to 8 ZF-like APAs with mutations in *KCNJ5*. The clinical data of the APA patients are showed in Table 1.1.

The finding of previously unsuspected genes with markedly up-regulated

expression in adrenal zona glomerulosa could provide insight to pathways involved in the regulation of aldosterone production. The top 20 of 213 of ZG-up-regulated genes are showed in Table 1.2.

The main genes studied are *ANO4* and *NEFM*. We have hypothesized that they may be involved in the regulation of aldosterone in normal ZG and, in case of NEFM, in ZG-like APAs. The primary aim is to determine the effects of over-expression and/or partial knockdown of each of these genes in human adrenal cells.

Sample ID	Age at surgery	Sex	SBP (mmHg)		DBP (mmHg)		Serum K^+ (mmol/L)		Plasma aldosterone (pmol/L)		Plasma renin (mU/L)	
			Pre	Post	Pre	Post	Pre	Post	Pre	Post	Pre	Post
ADR044	41	F	155	97	130	90	3.3	3.7	856	113	3	4
ADR061	43	F	160	120	100	80	2.7	4.7	846	195	1	26
ADR110	33	F	131	97	73	60	3	4	787	94	2	10
ADR111	46	M	133	125	90	74	3.3	5.1	3144	60	7	81
ADR118	45	M	152	130	84	80	3	4.5	658	151	3	56
ADR119	45	F	136	104	84	70	3	4.4	274	102	2	22
ADR131	73	F	144	131	72	77	4.5	4.5	638	234	7	11
ADR031	34	F	122	111	77	69	4.1	5	2301	172	<2.0	2
ADR032	49	M	225	133	115	81	3.8	4.5	>3300	108	33	127
ADR074	53	M	186	135	124	85	4.3	4.3	1522	94	5	7
ADR106	55	M	180	138	126	100	4.1	4	914	136	12	31
ADR113	35	F	170	128	110	80	2.9	4.5	884	136	2	91
ADR115	41	M	150	138	80	73	3.5	4.2	559	307	2	154
ADR121	45	M	158	130	96	80	3.6	4.1	301	72	6	11

Table 1.1: The clinical features of the patients with Conn's syndrome involved in the microarray assay. We did not have any clinical data about the Phaeocromocytoma patients. ZG: zona glomerulosa. APA: Aldosterone producing adenoma. AAG: adjacent adrenal gland.

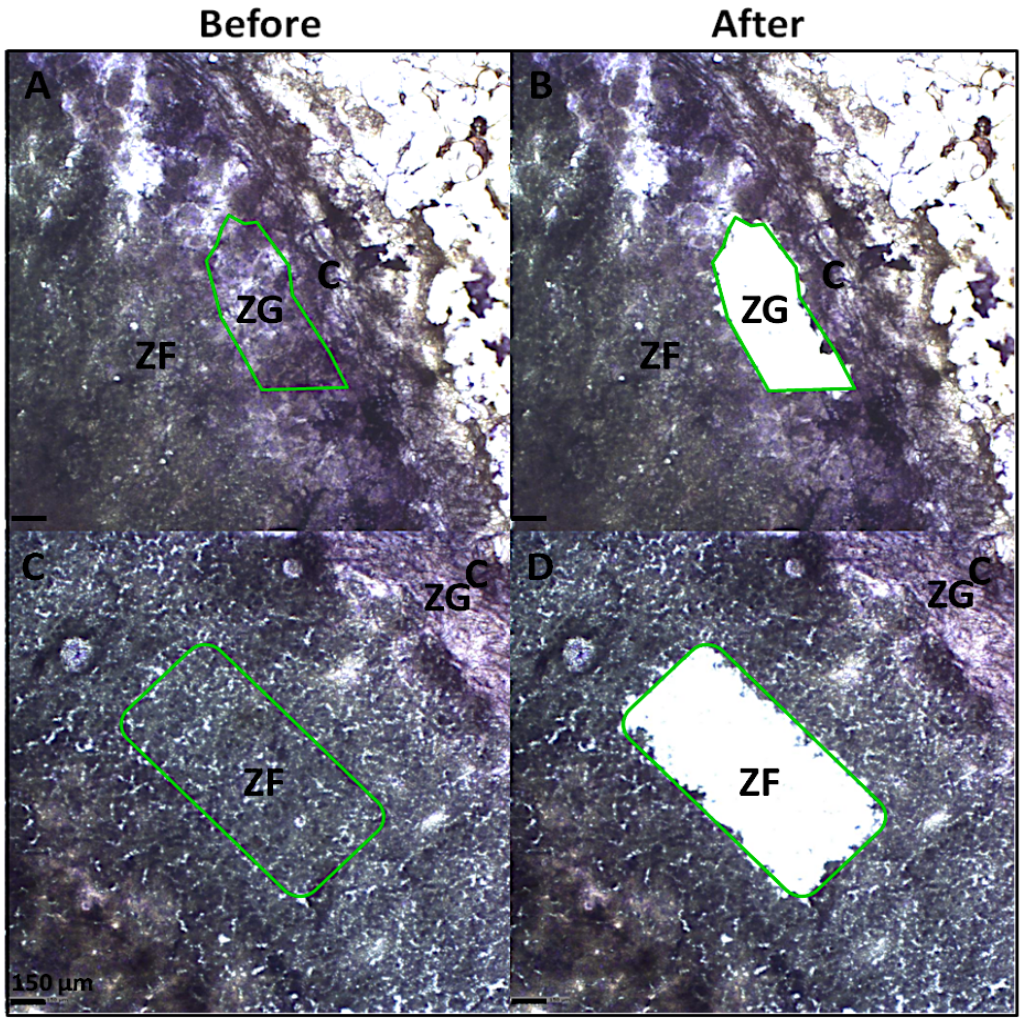

Figure 1.9: Histological images showing laser capture microdissection of ZG and ZF from adrenal sections.

Gene #	Gene Symbol	Fold-Change (ZG vs ZF)	P-value (ZG vs ZF)	Transcript ID	RefSeq
1	*LGR5*	25.05	1.57E-23	7957140	NM_003667
2	*VSNL1*	23.57	3.65E-23	8040430	NM_003385
3	***ANO4***	**19.89**	**6.58E-24**	**7957861**	**NM_178826**
4	***NEFM***	**14.80**	**9.16E-12**	**8145361**	**NM_005382**
5	*VCAN*	14.34	1.85E-13	8106743	NM_004385
6	*DACH1*	14.24	1.38E-21	7971950	NM_080759
7	*NR4A2*	10.90	6.16E-08	8055952	NM_006186
8	*KIAA1210*	8.90	5.40E-11	8174670	NM_020721
9	*SFRP4*	8.67	2.30E-10	8139087	NM_003014
10	*C12orf75*	7.22	4.37E-13	7958253	NM_001145199
11	*C9orf84*	6.95	5.10E-13	8163348	NM_173521
12	*VAT1L*	6.88	9.16E-17	7997336	NM_020927
13	*EDNRA*	6.50	1.18E-16	8097692	NM_001957
14	*OGN*	6.34	5.15E-12	8162373	NM_033014
15	*NR4A3*	5.92	3.06E-08	8156848	NM_006981
16	*SESN3*	5.89	6.10E-16	7951077	NM_144665
17	*LEF1*	5.88	4.29E-15	8102232	NM_016269
18	*PLD5*	5.86	2.55E-12	7925511	NM_152666
19	*CDH12*	5.81	4.45E-10	8111234	NM_004061
20	*HLF*	5.75	5.69E-16	8008588	NM_002126

Table 1.2: Top 20 of the 213 up-regulated genes in all zona glomerulosa (ZG) vs all zona fasciculata (ZF) (FC>5, P < 0.05) (Zhou et al., 2015).

Chapter 2: Study design and general methods

2.1 Study design

Small ZG-like APAs are undiagnosed because of their small size, although new imaging techniques such PET-CT scan can facilitate their detection.

In the following study, we have sought signature 'ZG-genes' which may provide insight to the frequency and pathology of ZG-like APAs. *ANO4* and *NEFM*, two top up-regulated ZG genes in our microarray result were subjects for further analyses due to their high selectivity in expression and probable role in aldosterone production regulation.

The role these genes on steroidogenesis was assessed in the human adrenocortical cell line, H295R, and in primary adrenal cells. This was done through silencing using short interfering RNAs and through overexpressing using a plasmid expression vector.

Further, due to association in literature of NEFM with the dopamine D1 receptor, we performed pharmacological and IF experiments investigating the effects of silencing NEFM on this receptor.

ANO4 effect on basal and stimulated aldosterone secretion was compared to those of other anoctamins, *ANO1* and *ANO6*. ANO4-mediated chloride currents were measured using YFP assay.

Further details on study design and specific methods are present in each chapter.

2.2 General Methods

2.2.1 Human adrenal tissue

Human adrenal tissues were obtained from patients with an APA or a Phaeocromocytoma who underwent adrenalectomy at Addenbrookes Hospital, Cambridge. Local ethical approval and informed consent were obtained from each patient.

Within half hour of the surgery, fresh adrenal tissues from adrenalectomy were separated from surrounded fat tissue. Subsequently, the tissues were processed differently for different purposes of future use:

(a) For RNA extraction: Tissue blocks of about 0.5×0.5×0.5 cm3 from tumor or normal tissue were dissected by an adrenal histopathologist and stored in RNAlater (Ambion, USA) in separate vials immediately. After keeping at 4°C overnight to allow the RNAlater enter the tissues, the solution was removed and the vials were stored at -70°C for long-term storage.

(b) For protein extraction: Same normal and tumor tissue blocks as prepared for RNA extraction were prepared for protein extraction. The sample was put into a vial sitting on ice with RIPA lysis buffer (Thermo Fischer) and complete protease inhibitor cocktail (Roche). Immediate homogenization was performed for the tissues. A maximum of twice homogenization was applied to tissues that were not well homogenized at the first time. Then the protein samples were stored at –70°C for future use.

(c) For cell culture: Pieces of normal and tumor adrenal glands were immersed in culture medium consisting of supplemented Dulbecco's Modified Eagle's Medium/Nutrient F-12 Ham immediately (supplemented with 100 U penicillin, 0.1 mg/ml streptomycin, 0.4 mM L-glutamine, insulin-transferrin-sodium selenite media, and 10 % fetal calf serum) and then proceeded to digestion by collagenase (3.3 mg/mL) for primary cell culture.

As we did not collect normal adrenal glands for ethic issues, we used only adjacent adrenal gland (AAG) cortex and classified this non-tumorous tissue as normal.

2.2.2 Primary cell culture from adrenal tissue

Freshly collected human adrenal tissue was moved to a culture dish with PBS. The medulla was carefully removed by a sterile surgery knife and the tissues minced in small pieces which were left into in 3.3 mg/ml collagenase (Sigma, USA) in warm media, at 37 °C for at least 2 hours to allow digestion. After that, the suspension was centrifuged to pellet the cells and discard the media with the enzyme. The cells were then washed by PBS twice and re-suspended in culture medium. The primary cells were cultured in 37 °C incubator in 5 % CO2 for at least 4-7 days, then plated for experiments.

2.2.3 Human adrenocortical cell line

H295R (NCI-H295R) cells are the only human adrenal cell line capable of proliferate and secrete aldosterone. This is a subgroup of NCI-H295 cells derived from a human adrenal carcinoma excised from a 48-year-old black female (Gazdar et al. 1990). All the major adrenocortical steroids are produced by NCI-H295 cells, including aldosterone, cortisol, corticosterone, androgens and respond to AngII and potassium. H295R cells are a strain of cells from NCI-H295 which grow faster and in a monolayer. They carry a mutation in *CTNNB1* gene (Tissier et al., 2005).

H295R cells (ATCC ® CRL-2128) were purchased from the American Type Culture Collection, and kept in liquid nitrogen until use. For resuscitation, a vial of cells was thawed rapidly in water bath at 37°C and transferred into pre-warmed culture medium. Only cells within passage of 10-19 were used.

2.2.4 Human brain and kidney tissue

Human kidney and brain tissues were used in this study as the positive control for IHC or Western Blotting. They were obtained from Human Research Tissue Bank of Addenbrookes hospital upon request. Ethical approval was granted for this project. The Tissue Bank does not provide clinical nor demographic data for these controls.

2.2.5 Human Embryonic Kidney 293 (HEK293) cell line

HEK293 is a cell line derived from human embryonic kidney cells grown in tissue culture. The source of the cells was a healthy, aborted fetus. Alex Van der Eb cultured the line in the early 1970s at his lab at the University of Leiden; Holland Frank Graham performed the transformation with adenovirus 5 DNA with the calcium phosphate technique invented by himself. The transformation resulted in the incorporation of approximately 4.5 kilobases from the viral genome (Graham et al. 1977).

The type of kidney cell that originated the HEK293 cell line is unknown, since embryonic kidneys contain almost all the types of cells present in the body. The cells may be neuronal in origin because of the presence of mRNA and gene products typically found in neurons, such as all the Neurofilament subunits (Shaw, Morse, Ararat, & Graham, 2002).

HEK293 cell line is very popular in research since they are easy to be cultured, to be transfected, have a good protein production after transfection and are capable of inducing tumours after the injection to animals.

2.2.6 Laser Capture Microdissection (LCM)

LCM was used to acquire samples of ZF, ZG and APA. For differentiation of ZG from ZF, sections were stained with cresyl violet using the LCM Staining Kit (AM1935, Ambion, USA).

Sections of fresh frozen AAG (14 μm) were thaw mounted on to polysine-coated slides and stored at -70°C. When required, sections were fixed in 95% ethanol, rehydrated in 75% and 50% ethanol, stained with 1% cresyl violet,

dehydrated in a graded ethanol series, and immersed in Histo-Clear (AGTC Bioproducts, Wilmington, Massachusetts, USA),. The ZG and ZF were microdissected using a PALM Microlaser System (P.A.L.M. 25 Microlaser Technologies). Total RNA was isolated and reverse transcribed into cDNA as described below with an additional step of purification using Wizard® SV 4 1 Gel and PCR Clean-Up System (Promega, Southhampton, UK)..

2.2.7 Microarray Assay

Microarray assay was performed using the Affymetrix Human Genome U133 Plus 2.0 Array by GenomicsCorelab, Cambridge. Fifty-six RNA samples acquired through laser capture microdissection were assayed—14 trios of ZF, ZG, and APA from patients with Conn's syndrome and a further 7 pairs of ZF and ZG adjacent to a phaeochromocytoma. Seven of the APAs contained a somatic mutation in *KCNJ5*, whereas the remaining 7 were wild-type. Microarray results were validated by quantitative real-time polymerase chain reaction.

2.2.8 Total RNA extraction

Human adrenal tissues were stored at -70°C till RNA extraction. 1 ml of Trizol (Life Technologies, USA) was added to every 50-100 mg of tissues.
For primary adrenal cells or H295R cells cultured in 24-well plates, the culture medium was removed and 400µl Trizol added per well.
Total RNA was isolated on silica columns using the TRIzol® Plus RNA Purification System (Life Technologies, USA). DNA-free RNA was prepared using PureLink® DNase Set (Life Technologies, USA) according to the manufacturer's instructions.

2.2.9 Reverse transcription

The concentration of RNA samples was quantified at NanoDrop. cDNA was synthesized using the Reverse Transcription System (Promega, USA). In

brief, 8.9 µl of RNA sample, 1 µl of random primers and 1 µl of Oligo-dT primers were mixed and then incubated at 70ºC for 10 min. After cooling down on ice, 9.1 µl of master mix (4µl of 25 mM MgCl2, 2 µl of 10X reverse transcription buffer, 2 µl of 10 nM dNTP mixture, 0.5 µl of RNase inhibitor, and 0.6 µl of AMV reverse transcriptase) was added per sample. The 20 µl systems were incubated at 22ºC for 15 min, 42ºC for 1 h, and 95ºC for 5 min. The cDNA samples were then stored at 4°C for short-term or –20°C for long-term. Negative control consisted of RNase free water instead of sample RNA template plus the master mix.

2.2.10 Quantitative Polymerase Chain Reaction (Real Time PCR, qPCR)

Targeted mRNA expression level was measured by amplifying and simultaneously detecting its relative cDNA quantity at ABI 7500 system (Life Technologies, USA).

In brief, 3.75 µl cDNA from previously described RT and 11.25 µl mix of (7.5 µl of Taqman Fast PCR Master Mix, 0.75 µl of 10X standard TaqMan ABI primer & probe of targeted gene, 3 µl of RNase free water) were added to each well of a 96-well plate in duplicate. After a short spin, the plates were incubated at 50 °C for 2 min to optimal Uracil N-glycosylase (UNG) enzyme activity, 95 °C for 10 min to activate AmpliTaq Gold enzyme, and then 45 cycles of PCR (95 °C for 15 sec to denature, 60 °C for 1 min to anneal and extend). Standard TaqMan ABI primer & probes were applied for all the targeted genes except for custom made *CYP11B1* and *CYP11B2*. The primers and probes used for these two genes are from previous literature, (Fallo et al., 2002) and produced by Eurofins Genomics, Ebersberg, Germany.18S rRNA was used as the housekeeping gene. The results were analyzed using the 2-ΔΔCT method. We have included two negative controls, one was RNase free water and the other one was the water control of reverse transcription.

2.2.11 Immunohistochemistry (IHC)

IHC on paraffin-embedded sections was performed at the Tissue Bank IHC service, Addenbrookes Hospital:

It was performed on formalin-fixed, paraffin-embedded sections (4 μm) using an automated immunostainer with cover tile technology (Bond-III system, Leica Biosystems). The commercial antibodies were used as the primary antibodies. The Antigen retrieval was carried out using the combination of heat and Bond Epitope Retrieval Solution 1 (Leica, AR9961) for 20 minutes. The optimal working dilution for NEFM was 1/500 and for DRD1 was 1/50. The Bond™ Polymer Refine Detection kit (Leica, DS9800) was used for detecting and visualising the antigens. Negative controls, in which primary antibodies were omitted, resulted in a complete absence of staining.

When performed in our lab the following was the protocol used:
Serial paraffin-embedded human adrenal or kidney sections (4 μm thickness) were prepared by Human Research Tissue Bank of Addenbrookes hospital upon request. The slides were de-paraffinized in 2 changes of histo-clear II, 10 min each and then transferred to 100% methanol for 2 changes, 5 min each. After this, the slides were transferred once through 90%, and 70% and methanol, 5 min each. The slides were rinsed by Milli-Q (MQ) purified water. To unmask the antigenic epitope, the slides were incubate at 100°C for 15 min in univer Vector® antigen unmasking solution (15 ml in 1600 ml MQ water, Vector laboratories Inc, USA) and left at room temperature for 20 min to cool down. Then the slides were incubated in 0.3% H_2O_2 solution in methanol at room temperature for 4 min to block the endogenous peroxidase activity. 300 μl of 5% goat serum were added to the sections on the slides to incubate in a humidified chamber at room temperature for 2 h for blocking. The blocking buffer was drained off and 300 μl of diluted primary antibody in 3% goat serum (made in PBS-T (0.1% (v/v) Tween 20 in 1x PBS)) were mounted on the sections to incubate in a humidified chamber at 4°C overnight. The following day, the slides were rinsed in PBS-T for 3 changes,

5 min each. Then, 300 µl of diluted secondary antibody in 3% goat serum (made in PBS-T) were mounted on the sections to incubate in a humidified chamber at room temperature for 1 h. The slides were rinsed in PBS-T for 3 changes, 5 min each. 300 µl of rabbit- Peroxidase Anti-Peroxidase (PAP)-conjugates (in 3% goat serum made in PBS-T) were added to the sections on the slides and incubated in a humid chamber at room temperature for 1 h. The slides were rinsed in PBS-T for 3 changes, 5 min each. 100 µl of DAB substrate solution (Sigma) were applied to the sections on the slides to reveal the color of antibody staining. The slides were allowed to develop color for about 2 min and then rinsed by MQ water. The slides were dehydrated in 4 changes of ethanol (95%, 95%, 100% and 100%), 5min each and then cleared in 3 changes of xylene and kept in xylene overnight. Finally, Depex was applied to the sections and the slides were covered by coverslips for permanent stock.

Positive controls were prepared by applying the same antibodies to the tissue biologically containing abundant amount of the respective antibody, such as human kidney tissue, which were obtained from the Human Research Tissue Bank of Addenbrookes hospital. We were not allowed to have any demographic or clinical data regarding these samples for ethical issues.

Tissue incubated with the antibody diluent alone and no primary antibody, followed by incubation with secondary antibodies and detection reagent was considered as negative control. This ensures that staining is produced from detection of the antigen by the primary antibody and not by the detection system or the specimen.

Images were captured using a standard bright field microscope, U-TV1-X digital camera and the CellD software (Olympus Ltd, UK). Some slides had been scanned by the Tissue Bank slide scanning service using an Aperio Digital Pathology Scanner.

2.2.12 Protein lysis and BCA™ protein assay

The protein samples lysed in RIPA buffer were briefly centrifuged to settle the debris. The supernatants were then collected as total protein of the samples. The components of RIPA buffer were as follows: 25mM Tris-HCl pH 7.6, 150mM NaCl, 1% NP-40, 1% sodium deoxycholate, 0.1% SDS.
The concentration of the lysate was detected by BCA™ protein assay (Pierce Biotechnology, USA). In brief, 10 µl of the lysate or standard curve sample and 80 µl of the BCA Working Reagent (50 parts of BCA Reagent A with 1 part of BCA Reagent B) were added to each well in a 96-well plate. The plate was then incubated at 37°C for 30 min. The plate was then measured the absorbance at 562 nm on a plate reader.

2.2.13 Western Blotting

Western blotting was conducted using total protein lysate. Protein lysates were boiled in sample buffer at 95°C for 5 min and then separated by electrophoresis in 8-20% SDS-PAGE gel. The electrophoresis was run at 110 V for 60 min until the protein ladder was well separated. The protein was then transferred from the gel to a PVDF membrane previously activated by methanol. After that, the membrane was blocked with blocking buffer (TBS-T with 5%onfat dry milk) for 30 min at room temperature and then incubated in appropriate dilutions of primary antibody in blocking buffer at 4°C overnight. The membrane was washed with TBS-T three times and then incubated in appropriate dilution of conjugated secondary antibody in blocking buffer at room temperature for 1 h. The membrane was washed with TBS-T again three times and the bands were detected using the Pierce ECL Western Blotting Substrate (Thermo Fisher Scientific, USA). Anti-GAPDH (#G8795, Sigma, UK; 1:10,000 dilution) was used as an internal control for protein abundance.

2.2.14 Aldosterone measurement

Commercially available Homogenous Time Resolved Fluorescence Resonance Energy Transfer (HTR-FRET or HTRF) assay from Cisbio Bioassays, France was used according to manufacturer's instructions. The aldosterone concentrations from H295R and primary cells were normalized to total cell protein.

HTRF is a competitive assay using a specific antibody labeled with Eu3+-Cryptate (donor) and aldosterone labeled with XL665 (acceptor).

When these dyes are in close proximity, the excitation of the donor with a light source (laser or flash lamp) triggers a Fluorescence Resonance Energy Transfer (FRET) towards the acceptor, which in turn fluoresces at a specific wavelength (665nm). The aldosterone present in the sample competes with the binding between the two conjugates and thereby prevents FRET from occurring. The specific signal, inversely proportional to aldosterone concentration, modulates negatively.

Briefly, the assay is performed as described: 10 ul of sample and standard curve points was plated in a 384 well plate in duplicate, followed by 5 ul of aldosterone-XL665 (100-fold stock solution previously diluted in detection buffer) and 5 ul of aldosterone-Cryptate antibody (100-fold stock solution previously diluted in detection buffer). The plate was sealed and incubated in the dark for at least one hour. The plate was then read in a compatible HTRF reader**.**

2.2.15 Confocal Imaging

H295R and primary cells were cultured in supplemented media on sterilised and poly L-lysine coated coverslips for 24-h.

Cell plasma membranes were stained with Wheat Germ Agglutinin, Alexa Fluor® 633 Conjugate (W21404, Life Technologies) diluted in growth media (2 ug/mL) for 10 min at 37 °C. Cells were then washed twice with PBS (5 min each), fixed with 4% paraformaldehyde for 10 minutes and permeabilised with 1% triton-X100 in PBS, 5 min at room temperature. Cells were incubated with blocking buffer (3% BSA in PBS-T) for 1 hr at room temperature and overnight with the primary antibody at optimized dilution in 3% BSA-PBS-T. Goat anti-

Rabbit IgG, or goat anti-Mouse Alexa Fluor® Conjugates (Life Technologies) were used as secondary antibody at 1:500 dilution in 3%BSA-PBST for 1-h at room temperature. Finally cells were washed three times in PBS and cover slips were mounted on slides using VECTASHIELD Antifade Mounting Medium with DAPI (H-1200, Vector Laboratories). Confocal images were taken (63X) using Zeiss LSM510 Meta confocal microscope and analysed using Zen 2011 software.

2.2.16 siRNA

H295R cells were seeded at 1.0×10^5/well in 24-well plates in antibiotic-free complete culture medium the day before.

The next day, the medium was removed and 500 µl of antibiotic-free medium with pool or individual ON-TARGETplus siRNA and non-targeting siRNA as control (Dharmacon) was added to the cells. The cells were then incubated at 37°C in 5% CO_2 for 48 h and the medium harvested to measure aldosterone and/or protein assay or mRNA expression studies.

For overexpression experiments H295R were seeded at the same density as for silencing. The growth media was then replaced with un-supplemented media to starve the cells and increase the transfection efficiency. After at least six hours the media was replaced by 500 ul transfection media containing 50 ul Optimem, 1.5 ul Lipofectamine reagent 3000, 2 ul Lipofectamine P3000 reagent and 500 ng of plasmid per well. The cells were harvested after 48 hours for RNA or protein experiments.

2.2.17 Live cell imaging

H295R cells were transfected with non-targeting control and NEFM siRNA and IncuCyte Kinetic Live Cell Imaging System (Essen BioScience) was used to measure live cell growth at 37°C and 5% CO_2 in 5 wells per treatment over 72 hours.

After plating 10^5 cells per well in a 24 well plate, the antibiotic-free growth media has been replaced by media with 10nM of Si-RNA (or non-targeting in

controls) and the plate immediately placed in in vitro live-cell imaging system (Incucyte). The measurement of the occupied area (% confluence) of cell images over time monitors cell proliferation. As cells proliferate, the confluence increases.

2.2.18 Colony formation assay

The colony formation assay (or clonigenic assay) helps evaluating the ability of a single cell to generate a colony of 50 or more cells (or progeny) after any treatment (drugs, radiation, genetic modifications).

A clonigenic experiment has three steps: 1) cells treatment, 2) preparation of single cell suspension, counting and plating a known and equal number of cells in six wells plate and, 3) fixing and staining colonies following a relevant incubation period (3-4 weeks for H295R cells).

For our experiments, H295R were transfected with shRNA for NEFM in 24 well plates by using Lipofectamine 3000 as described before. After 48 hours incubation, cells were washed with PBS, trypsinized to obtain single cell suspension and counted at hemocytometer. Three hundred cells were seeded per well (every treatment had triplicates) and incubated at 37°C in a 5% CO2 environment for 3 weeks. Media was changed every week. After this incubation period, the cells were fixed and stained: the media was aspirated from each well and the cells washed with PBS twice. The colonies were fixed on ice with ice-cold methanol for 10 minutes. The methanol was aspirated and the cells washed again with PBS. The staining was performed with 0, 1% (w/v) crystal violet in dH_2O left for 30 minutes. The crystal violet was then removed the wells washed with dH_2O. After drying overnight the plates were photographed and the individual colonies counted using Image J.

2.2.19 Escherichia coli (E. coli) Transformation

50 µl of One Shot® TOP10 E. coli Competent Cells (Invitrogen, USA) was thawed on ice and mixed with about 100 ng of plasmids which carried the

gene for Ampicillin resistance. After 15 min incubation on ice the cells underwent a 42°C heat shock in water bath for 45 seconds, followed by 2 min incubation on ice. After this 250 µl of SOC medium was added and the cells were incubated at 37°C for 1 h shacking at 250 rpm. Finally, the cells were pelleted by centrifugation at 14,000 rpm for 30 seconds. The cells were re-suspended and seeded in a pre-warmed LB Agar plate with ampicillin. 50 µl of nuclease-Free Water was used as negative control. The plates were incubated at 37°C overnight. The next morning, 3-5 single colonies were picked for miniprep and maxiprep from the positive plate.

2.2.20 Miniprep

A single colony of E. coli from the seeded plate was picked and transferred to 5 ml of LB broth medium supplemented with ampicillin and incubated at 37°C overnight -shaking at 250 rpm. 4.5 ml of the suspension was used for miniprep to obtain enough plasmid to be sequenced and the other 0.5 ml was stored at 4°C for maxiprep. The QIAprep Spin Miniprep Kit (Qiagen, UK) was used for miniprep according to the manufacturer's instructions.
In brief, the bacteria were pelleted by centrifugation and resuspended in buffer P1 (Resuspension Buffer: 50mM Tris-Cl, pH 8.0, 10mM EDTA, 100ug/mL RNase A), plus buffer P2 (Lysis Buffer: 200mM NaOH, 1% SDS) and buffer P3 (Neutralization Buffer: 3.0M potassium acetate, pH 5.5). The mixture was centrifuged and the supernatants moved to the QIAprep spin column and centrifuged. The plasmid DNA in the spin column was washed using buffer PE, then eluted in RNase free water. The concentration of the plasmid DNA was measured at NanoDrop. A sample of each miniprep was sent for Sanger sequencing to select the right colony with expected sequence of plasmid DNA.

2.2.21 Maxiprep

The saved bacterial cell suspension from the original colony was added to 500 ml of LB broth containing ampicillin (final concentration 100 µg/mL) and

incubated at 37°C for maximum 16 h at 250 rpm. The next day, the bacteria suspension was centrifuged at 3200 rpm for 1 h at 4°C and maxiprep was performed using the EndoFree Plasmid Kits (Qiagen, UK) according to the manufacturer's instructions.

In brief, the bacterial pellet was suspended in buffer P1, buffer P2 and chilled buffer P3. The lysate was poured into a QIAfilter Cartridge and kept at room temperature for 10 min. The cell lysate was then pressed and filtered. After that, buffer ER was added (1:10) and incubated on ice for 30 min. Subsequently, the cell lysate was poured into a QIAGEN-tip 500 column with an equilibrated membrane where the plasmid DNA attached after the lysate went across by gravity. The column was washed with buffer QC twice and the DNA was eluted in buffer QN, and precipitated by isopropanol and centrifuged at 3200 rpm for 1 h at 4°C. The DNA pellet was washed by 70% ethanol once and air-dried until the residual ethanol evaporated. The DNA pellet was eluted in endotoxin-free RNase free water and nanodropped to determine the DNA concentration.

2.2.22 Polymerase chain reaction (PCR)

Most of the polymerase chain reaction (PCR) in this study used the following fast PCR reaction system and program as suggested by the protocol (Applied Biosystems, USA):

Fast PCR reaction system:

1. Forward primer (5 μM) 2 μl;
2. Reverse primer (5 μM) 2 μl;
3. Human adrenal or blood sample template (50-200 ng) 6 μl;
4. AmpliTaq Gold®Fast PCR Master Mix (Applied Biosystems, USA) 10 μl, UP (2×).

Fast PCR program:

1. 95 ºC 10 min to start the enzyme;
2. 35 Cycles of the following steps:

1> 96 ºC 3 seconds for denature;
2> Primer Melting Temperature for 3 seconds;
3> 68ºC 5 seconds for extension;

3. 72 ºC 10 seconds for Final elongation.

For the KCNJ5 gene sequencing, the regions including the selectivity filter and inner helix were sequenced using the following sets of primers:

Set 1 forward primer: 5'-TTG AAA ACC TCA GTG GCT TC-3'
Set 1 reverse primer: 5'-GCA GCT GAG CCT GAG ACA TC-3'
Set 2 forward primer: 5'-GAT GGT GTC TTT TTA ACT CAA AGC-3'
Set 2 reverse primer: 5'-CTG AGG AGG ACA AAG CGC C-3'
Set 3 forward primer: 5'-ATG GCT GGC GAT TCT AGG AAT GCC-3'
Set 3 reverse primer: 5'-TCA CAC CGA GCC CCT GGC CTC C-3'.

Chapter 3: Role of *NEFM*, a ZG-selective gene, in human adrenal

3.1 Abstract

Heterogeneity among APAs has been highlighted by the discovery of somatic mutations. Frequent *KCNJ5* mutations are usually present in large ZF-like APAs; mutations in *CACNA1D*, *ATP1A1*, *ATP2B3* and *CTNNB1* had been found in small APAs with ZG-like histological features. Microarray comparison of *KCNJ5* mutant versus wild-type APAs revealed significant differences in transcriptomes. NEFM, one the neurofilament subunits and a dopamine receptor D1R interacting protein, was 4-fold-upregulated in *KCNJ5* wild-type ZG-like vs *KCNJ5* mutant ZF-like APAs, and 14-fold more expressed in normal ZG vs ZF.

Immunohistochemistry confirmed selective expression of NEFM in ZG from adjacent adrenal cortex and in ZG-like APAs.

Silencing *NEFM* in H295R cells increased basal aldosterone secretion and cell proliferation. Moreover, it also amplified aldosterone stimulation and inhibition in response to D1R agonist fenoldopam and antagonist SCH23390, respectively. NEFM co-immunoprecipitates with D1R and its expression is stimulated by fenoldopam, thus suggesting that it plays a role in preventing D1R accumulation to the plasma membrane.

Immunohistochemistry for D1R differed between the two APA subtypes. In ZG-like APAs was mainly intracellular, membranous in ZF-like APAs.

Aldosterone secretion in response to fenoldopam in primary cells from ZF-like APAs was significantly higher than in cells from ZG-like APAs.

In conclusion: (1) NEFM is a negative regulator of aldosterone production and cell proliferation; (2) it prevents D1R trafficking to plasma membrane; (3) its down-regulation in ZF-like APAs may contribute to a D1R/D2R imbalance underlying variable pharmacological responses to dopaminergic drugs among patients with APAs.

3.2 Introduction

Transcriptome comparison between human adrenal ZG and ZF found unsuspected genes up-regulated -up to 25-fold- in ZG vs ZF 3.
Of these, 7 genes were more than ten-fold up-regulated (*LGR5, VSNL1, ANO4, NEFM, VCAN, DACH1* and *NR4A2*), but only *VSNL1* and *NR4A2* have previously been investigated in zona glomerulosa (Bassett et al. 2004; Williams et al. 2012). *NEFM* expression and function in the adrenal ZG has been further investigated.

Its expression was 14.8 fold up regulated in ZG vs ZF ($p=9.16^{-12}$) and 3.2 fold down-regulated in overall APA vs ZG ($p=1.38^{-03}$). Of note, the two APA subtypes showed different expression levels: *NEFM* expression was 3.96 fold down-regulated in *KCNJ5* mutant APAs in comparison to wild type ($p=4.35^{-03}$).

NEFM is one of the subunits forming the Neurofilament (NF), the type IV intermediate filament of mature neurons, one of the most abundant proteins in the nervous system. Instead of other intermediate filaments types expressed in different cell types that are homo-polymers, NFs are hetero-polymers composed of four subunits: NEFL, NEFM, NEFH (classified according to their molecular weight), plus alpha-internexin in the central nervous system or peripherin in peripheral nervous system.

The four subunits have a common structure: a conserved central-helical rod region, and non-helical regions, the head domain at the N-terminus and a tail of variable length at the C-terminus. The rod domain contains highly conserved motifs, while head and tails are less conserved. The head domain is rich for serine and threonine. The tail domain is the distinctive feature of NF proteins. NEFL tail is short and rich in glutamic acid, whereas it is longer in NEFM and NEFH, and contains not only several glutamic acid residues but also multiple repeats of' phosphorylation sites lysine–serine–proline (KSP) (Perrot et al. 2008).

The complex regulation of head and tail phosphorylation distinguishes NF subunits from other intermediate filaments, beyond the structural role as cytoskeletal proteins. Phosphorylation controls turnover, subunit polymerisation and tail extension, but other functions are expected.

NF subunits explicate extra-cytoskeletal roles in the neuronal synapses as receptors-interacting proteins, while recent studies have showed that NEFM, NEFL and NEFH can also be considered onco-suppressor genes in different cancer types, in which their epigenetic silencing affects cell proliferation, and correlates with aggressiveness and prognosis (Calmon et al., 2015; Peng et al., 2015; Shen et al., 2016; Wang et al., 2015).

Regarding the synapses, the previous conception as simple NF degradation site has been overtaken by the finding that synaptic NF proteins constitute a pool with different features in comparison to those expressed in other regions of the neurons (Yuan et al. 2015; Yuan & Nixon 2016).
First of all, NF proteins in synapses are oligo- or monomeric and can be either transported in axons or locally synthesized. They are more abundantly present in the post-synaptic density rather than the presynaptic terminal. So far NEFL and NEFM synaptic roles have been elucidated as for their interaction with different neurotransmitter receptors.

NEFL interacts directly with the C-terminus of NR1, a subunit of N-methyl-d-aspartate (NMDA) receptor highly concentrated in postsynaptic membranes of glutamatergic synapses. Co-expression of NEFL with NR1 increases surface abundance of NR1 by 20% and reduces its ubiquitination process, thus facilitating NMDA receptor trafficking into the plasma membrane and contrasting its degradation. (Ehlers et al. 1995; Ehlers et al. 1998) Moreover, NEFL binds to protein phosphatase-1 (PP1), which can affect the phosphorylation state of NF proteins and NR1 (Terry-Lorenzo et al. 2000).

NEFM is abundantly present in the synaptic NF population, and it is characterized by lower phosphorylated state if compared to other neuron cell regions. In 2002 Kim et al. found, by using a yeast-two-hybrid screening approach, that NEFM directly and specifically interacts with the cytoplasmic loop of D1R, one of the dopamine receptors highly expressed and localised in the postsynaptic density of dopaminergic neurons.
Co-expression of NEFM and D1R in HEK293 cells caused a 50% reduction of the receptor binding and of the consequent cAMP synthesis induced by D1R activation.
It also reduced D1R localization at the cell surface and promoted its cytoplasmic accumulation. Functionally, co-expression of NEFM with D1R reduced the agonist-induced desensitization of D1R. NEFM and D1R localized in the rat frontal cortex. NEFM-KO mice brains showed a reduction in D1R expression (Kim et al. 2002).

More recently, the NEFM/D1R interaction at synaptic level was more deeply investigated in an animal model. In wild-type mice, NEFM co-localizes with the D1R in synaptic densities. The specific deletion of NEFM, but not of NEFL or NEFH subunits, amplified the D1R-mediated motor responses to cocaine and caused the redistribution of postsynaptic D1R to the plasma membrane from the endosome recycling compartment (Yuan et al. 2015).

Further evidence that NF proteins are correlated to D1R comes from animal models of drug addiction, such as cocaine or nicotine, involving the release of dopamine and increasing its synaptic concentrations in the mesolimbic system. In these animals drugs affect NF proteins expression.
More in detail, in one study NEFL, NEFM and NEFH were decreased 15-50% by chronic administration of morphine or cocaine in rats (Beitner-Johnson et al. 1992), but more recently it has been found that in the synaptosomal fractions NEFM increases after administration of D1R binding cocaine in rats (Kovacs et al. 2010).

The response to antipsychotics acting on D1R also depends on genetic variances of NEFM (Strous et al. 2007).
A further evidence of NEFM/D1R interaction comes from the D1R knockout mouse in which NEFM expression in the brain was suppressed, while all the other NF subunits were not affected (Stanwood et al. 2005).

NF proteins expression is deregulated in cancer: the three NF subunits are epigenetically inactivated (mainly by DNA methylation) in several tumors such as breast, pancreas, gastric, and colon cancer.
Their epigenetical silencing correlates with the prognosis and progression and staging of the disease. One study found that overexpression of NEFH reduces cell proliferation and stops cells cycle progression at Go/G1 phase transition, with a reduction in migration and invasion in breast cancer cells (Calmon et al. 2015).
Another epigenetic mechanism involved in silencing NF subunits is the expression of micro-RNA. NEFL is as instance silenced in aggressive brain cancer and in head and neck carcinomas because of the overexpression of miR-25 (Peng et al. 2015).
More than one pathway can be involved: silencing NEFL in a lung cancer derived cell line increased invasion and migration via inhibition of the NF-kB pathway (Shen et al. 2016).
DNA methylation of the NEFH promoter and down-regulation of expression activates the AKT/b-catenin pathway in renal carcinoma cells.
NEFL silencing in head and neck cancer causes an activation of mTOR signaling (Dubrowinskaja et al. 2014).

3.3 Study design

In order to investigate the role of NEFM in the adrenal, we have characterized its protein expression in human adrenals and co-localized NEFM with D1R staining. We also investigated the function of NEFM on adrenal steroidogenesis and its effect on the cell proliferation. For its known interaction with synaptic D1R we have investigated the functional interaction between NEFM and D1R by evaluating co-localisation, co-immuno-precipitation, D1R cellular trafficking in relation to NEFM expression and aldosterone response to drugs targeting D1R in both H295R cells and primary cells from the two different APA subtypes.

3.4 Specific Methods

3.4.1 Antibodies testing

The rabbit polyclonal anti-D1R antibody (Sigma) was tested for specificity at IHC using a competing peptide (Sigma). The rabbit polyclonal anti-NEFM antibody was tested in lysates of nontargeting and *NEFM*-specific siRNA-transfected H295R. Kidney and brain slides were used as positive control at IHC, respectively.

3.4.2 Co-immunoprecipitation

500 µg of whole-cell lysates protein with a final volume of 1 ml were pre-cleared by incubation with 10 µl of Protein A/G PLUS-Agarose (Santa Cruz, sc-2003) at 4 °C for 1 hour followed by centrifugation at 4 °C for 1 min at 4000 rpm. The supernatant was subjected to immunoprecipitation by the addition of 1 µg of mouse anti D1R (Santa Cruz, sc-33660) antibodies and incubated overnight at 4 °C, followed by incubation with Protein A/G PLUS-Agarose for 2 h. After washing with lysis buffer and buffer A (50 mM Tris and 0.1 mM EGTA) twice, the beads were incubated in 2 × SDS loading buffer at room temperature, then transferred to a SpinX tube and centrifuged for 3 minutes at 14000 rpm. The eluent was collected and reducing agent beta-

mercaptoethanol was added. The samples were resolved by SDS-PAGE and subjected to Western blot analysis, as previously described. Rabbit Anti NEFM 1:500 (Sigma) was used to probe the membrane.

3.4.3 shRNA

In order to visualize cells at confocal microscopy, we have transfected cells with shRNA plasmid expressing eGFP. pLVTH was a gift from Didier Trono (Addgene plasmid # 12262). shRNA sequence targeting NEFM was cloned into pLVTH plasmid using Q5 site directed mutagenesis kit (NEB) and primers (5'ATCCGTTGCGCTCCACCGTGATGTTTTTTGGAAAAGCTTATCGATACC-3' and 3' – ATCAATTGCGCTCCACCGTGATGTGGGGATCTGTGGTCTCATAC- 5'). Stem loop sequence used was sense 5- ACAUCACGGUGGAGCGCAA- 3' and 5'- UGUAGUGCCACCUCGCGUU- 3'. Loop sequence used was 5'-TTGATATCCG-3'. Sanger sequencing verified the shRNA sequence insertion and Lipofectamine 3000 was used to transfect cells.

3.4.4 Mitochondrial staining with MitoTracker Orange CMTMRos

Cells were grown and transfected with shRNA on coverslips. After 48 hours the media was removed and replaced by pre-warmed (37°C) complete media containing MitoTracker probe (at 250 nM). The incubation time was 30 minutes at 37°C and 5% CO_2. After staining, the cells were washed in PBS three times (5 minutes each), and fixed with 4% paraformaldehyde for 10 minutes. After fixation, the cells were washed three times in PBS and cover slips were mounted on slides using VECTASHIELD Antifade Mounting Medium with DAPI (H-1200, Vector Laboratories). MitoTracker Orange CMTMRos has an emission of 554 nm and excitation of 576 nm.

3.5 Results

3.5.1 Microarray

Microarray comparison of ZG vs ZF from 21 humans found that *NEFM* was the fourth most up-regulated gene (14.8 Fold-change, p= 9.16^{-12}).

When the transcriptome of ZF-like, *KCNJ5*-mutant APAs was compared to ZG-like, *KCNJ5* wild-type APAs, *NEFM* resulted to be the fourth most down-regulated gene in the former (-3.96 Fold-change, p=4.35^{-03}, Figure 3.1) .

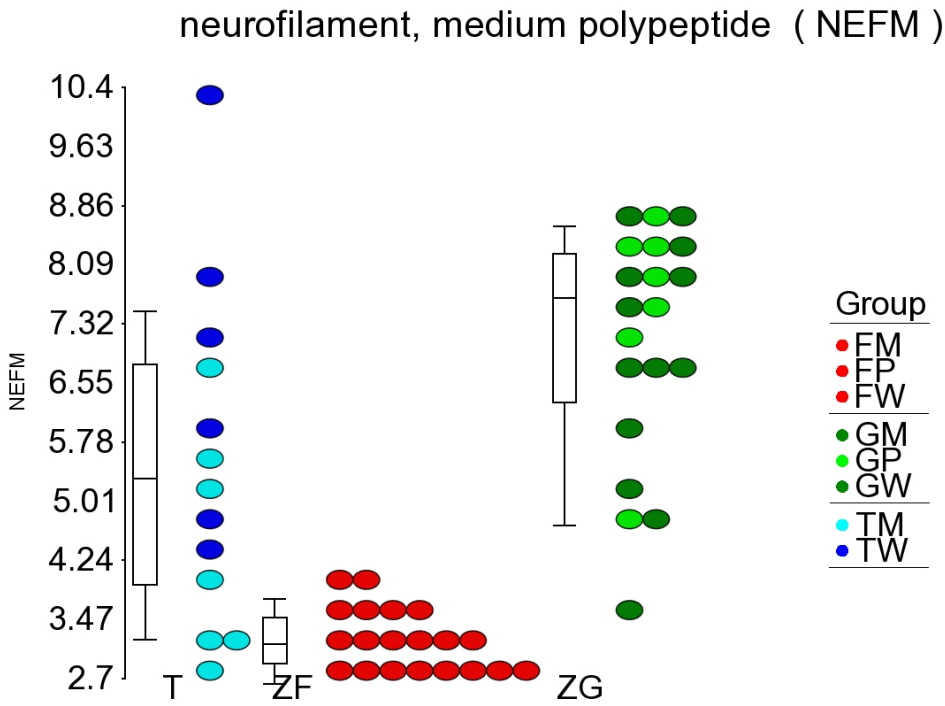

Figure 3.1: Representative RMA values of *NEFM* automatically clustered ZF, ZG and APA separately. RMA: Robust Multichip Average. T: Tumor (Aldosterone-Producing Adenoma). ZF: Zona Fasciculata. ZG: Zona Glomerulosa. Group legend: FM: ZF-Mutant KCNJ5. FP: ZF-Phaeocromocytoma. FW: ZF- wild-type KCNJ5. GM: ZG-Mutant KCNJ5. GP: ZG-Phaeocromocytoma. GW: ZG-KCNJ5 wild-type. TM: Tumor - mutant KCNJ5. TW: Tumor- Wild-type KCNJ5.

The microarray results were validated and confirmed by qPCR performed on LCM samples (Figure 3.2).

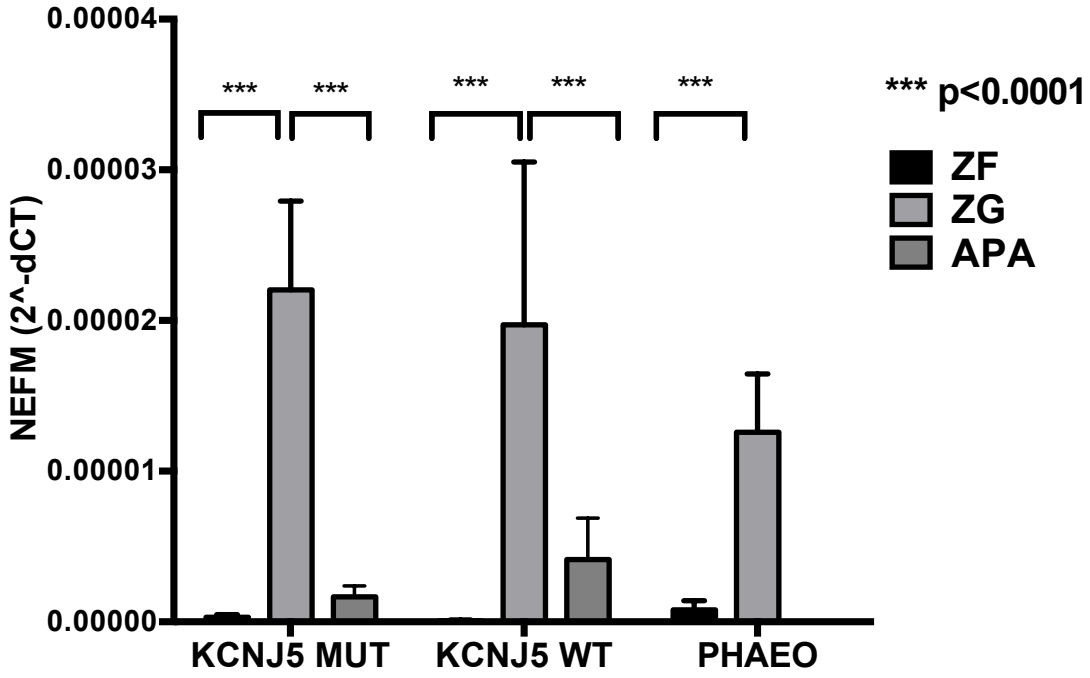

Figure 3.2: *NEFM* qPCR validation of microarray findings performed on LCM samples from ZG, ZF and APAs of 7 patients with phaeocromocytoma, 7 patients with *KCNJ5* mutant, and 7 patients with *KCNJ5* wild-type APAs. Results are expressed as Mean and S.E.M of 2^{-dCT}. Multiple t-tests were applied.

3.5.2 Antibodies testing

The rabbit polyclonal anti-D1R antibody (Sigma) was tested for specificity at IHC using a competing peptide (Sigma). The rabbit polyclonal anti-NEFM antibody was tested in lysates of nontargeting and *NEFM*-specific siRNA-transfected H295R.

The disappearance of D1R staining after the competing peptide experiment and of NEFM band in silencing experiments allowed us to confidently rely on the specificity of these two commercial antibodies.

Kidney and brain slides were used as positive control at IHC, respectively.

IHC of D1R showed staining mainly in proximal tubules but not in the glomeruli. IHC of NEFM showed that neuronal perikarya and axonal fibers were all NEFM-positive (Figure 3.3).

No primary antibody control was performed by incubating tissue with the antibody diluent alone and no primary antibody, followed by incubation with secondary antibodies and detection reagents. The absence of staining confirmed that the staining from primary antibody experiment is produced from its detection of the antigen and not by the detection system or the specimen (Figure 3.4).

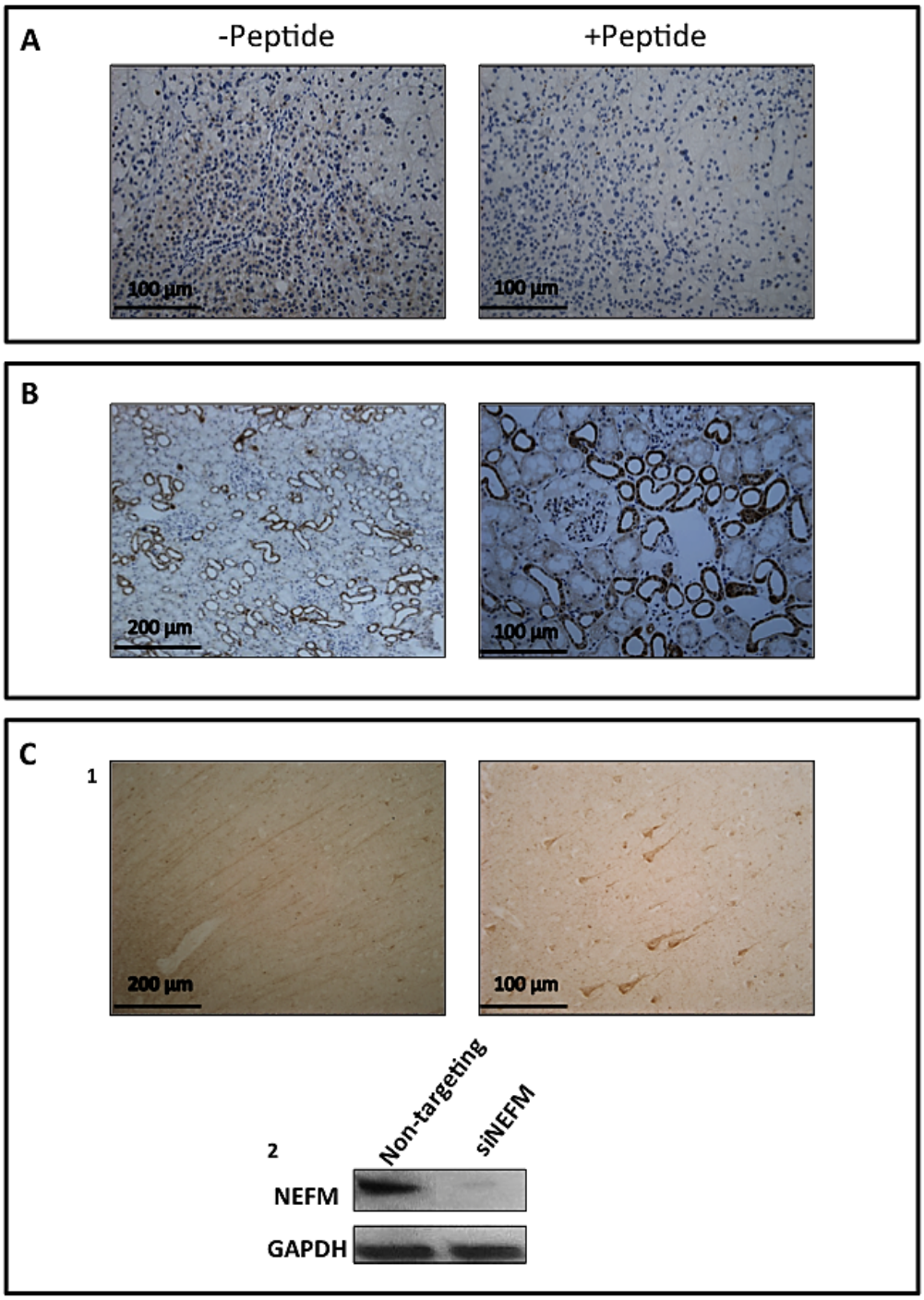

Figure 3.3: Antibodies validation. Panel A: IHC analysis of paraffin-embedded APA slides, using rabbit anti D1R (Sigma) pre-incubated without (Left) and with blocking Peptide (100X molar excess, Right). The staining disappears in presence of the blocking peptide.

Panel B: IHC of D1R of paraffin-embedded human kidney slides, used as positive control, at two magnifications. The staining was mainly in proximal tubules but not in the glomeruli. Panel C 1: IHC of NEFM of

paraffin-embedded human brain slides, used as positive control, at two magnifications. Neuronal perikarya and axonal fibers are all NEFM-positive. Panel C 2: Western blot analysis of lysates from H295R cells transfected with either nontargeting siRNA or *NEFM* specific siRNA. Downregulation of signal from the anti-NEFM antibody confirms target specificity. Anti GAPDH was used as loading control.

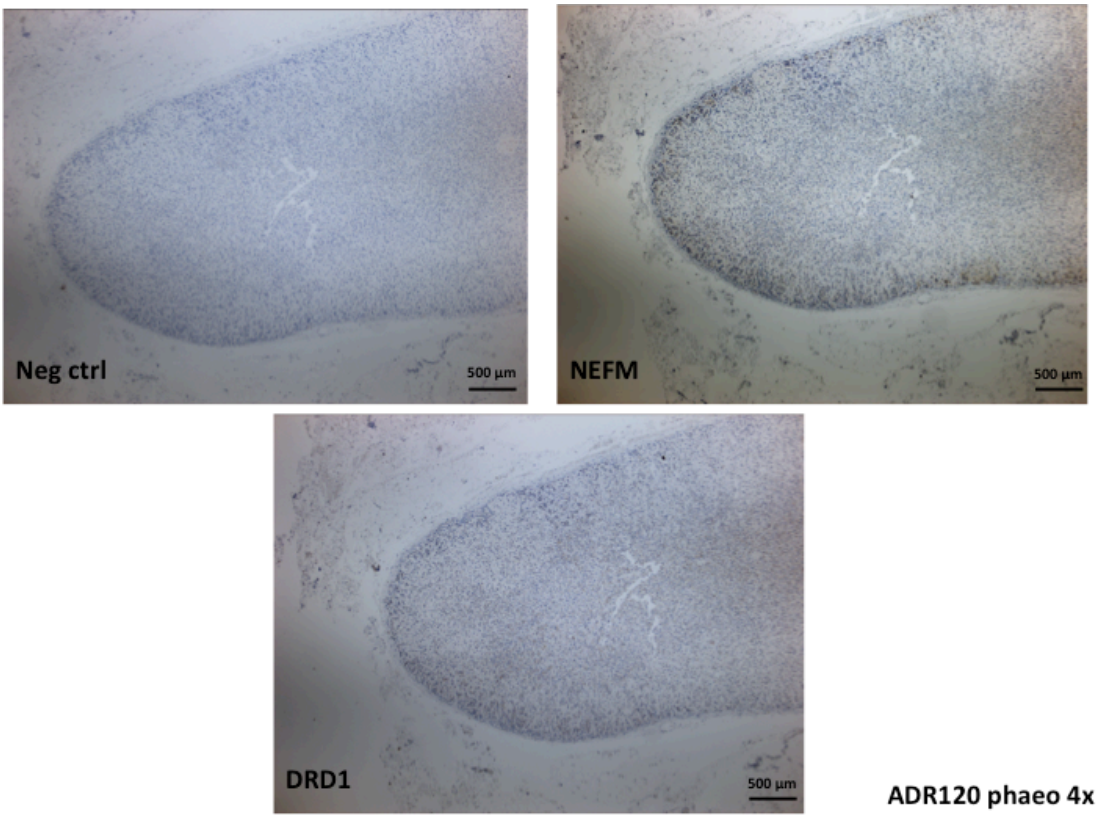

Figure 3.4: No primary antibody control of paraffin-embedded adrenal slides from adjacent adrenal gland next to a phaeocromocytoma. Tissue is incubated with the antibody diluent alone and no primary antibody, followed by incubation with secondary antibodies and detection reagents. This ensures that staining is produced from detection of the antigen by the primary antibody and not by the detection system or the specimen.

3.5.3 NEFM protein expression in AAG and APA

NEFM protein was highly and selectively expressed in the ZG of adjacent adrenal glands (AAG) next to an APA or AAG next to a Phaeocromocytoma (Figure 3.5 panel A). In the positive control sections (human cerebral cortex sections), NEFM staining was observed in the neuron bodies and axons as expected (Figure 3.3). In the adrenal ZG the staining was cytoplasmic.
Cytoplasmic staining of NEFM was found in APAs (Figure 3.5, panel B). ZG-like APAs appeared to express higher levels of NEFM protein in comparison to ZF-like APAs (see also Figure 3.7).

We also compared NEFM staining with other ZG/ZF markers including the ZG markers, CYP11B2 and KCNJ5, and the ZF marker, CYP11B1. The distribution of NEFM appeared more ZG-selective of all the ZG markers (Figure 3.6). As previously noted, CYP11B2 was patchy in the ZG.

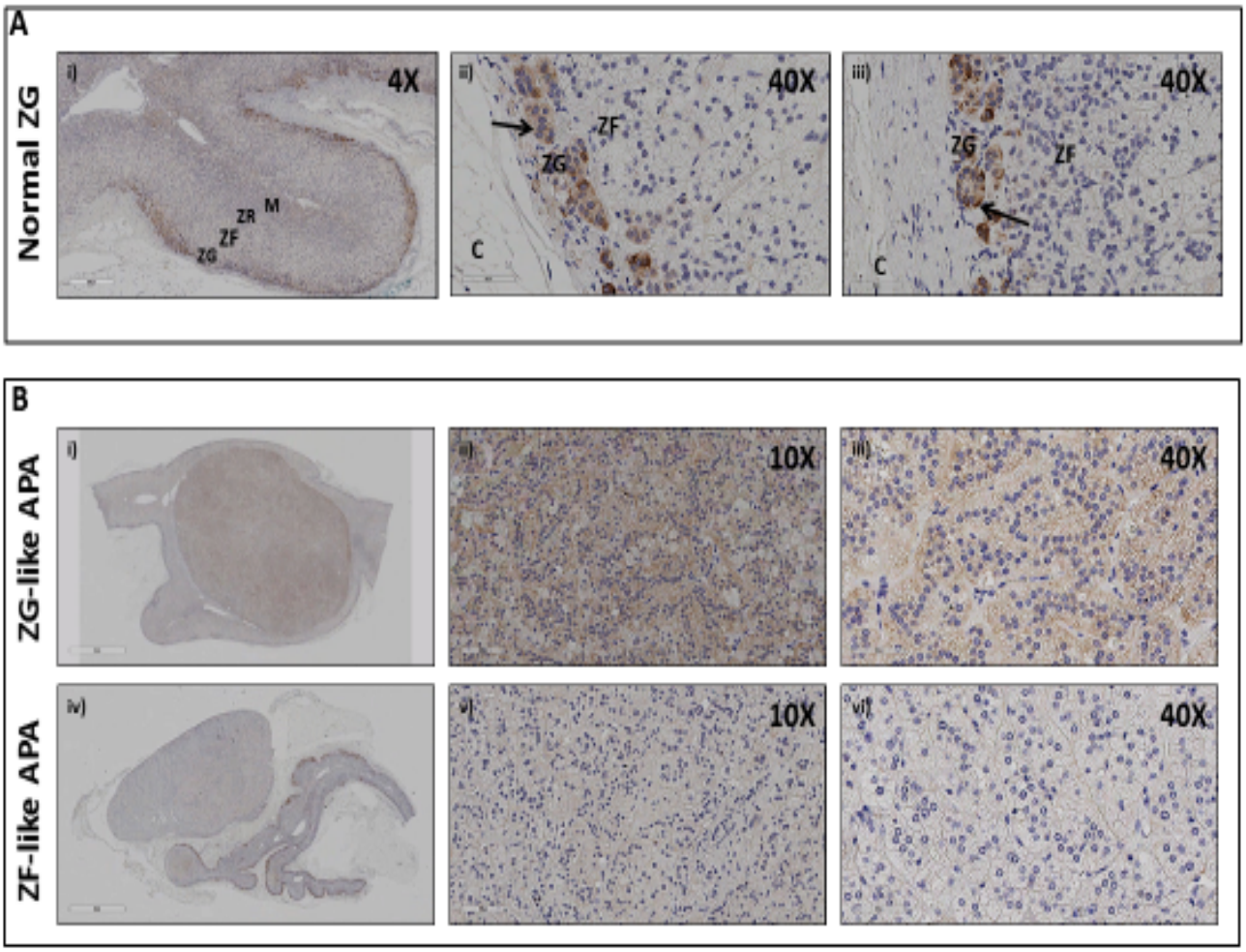

Figure 3.5: Immunohistochemistry (IHC) of NEFM in formalin-fixed paraffin embedded human adrenal sections.
A, IHC of NEFM in adjacent normal adrenal cortex. NEFM is highly expressed in zona glomerulosa (ZG) cell's cytoplasm.
B, IHC of NEFM in APAs. NEFM is more expressed in ZG-like than ZF-like APAs i) and iv) whole slide scanned images Ii), iii), v), vi) zoomed insets of left panels.

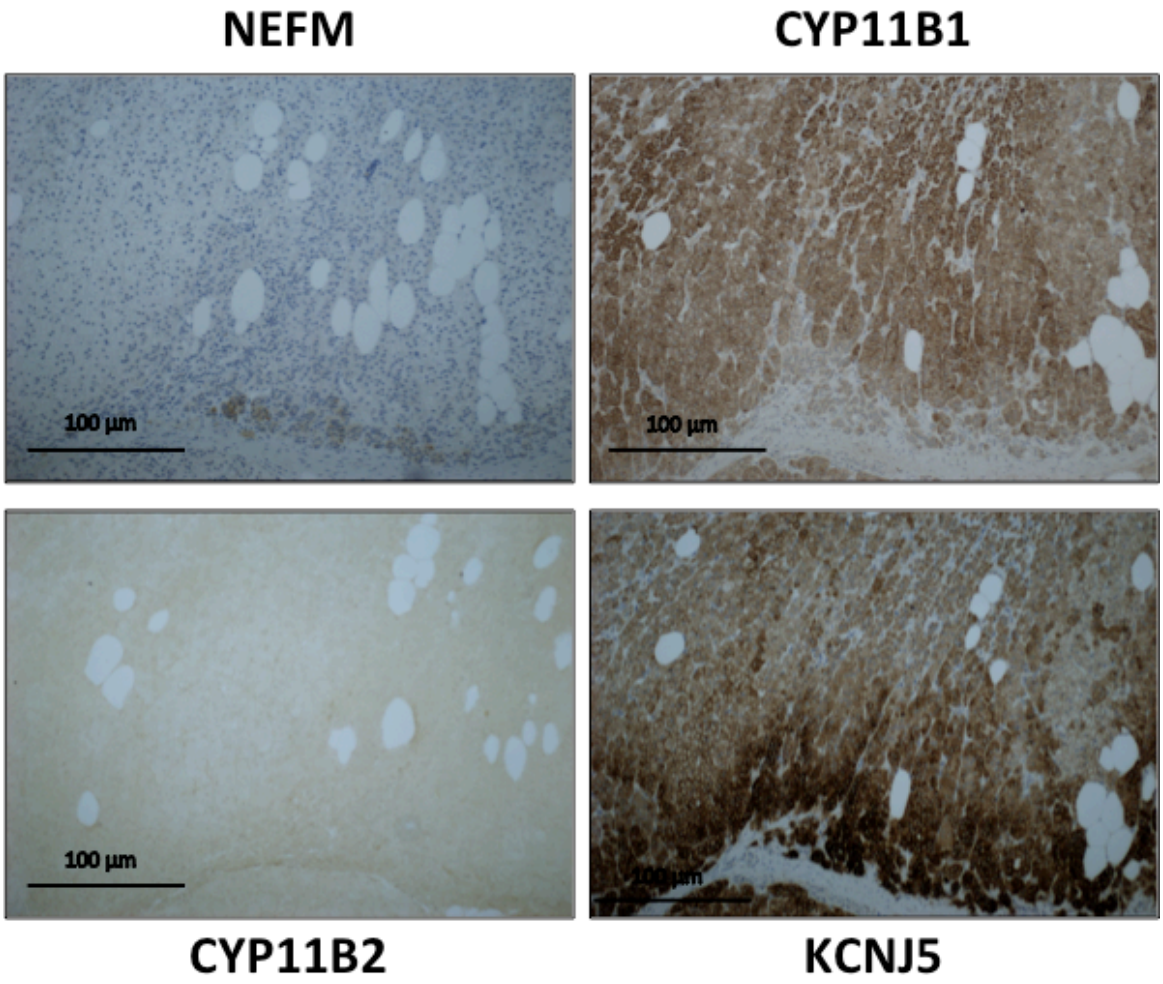

Figure 3.6: IHC of NEFM, ZF marker *CYP11B1*, and ZG markers C B, IHC of NEFM in APAs. NEFM is more expressed in ZG-like than ZF-YP11B2 and *KCNJ5*, in serial sections from adjacent normal cortex in a patient with APA.

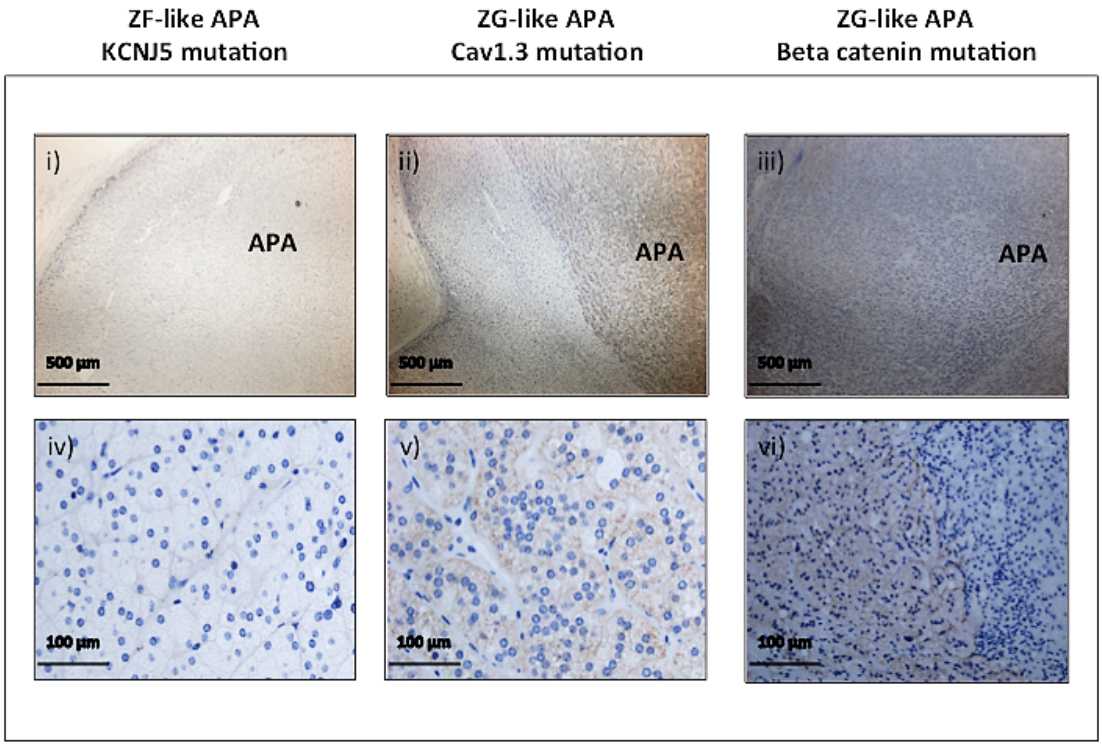

Figure 3.7: Immunohistochemistry (IHC) of NEFM in formalin-fixed paraffin-embedded APAs sections. Three different genotypes (*KCNJ5*, Cav1.3 and beta-catenin mutants) are shown, differing in terms of NEFM expression levels. ZF-like, *KCNJ5* mutant APAs have very low NEFM expression. ZG-like, Cav1.3 and beta-catenin mutant APAs express higher NEFM protein levels.

3.5.4 NEFM expression in H295R and HEK293 cells: Immunofluorescent staining.

We have evaluated NEFM expression pattern in H295R cells and compared it to HEK293 by confocal microscopy. The latter expresses several neuronal markers, including NEFM itself (a neuronal origin of this popular cell line has been in fact hypothesized). The cells were counter stained with plasma membrane marker WGA and nuclear staining DAPI. We can notice a different NEFM staining pattern in the two cell lines: in H295R cells it is not only cytoplasmic but also nuclear and not organized in filaments resembling cytoskeletal proteins (Figure 3.8), whereas in HEK293 cells NEFM protein appears to be localized in the cytoplasm only and to assemble in filaments (Figure 3.9).

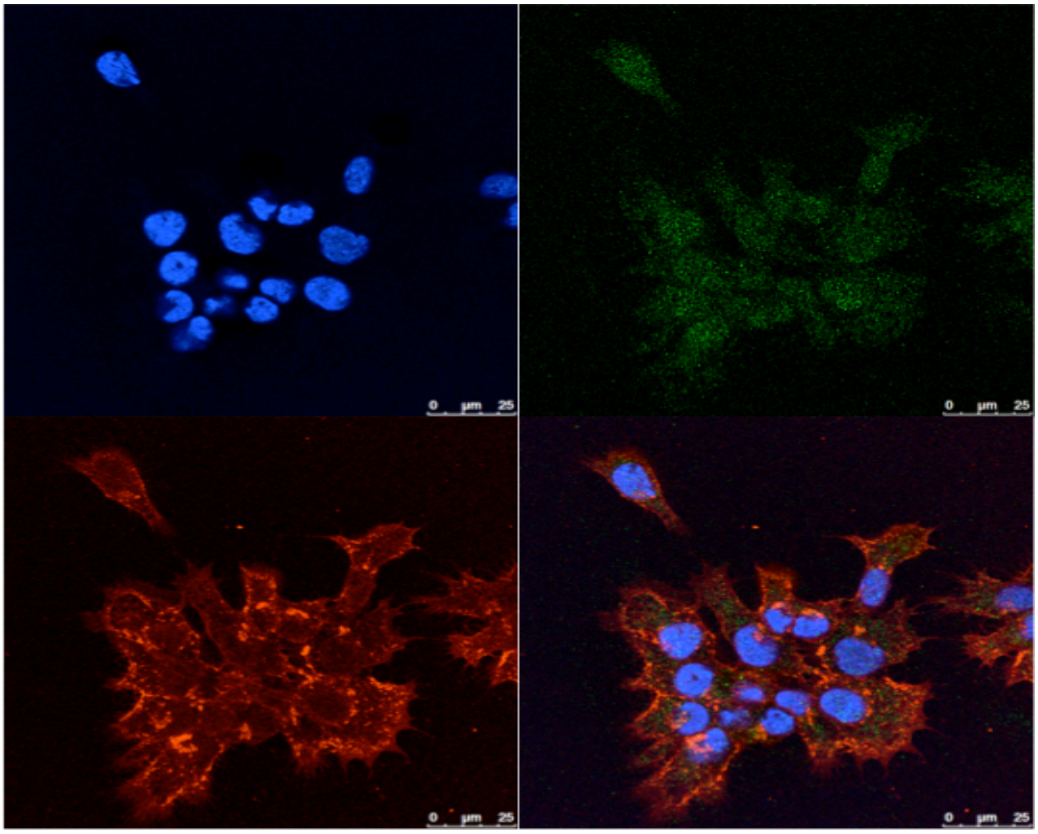

Figure 3.8. Confocal microscopic images of immunofluorescent staining showed endogenous NEFM staining (green), plasma membrane (red), nuclei (blue) and the overlay of them in the same sight field in H295R cells. NEFM staining is cytoplasmic but also nuclear and not organized in filaments resembling cytoskeletal proteins. Pictures are representative of three fields.

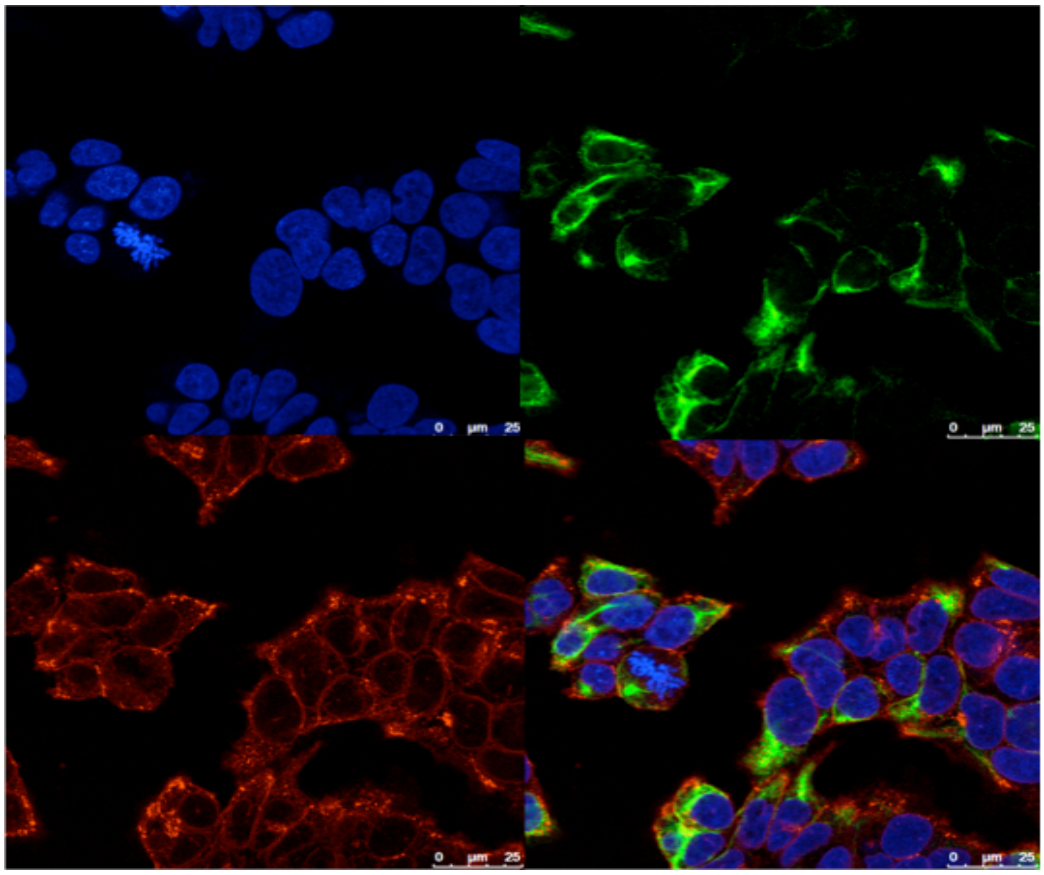

Figure 3.9: Confocal microscopic images of immunofluorescent staining showed endogenous NEFM staining (green), plasma membrane (red), nuclei (blue) and the overlay of them in the same sight field in HEK293 cells. NEFM staining is cytoplasmic and more condensed. Pictures are representative of three fields.

3.5.5 Silencing *NEFM* in H295R cells by siRNA and shRNA

H295R cells silenced by 10 nM Si-*NEFM* (ACAUCACGGUGGAGCGCAA) for 48 hours had a reduced *NEFM* expression both at mRNA and protein level in comparison to non-targeting siRNA (UGGUUUACAUGUCGACUAA).
The single oligonucleotide and the concentration were chosen after optimization and comparison to the other 3 single oligonucleotides included in the pool (Figure 3.10).

Comparing to the non-targeting control, the *NEFM* mRNA was decreased by 51% (N=6, P< 0.0001; Figure 3.11). This change resulted in a significant 38% increase in aldosterone (N=12, from 102 to 140 pM/ug protein, P<0.05, Figure 3.14)
The mRNA level of aldosterone synthase, *CYP11B2*, was decreased by 57% (N=6, P<0.01, Figure 3.12), and the *CYP11B2* transcription factor *NR4A2* mRNA levels were consistently decreased by 64% (N=6, P<0.05; Figure 3.13).

Analogous results were achieved by shRNA plasmid transfection. GFP-tagged shRNA was used to identify the transfected cells at the microscope and analyse fluorescent staining for D1R and other proteins.
At 48 hours from transfection, shRNA caused a decrease of *NEFM* mRNA levels by 59% (N=3, P<0.05, Figure 3.15 panel A). Consistently with siRNA results, it caused a reduction of *CYP11B2* mRNA levels by 55% (N=3, P<0.05, Figure 3.15, panel B) and an increase of basal aldosterone levels by 23% (N=4, P<0.05, Figure 3.15, panel C).

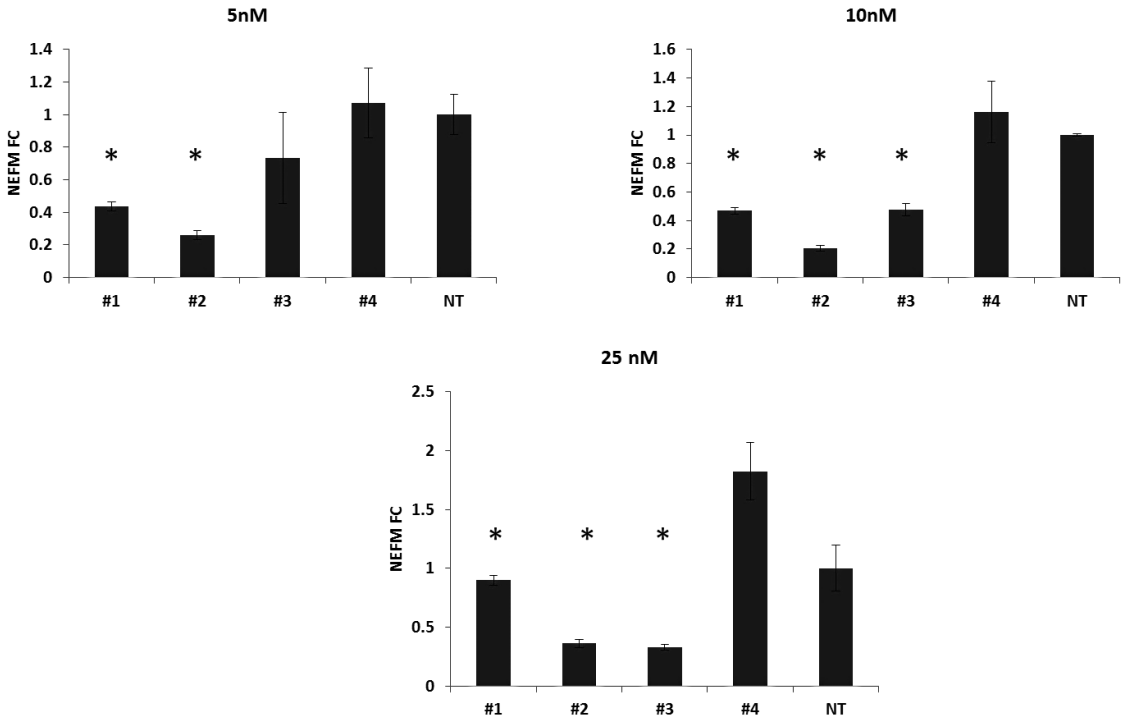

Figure 3.10: Effect of single RNA oligonucleotides (numbered from #1 to #4) targeting *NEFM* on *NEFM* mRNA expression in H295R cells at 48 hours. Different concentrations (from 5 to 25 nM) had been tested. We have chosen oligonucleotide #2-sequence reported in the paragraph- at 10 nM as it gave the best mRNA knock-down. NT: non targeting. Results are expressed as geometric mean values with SEM and compared using multiple Student t test vs NT. The significance level of P<0.05 (*) was considered to indicate statistical significance.

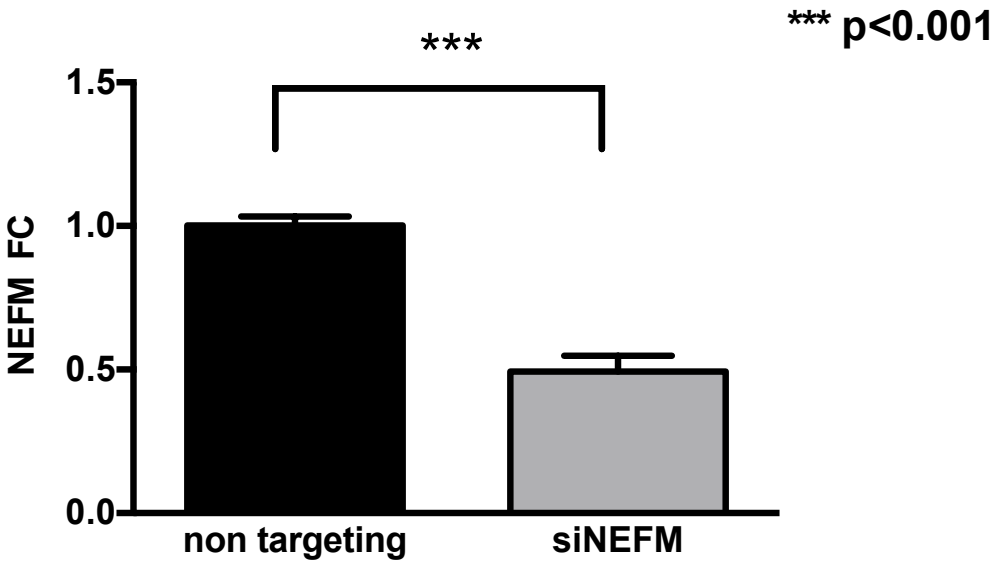

Figure 3.11: Effect of Si-*NEFM* on *NEFM* mRNA expression in H295R cells. 10 nM of Si-*NEFM* transfection decreased the *NEFM* expression by 51%, comparing to 10 nM of non-targeting transfection (P<0.001). Results are expressed as geometric mean values with SEM and compared using the 2-sided Student t test. The significance level of P<0.05 was considered to indicate statistical significance.

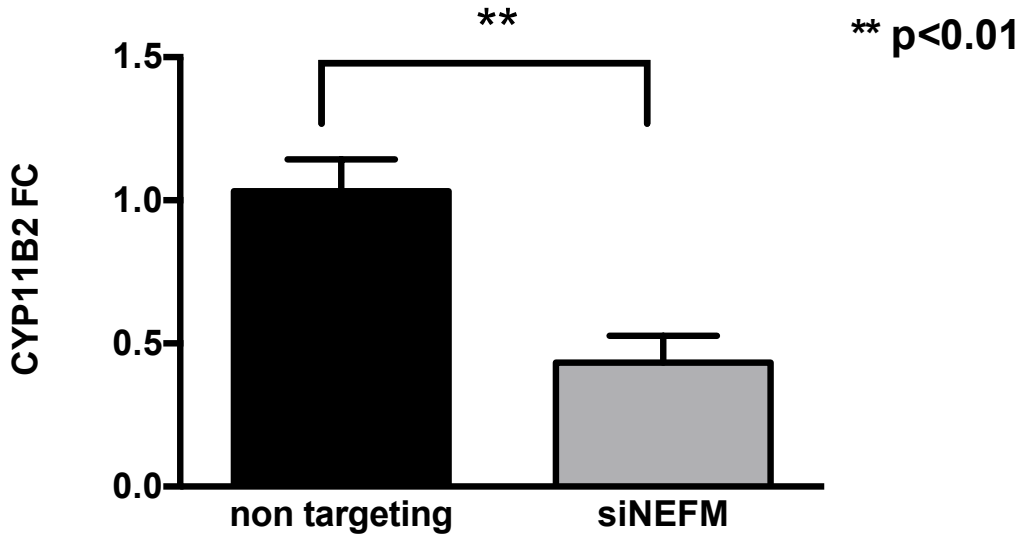

Figure 3.12: Effect of Si-*NEFM* on *CYP11B2* mRNA expression in H295R cells. 10 nM of Si-*NEFM* transfection decreased the *NEFM* expression by 51% comparing to 10 nM of non-targeting transfection (P<0.01). Results are expressed as geometric mean values with SEM and compared using the 2-sided Student t test. The significance level of P<0.05 was considered to indicate statistical significance.

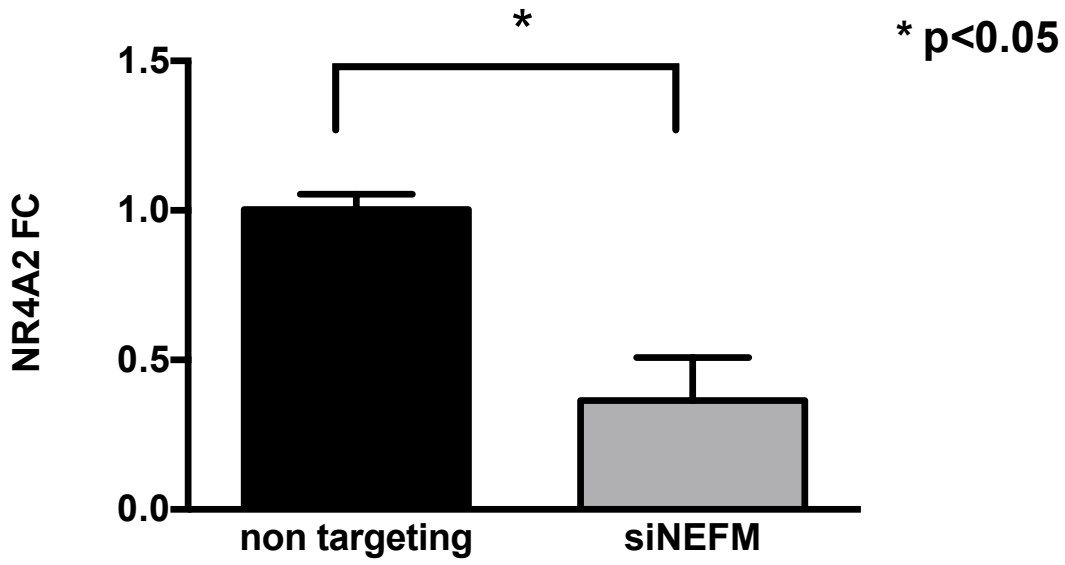

Figure 3.13: Effect of Si-*NEFM* on *NR4A2* mRNA expression in H295R cells. 10 nM of Si-*NEFM* transfection decreased the *NEFM* expression by 51%, comparing to 10 nM of non-targeting transfection (P<0.05). Results are expressed as geometric mean values with SEM and compared using the 2-sided Student t test. The significance level of P<0.05 was considered to indicate statistical significance.

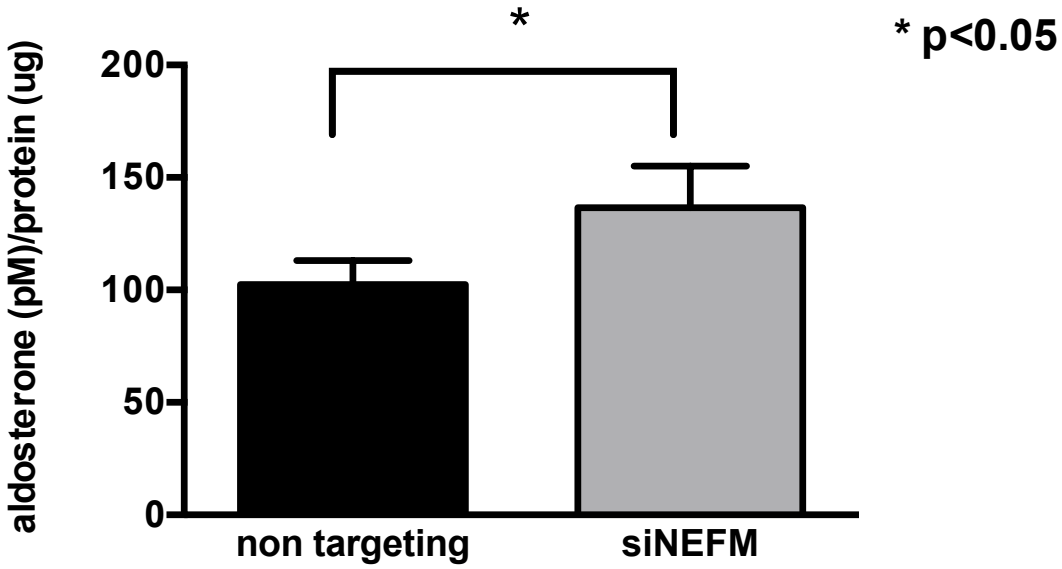

Figure 3.14: Effect of Si-*NEFM* on aldosterone production in H295R cells. 10 nM of Si-*NEFM* transfection increased the aldosterone production by 38% in comparison to 10 nM of non-targeting (P<0.05). Aldosterone production was normalized by total protein from the same wells. Results are expressed as geometric mean values with SEM and compared using the 2-sided Student t test. The significance level of P<0.05 was considered to indicate statistical significance.

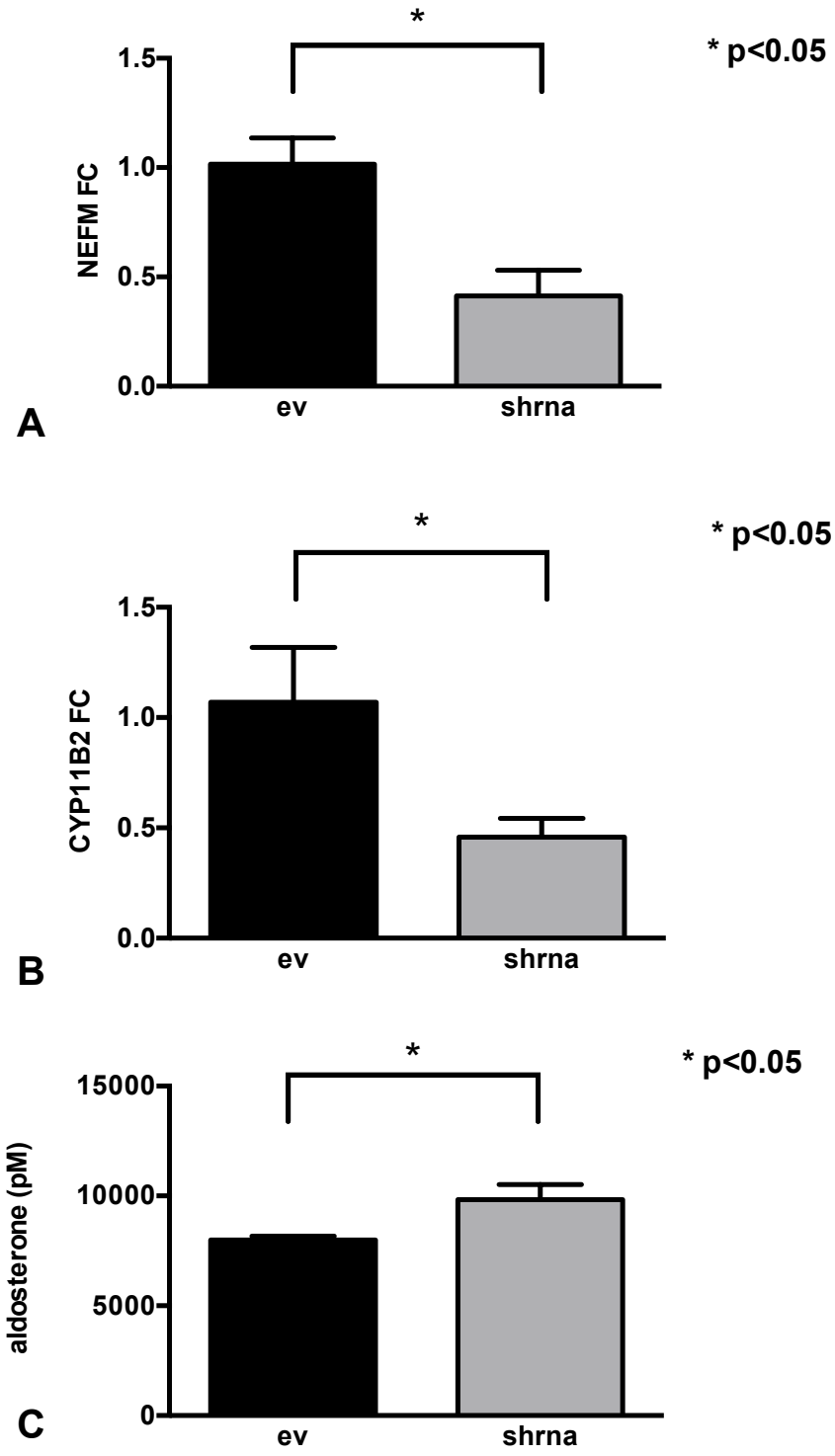

Figure 3.15: effect of *NEFM*-shRNA on *NEFM*, *CYP11B2* mRNA and aldosterone levels (panels A, B and C, respectively) in H295R at 48 hours from transfection. Results are expressed as geometric mean values with SEM and compared using the 2-sided Student t test. The significance level of P<0.05 was considered to indicate statistical significance.

3.5.6 *NEFM* affects adrenal cells proliferation.

The top hit genes up-regulated in ZG vs ZF studied so far (*LGR5, VSNL1, DACH1)* have been shown to regulate apoptosis and cell proliferation. Moreover, as mentioned before, *NEFM* and other NF subunits are silenced in cancer and play a role in cell proliferation. Therefore, we have investigated the effects of knocking down *NEFM* in H295R cells on cell confluence and proliferation with two different techniques.

After plating 10^5 cells per well in a 24 well plate, the antibiotic-free growth media has been replaced by media with 10nM of Si-RNA (or non-targeting in controls) and the plate immediately placed in in vitro live-cell imaging system (Incucyte). The measurement of the occupied area (% confluence) of cell images over time monitors cell proliferation. As cells proliferate, the confluence increases.
Kinetic live-cell imaging of si-*NEFM* transfected cells directly quantified a 15 ± 1.3% increase in the proliferation of H295R cells (N=4, P< 0.0001, Figure 3.16).

Consistently, an increase in cell proliferation and clonigenic ability of H295R after silencing *NEFM* was confirmed by using a different silencing technique and by a different assay, the colony-forming assay.
At 3 weeks from transfection of shRNA, the number of colonies was significantly higher in H295R cells transfected with shRNA in comparison to empty vector (ev) (N=3, 162 vs 93 colonies, P<0.05, Figure 3.17).

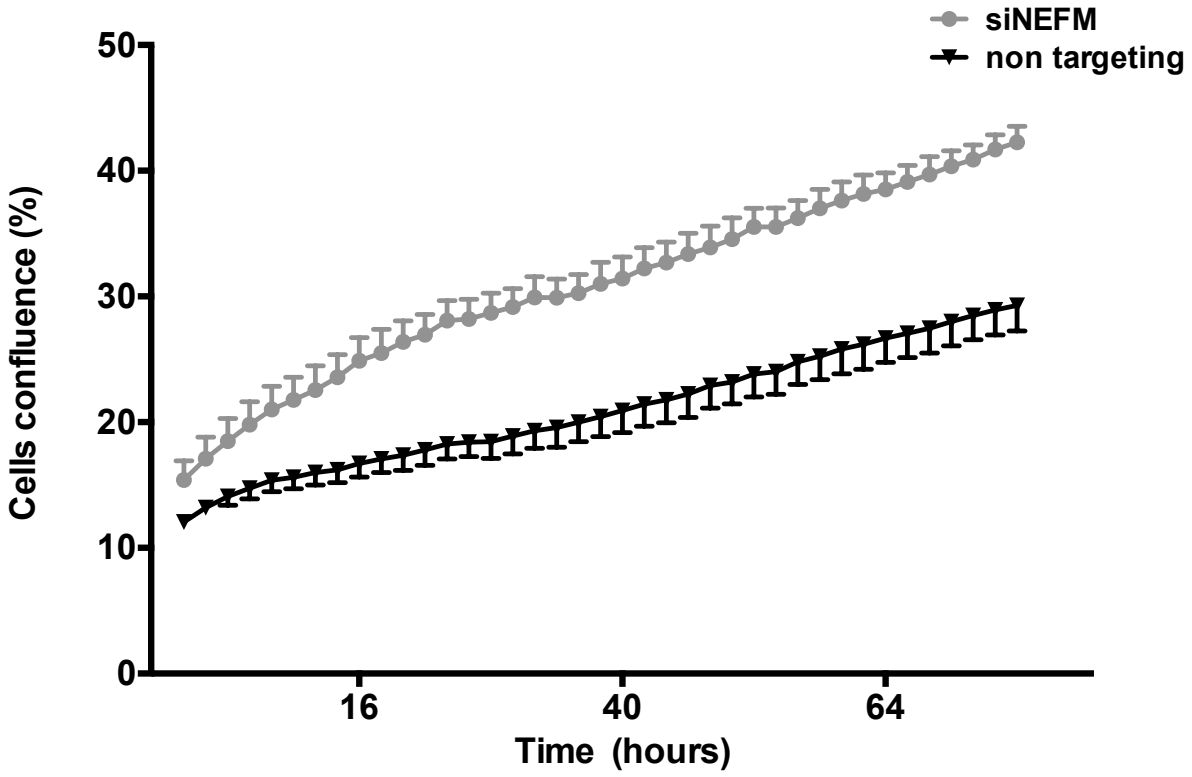

Figure 3.16: Effect of silencing *NEFM* on cell proliferation evaluated at Incucyte. Calculation of cell confluence was performed every 2 hours and for 72 hours. Kinetic live-cell imaging of Si-*NEFM* transfected cells directly quantified a 15 ± 1.3% increase in the proliferation of H295R cells (P< 0.0001). Results are expressed as mean values with SEM and compared using the 2-sided Student t test. The significance level of P<0.05 was considered to indicate statistical significance.

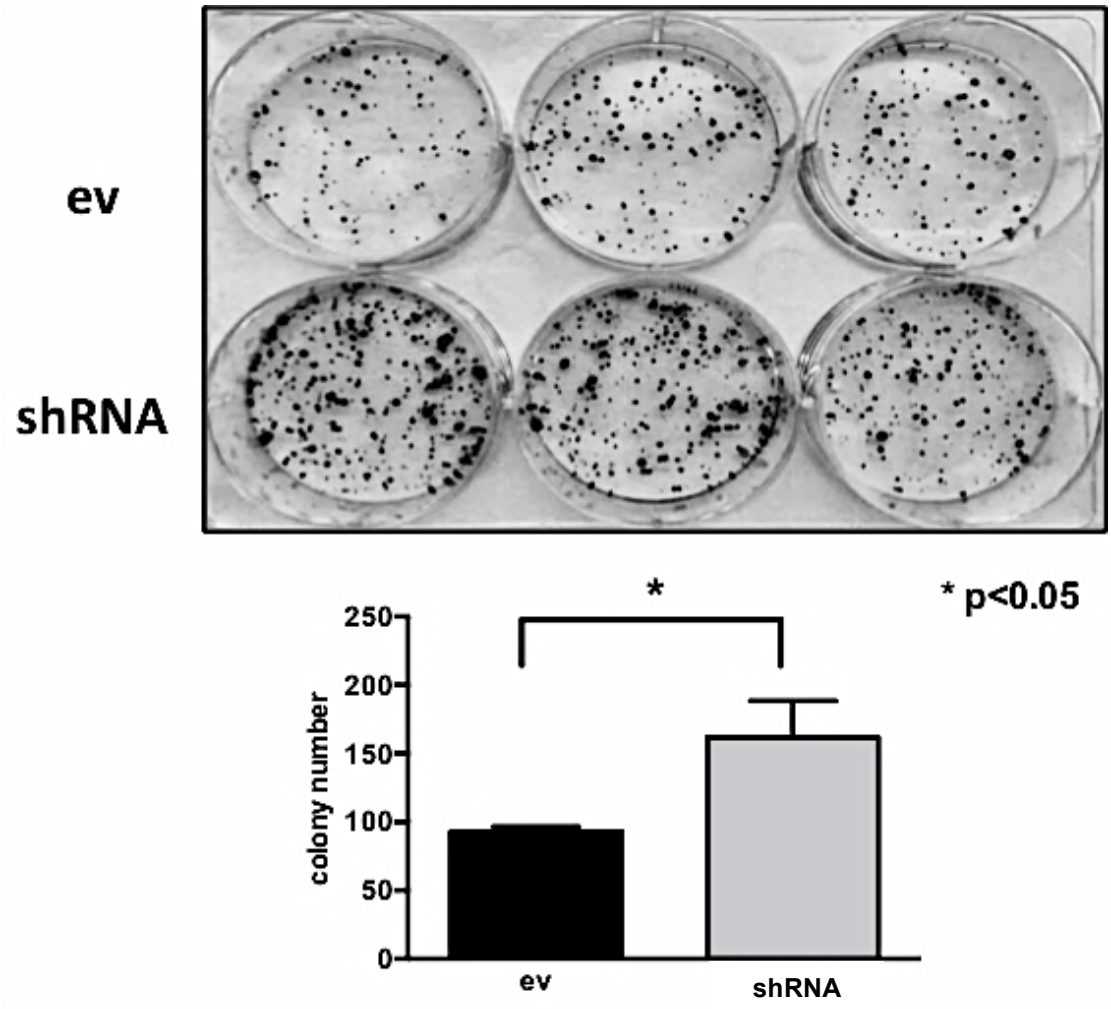

Figure 3.17: Effect of silencing *NEFM* by shRNA At 3 weeks from transfection of shRNA, the number of colonies was significantly higher in H295R cells transfected with shRNA in comparison to empty vector (ev) (162 vs 93 colonies, data expressed as mean ± SEM).

3.5.7 Silencing *NEFM* affects mitochondrial membrane potential

In neurons NF interacts with mitochondria and regulate both localisation and membrane potential. Positioning of mitochondria is important in axons where high amount of ATP is required but these organelles also buffer Ca^{2+} to regulate neurotransmission. NF binding to mitochondria affects their metabolic activity by reducing their mobility.

Mitochondrial membrane potential changes can affect cell proliferation since this is the main driver for cytoplasmic Ca^{2+} to entry into the mitochondria and stimulate cell proliferation (Nunez et al., 2006). Therefore we have hypothesized that silencing *NEFM* stimulates proliferation by affecting mitochondrial membrane potential and performed a staining with MitoTracker Orange CMTMRos in adrenocarcinoma cell line H295R, whose signal intensity is directly proportional to the mitochondrial membrane potential.

At 48 hours from shRNA transfection, the MitoTracker Orange CMTMRos staining was more intense in GFP-positive, shRNA transfected cells, in comparison to not transfected cells in the same field, thus indicating an increased mitochondrial membrane potential (which could increase Ca^{2+} intake) and mitochondrial metabolic activity (Figure 3.18).

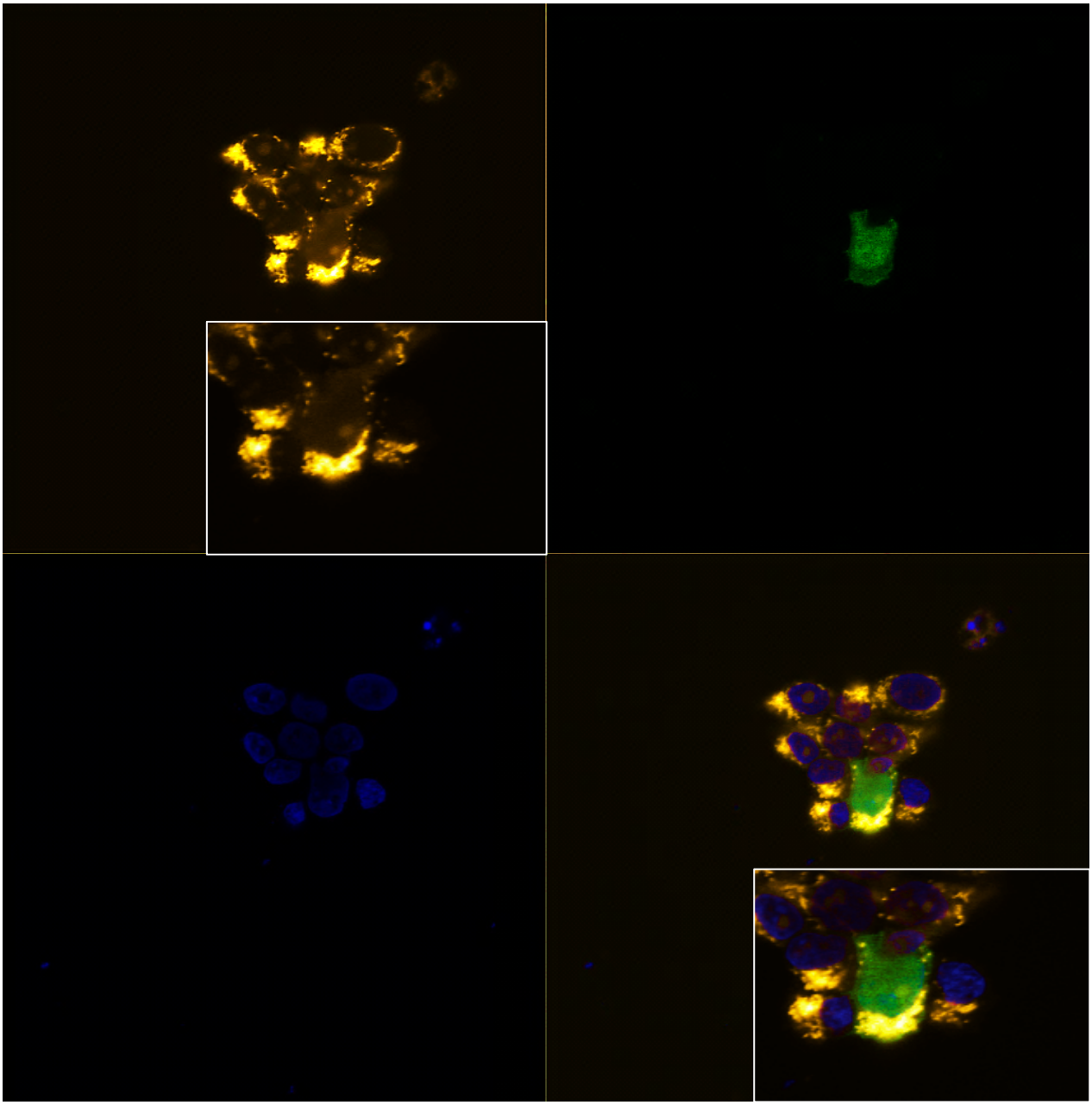

Figure 3.18: Mitochondrial staining with MitoTracker Orange CMTMRos in H295R cells transfected with GFP-tagged shRNA. The MitoTracker Orange CMTMRos staining appears to be more intense in the GFP-positive transfected cell (zoomed in the small square), suggesting that in absence of *NEFM* the mitochondria are more depolarized and likely to uptake Ca^{2+} and stimulate proliferation.

3.5.8 NEFM expression levels correlates with D1R subcellular localisation in the two APA subtypes

NEFM interacts with D1R in the neuronal synapses, where it mediates its internalization in response to the agonist. NEFM knockout mice have amplified D1R-mediated motor responses to cocaine. These evidences suggest that the expression levels of *NEFM* could affect D1R subcellular localization; plasma membrane trafficking and consequently any D1R mediated biological response.
Our microarray analysis showed that *NEFM* expression levels differ between the two APA subtypes, and it resulted to be higher in *KCNJ5* wild-type, ZG-like than in *KCNJ5* mutant, ZF-like APAs.
We have therefore hypothesized that the two subtypes would differ also in terms of D1R expression pattern and aldosterone response to D1R activation due to agonist (fenoldopam) binding.

To answer the first question, we have compared the D1R staining pattern at IHC in formalin-fixed, paraffin-embedded sections of the two APAs subtypes.

We have found that D1R protein expression in ZG-like, *KCNJ5* wild-type APAs, which express high *NEFM* levels, is mainly cytoplasmic, whereas in ZF-like, *KCNJ5* mutant APAs D1R protein is mainly localised on plasma membrane, thus suggesting that more D1R is available on cell surface (Figure 3.19).

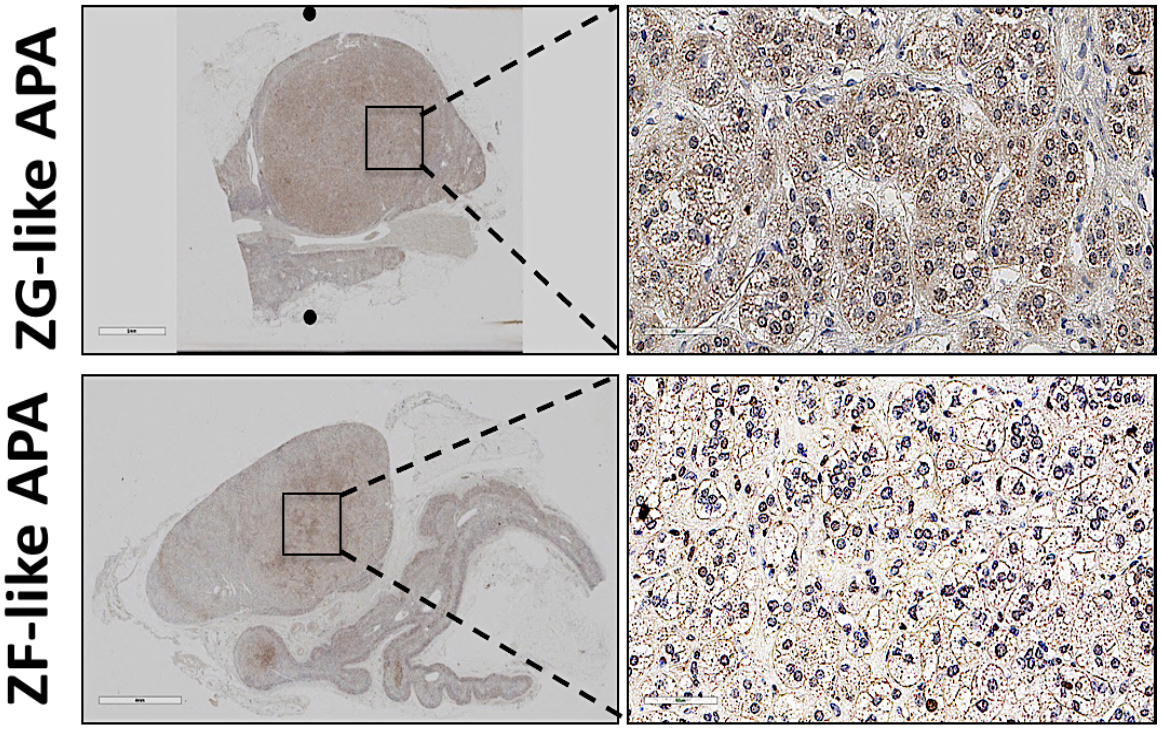

Figure 3.19: : IHC for D1R of paraffin-embedded human adrenal sections including ZG-like (i), ii) ,iii)), and ZF-like APAs (iv) ,v) ,vi)) in ZG-like APA D1R is mainly localized in the cytoplasm. In ZF-like APAs D1R is mainly localized on the plasma membrane. i),iiii) scanned images. Ii), iv), zoomed insets of left panels.

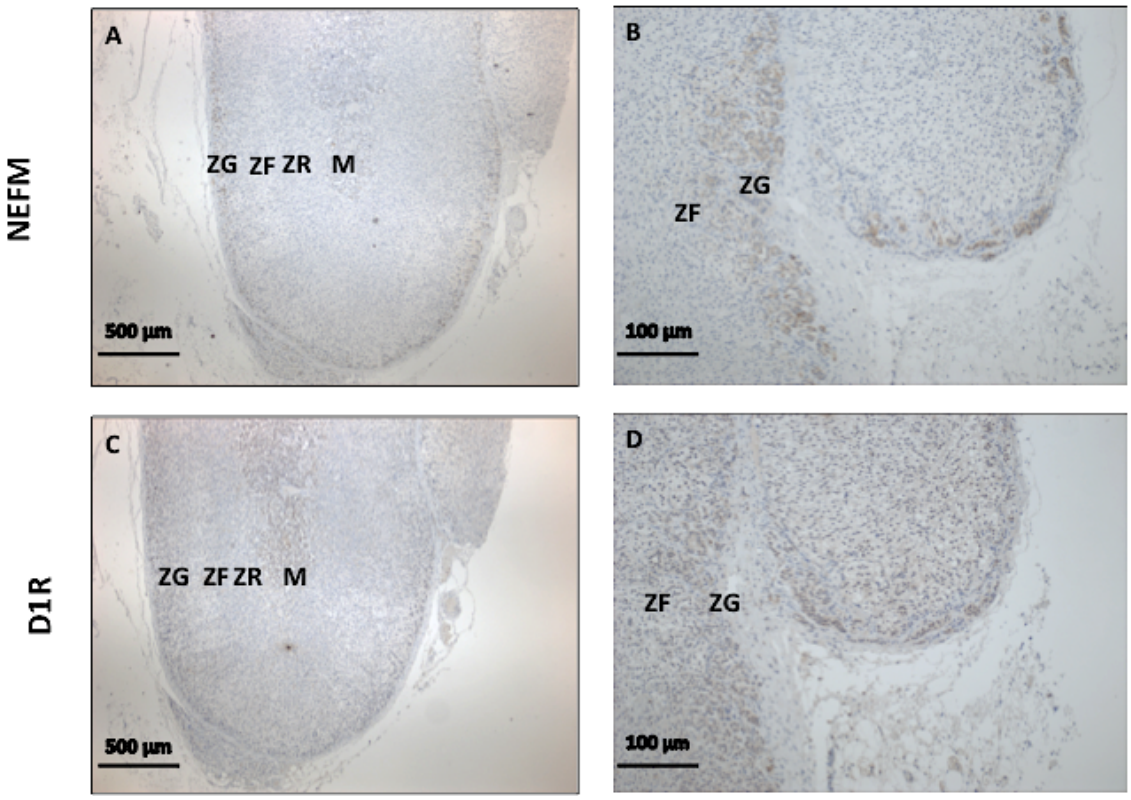

Figure 3.20: NEFM (Panels A and B) and D1R (Panels C and D) staining in the normal adrenal cortex. NEFM staining appears to be ZG-selective and cytoplasmic. D1R appears to be expressed in the adrenal medulla and in the adrenal cortex although it seems to be more cytoplasmic in ZG and membranous in ZF.

3.5.9 Aldosterone response to D1R agonist fenoldopam varies in primary cells from two APA subtypes with different *NEFM* expression

Because of the different *NEFM* expression levels and D1R subcellular localisation in the two APA subtypes, we have measured aldosterone in response to D1R agonist fenoldopam in primary cell cultures derived from four ZF-like, *KCNJ5* mutant and four ZG-like, *KCNJ5* wild-type APAs.

After 4-6 days in culture in a 75-cm^2 flasks, the cells were seeded in 24 well plates. The day after seeding, cells were starved in nil media for six hours, and then treated with fenoldopam (at only two different doses because of the scarcity of cells). After 24 hours, the media was collected and cell harvested in RIPA buffer. Aldosterone was measured by HTRF assay and normalized per protein concentration measured by BCA, as explained in the first chapter.

Primary cells from both adrenal subtypes responded to fenoldopam, but the stimulation by fenoldopam at maximal dose (10^{-7} M) was bigger in those from *KCNJ5*-mutant, ZF-like APAs (from 1±0.07 at 0 M to 1.24±0.106 at 10^{-8} M and 1.38±0.103 at 10^{-7} M in ZG-like APA cells vs 1±0.15 at 0 M to 1.49±0.23 and 2.28 ± 0.35 at 10^{-8} and 10^{-7} M, respectively, in ZF-like APA cells, $P<0.05$ at 10^{-7} M). M stands for mol/L.

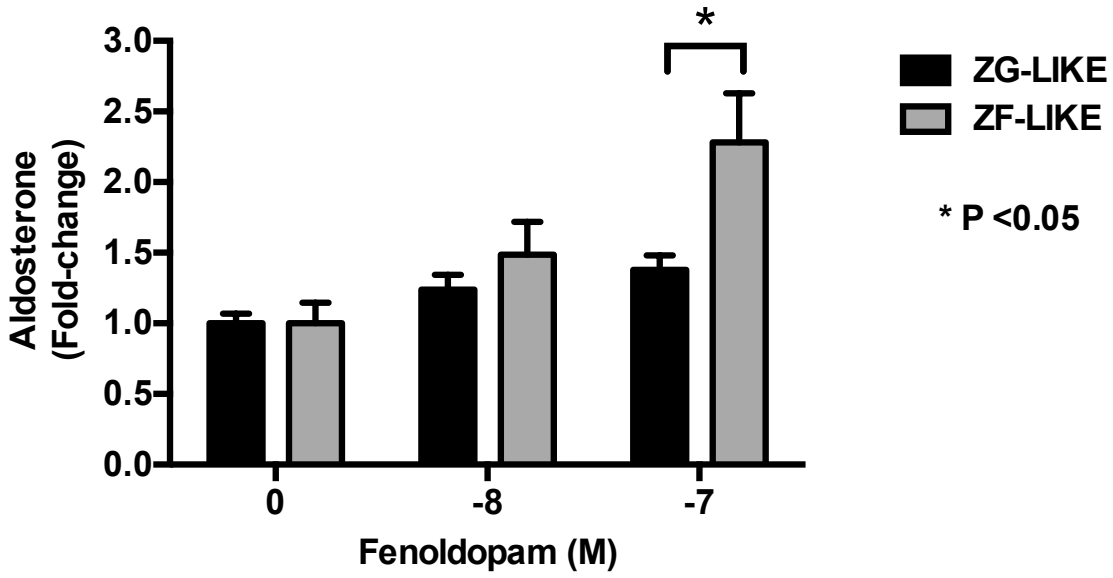

Figure 3.21: Aldosterone secretion in primary adrenal cells from ZG-like and ZF-like APAs (n = 4 each) in response to fenoldopam.
Each concentration was replicated 4 times within each individual patient samples. Aldosterone results shown here are relative to 0 M of treatment. Two-way ANOVA was used to calculate overall significance. The stimulation by fenoldopam at maximal dose (10^{-7} M) was bigger in *KCNJ5* mutant, ZF-like APAs (P<0.05 at 10^{-7} M). M stands for mol/L.

3.5.10. Silencing *NEFM* attenuates dopamine inhibition on aldosterone response

To further evaluate the effect of *NEFM* expression levels on D1R response, we performed drug experiments in the adrenocarcinoma cell line H295R after si-*NEFM* transfection. We investigated aldosterone secretion in response to dopamine, which is known to have a D2R effect and inhibit aldosterone, but also treated cells with D1R agonist and antagonist and D2R antagonist metoclopramide.

In brief, H295R cells transfected with 10 nM si-*NEFM* and non-targeting were starved for six hours at 42 hours from transfection, then treated with increasing doses of dopamine in presence of AngII at 10^{-8} M, and antioxidant vitamin C 0.1% for 24 hours. Aldosterone has been normalized per protein concentration and all values are normalized to the aldosterone/protein concentration at 0 M.

In non-targeting siRNA transfected cells, 10^{-8} M, 10^{-7} M and 10^{-6} M dopamine caused a reduction of aldosterone secretion by 23±4, 34±10 and 24±6%, respectively ($p < 0.05$ at 10^{-7} M). Silencing *NEFM* attenuated the expected dopamine inhibition of aldosterone secretion. Dopamine did not inhibit but slightly stimulated aldosterone production by 13±8, 26±15 and 16±10% at 10^{-8} M, 10^{-7} M, and 10^{-6} M, respectively. The differences between si-*NEFM* and non-targeting at each dose were significant at two-way ANOVA comparison (10^{-8} M $P<0.05$, 10^{-7} M, $P< 0.001$, 10^{-6} M $P<0.05$, Figure 3.22).

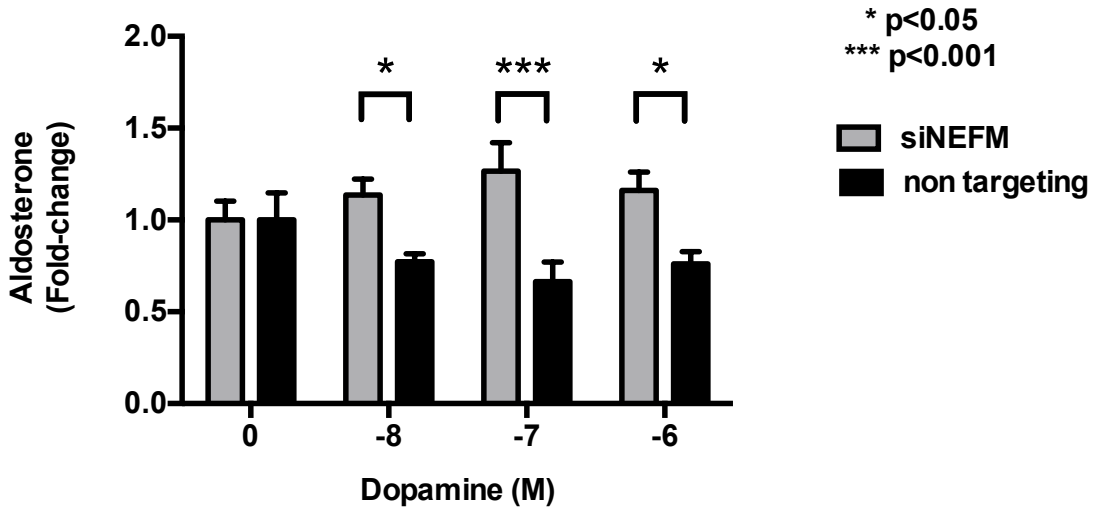

Figure 3.22: Silencing *NEFM* attenuates dopamine inhibition on aldosterone response. Dopamine inhibits aldosterone in non-targeting control cells (by 40%), and this effect is attenuated in si-*NEFM* transfected cells in which dopamine slightly stimulates aldosterone production by 13±8, 26±15 and 16±10% at 10^{-8}M, 10^{-7}M, and 10^{-6} M, respectively. The differences between si-*NEFM* and non-targeting at each dose were significant with two-way ANOVA comparison (10^{-8}M P<0.05, 10^{-7} M, P< 0.001, 10^{-6} M P<0.05). Data shown are mean ± SEM and normalized to 0 M. M stands for mol/L.

3.5.11 *NEFM* inhibits aldosterone response to D1R activation.

Since *NEFM* knocking-down prevented aldosterone inhibition by dopamine, we have investigated whether this effect was mediated by D1R or D2R.
We have examined aldosterone response to 24 hours treatment with D1R selective agonist fenoldopam or antagonist SCH23390 in si-*NEFM* transfected cells and controls. The drugs had been diluted at increasing concentrations in nil media containing AngII at 10^{-8}M, Dopamine at 10^{-7}M, antioxidant vitamin C 0.1%.

Fenoldopam increased aldosterone secretion by 23 ±13 and 17.3±12 in non-targeting (ns). Silencing *NEFM* amplified the stimulatory effect of fenoldopam on aldosterone secretion by 34± 10, 51±20 and 75±28 % at 10^{-8}M, 10^{-7}M and 10^{-6}M respectively ($p < 0.05$ at 10^{-6}M, Figure 3.23).

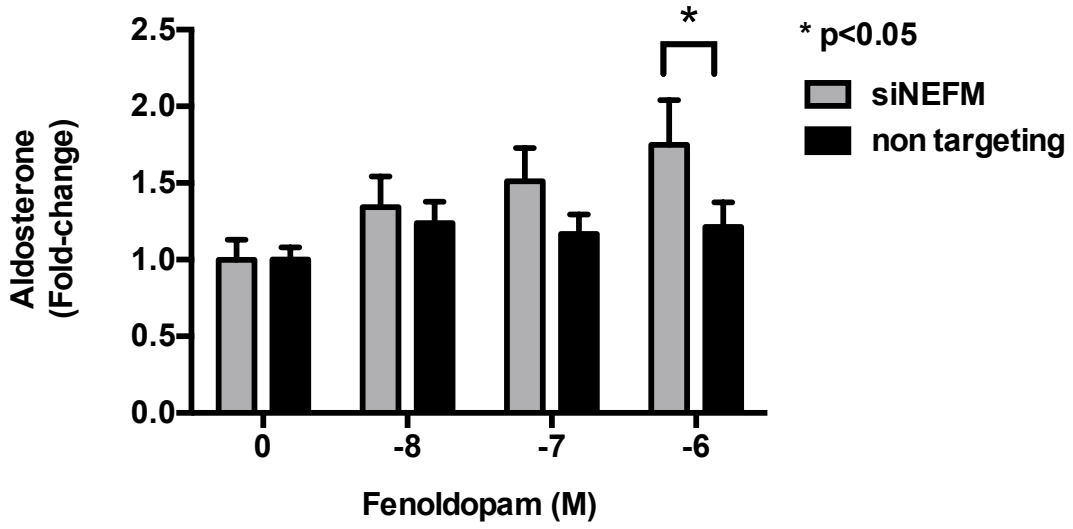

Figure 3.23: Silencing *NEFM* amplifies fenoldopam stimulation on aldosterone. Fenoldopam increases aldosterone by max 24% in controls cells, but this effect is amplified in si-*NEFM* transfected cells.
The differences between si-*NEFM* and non-targeting were significant with two-way ANOVA comparison (10^{-7} M and 10^{-6} M $P<0.05$). Data shown are mean ± SEM and normalized to 0 M. M stands for mol/L.

Treatment with D1R antagonist SCH23990 caused a slight, not significant decrease of aldosterone by 13±7, 9±5 and 9±4 % at 10^{-8}M, 10^{-7}M and 10^{-6} M, respectively, in controls. Silencing *NEFM* amplifies aldosterone inhibition by SCH23990 (by 36±4, 37±6 and 41±4 at 10^{-8}M, 10^{-7}M and 10^{-6} M, respectively ($P<0.05$ at 10^{-7}M and 10^{-6} M, Figure 3.24).

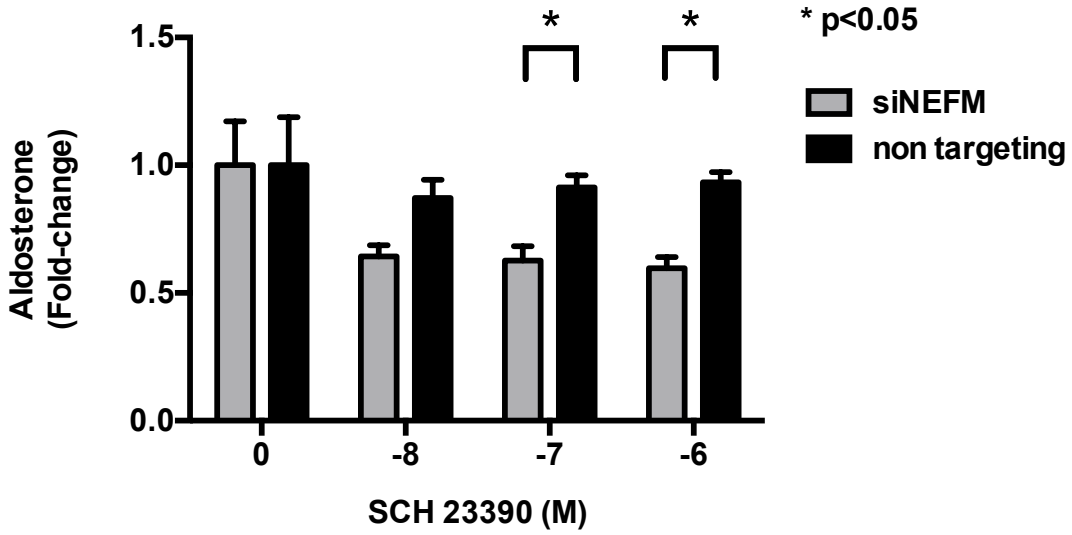

Figure 3.24: Silencing *NEFM* amplifies D1R antagonist SCH23390 inhibition on aldosterone secretion. SCH23390 slightly inhibits aldosterone in non-targeting control cells, but this effect is amplified in si-*NEFM* transfected cells in which the antagonist significantly decreases aldosterone production by 36±4, 37±6 and 41±4 at 10^{-8}M, 10^{-7}M and 10^{-6} M, respectively ($P<0.05$ at 10^{-7}M and 10^{-6} M). M stands for mol/L.

We have also questioned if *NEFM* silencing would affect aldosterone stimulation by D2R antagonist. Hence, we have treated the cells with increasing doses of metoclopramide, at the same time points of the previously described experiments. Metoclopramide stimulated aldosterone secretion but with no significant difference between si-*NEFM* and non-targeting (Figure 3.25).

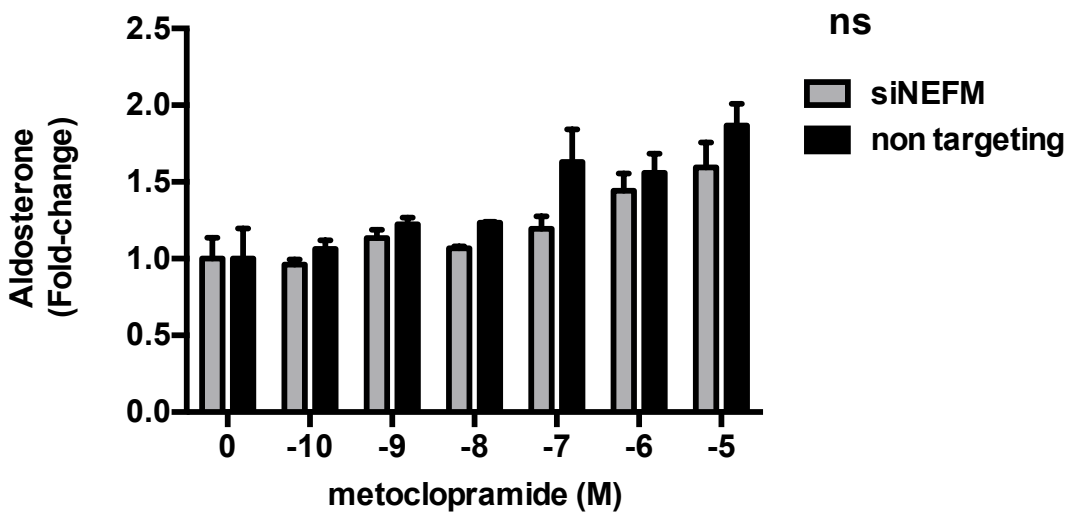

Figure 3.25: Aldosterone response to D2R antagonist metoclopramide is not affected by silencing *NEFM*. A non-significant difference has been found between si-*NEFM* and non-targeting. Two-way ANOVA was used to calculate overall significance. Ns=non-significant. M stands for mol/L.

3.5.12 D1R/NEFM protein interaction

NEFM and D1R interact in mammalian cells. This has been demonstrated in mice synaptosomal fraction (by co-immunoprecipitation) and previously by yeast two-hybrid system (Yuan et al. 2015; Kim et al. 2002).

To confirm the physical interaction between endogenous NEFM and D1R in H295R cells, co-immunoprecipitation assay was performed. Monoclonal mouse anti-D1R (or PBS as negative control) was first used to precipitate the protein complexes containing D1R, and the presence of NEFM protein in these complexes was subsequently examined by immunoblotting with a polyclonal rabbit anti-NEFM antibody. The presence of NEFM protein was markedly detected in the cellular lysates with IP by anti-D1R antibody, not by control, indicating a specific interaction of NEFM with D1 (Figure 3.26).

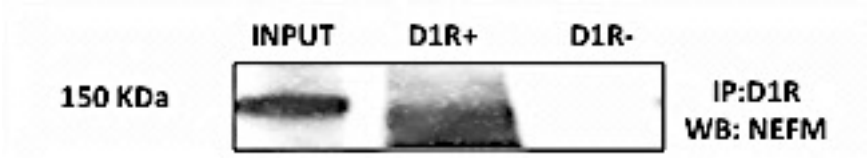

Figure 3.26: Co-immunoprecipitation of D1R pulls down NEFM, confirming the interaction between NEFM and D1R in H295R.
Monoclonal mouse anti-D1R (or PBS as negative control) was used to precipitate the protein complexes containing D1R, and the presence of NEFM protein in these complexes was subsequently examined by immunoblotting with a polyclonal rabbit anti-NEFM antibody.

3.5.13 Effects of fenoldopam on *NEFM* expression

Since NEFM interacts with D1R and regulates its trafficking and plays a role in the agonist-induced desensitization of D1R, we evaluated the changes in *NEFM* expression at both mRNA and protein level in H295R cells after 24 hours treatment with D1R agonist fenoldopam.

Fenoldopam caused a significant 2.28 and 2.9 fold increase of *NEFM* mRNA levels at 10^{-7} and 10^{-6} M, respectively ($P<0.05$ at 10^{-7}M and $P<0.001$ at 10^{-6}M, Panel A, Figure 3.27). We have observed the same increase at protein level (Panel B, Figure 3.27).

Of note, the forskolin hydrophilic equivalent NKH477, which is an activator of adenyl cyclase therefore causing an increase in cAMP (the second messenger of D1R activation signaling) affected in the opposite direction the *NEFM* mRNA levels (Figure 3.29), suggesting that the mechanisms of *NEFM* up-regulation following D1R activation are cAMP independent.

When treated for 24 hours with NKH477 at three different concentrations, H295R increased aldosterone secretion as expected (by 1.8 and 2.4 fold change at 10^{-6} and 10^{-5}M respectively, in comparison to 0 M, $P<0.0001$, Figure 3.28). The same treatment caused a dose-dependent decrease of *NEFM* (up to 96% at 10^{-5}M, Figure 3.29).

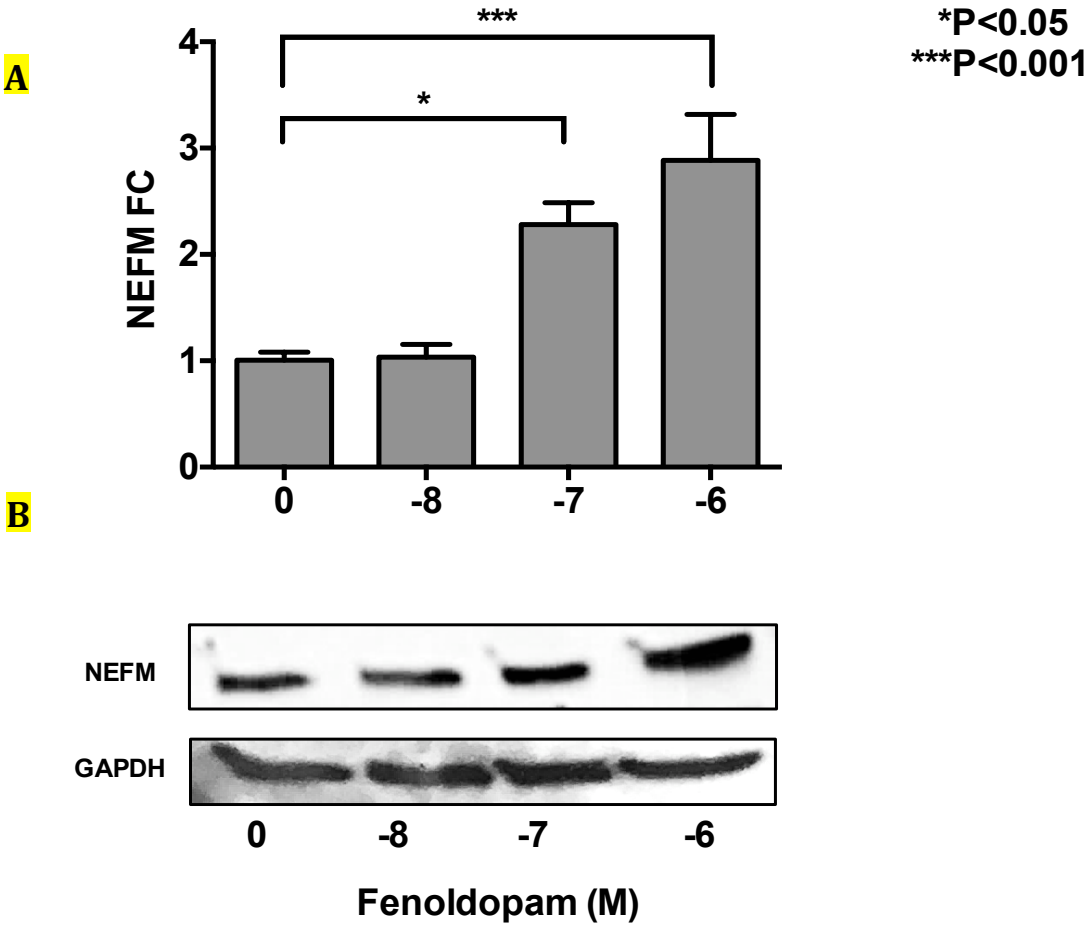

Figure 3.27: H295R treated with fenoldopam for 24 hours increased *NEFM* mRNA expression by 230 and 280 % at 10^{-7}M and 10^{-6}M, respectively (Panel A, P<0.05 and P<0.001). Similar increases were observed at protein level (Panel B). Results are expressed as geometric mean values with SEM and compared using the 2-sided Student t test vs 0 M. The significance level of P<0.05 was considered to indicate statistical significance. M stands for mol/L.

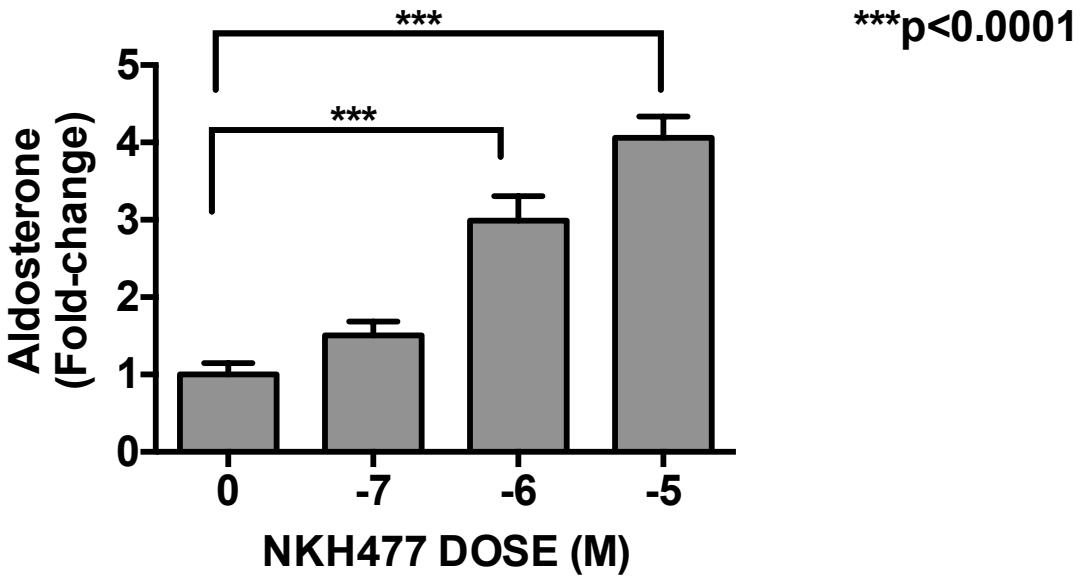

Figure 3.28: H295R treated with forskolin analogue NKH477 for 24 hours increased aldosterone secretion by 50, 298 and 400% at 10^{-7}M 10^{-6}M, and 10^{-5}M, respectively (P<0.001). Results are expressed as geometric mean values with SEM and compared using the 2-sided Student t test vs 0 M. The significance level of P<0.05 was considered to indicate statistical significance. M stands for mol/L.

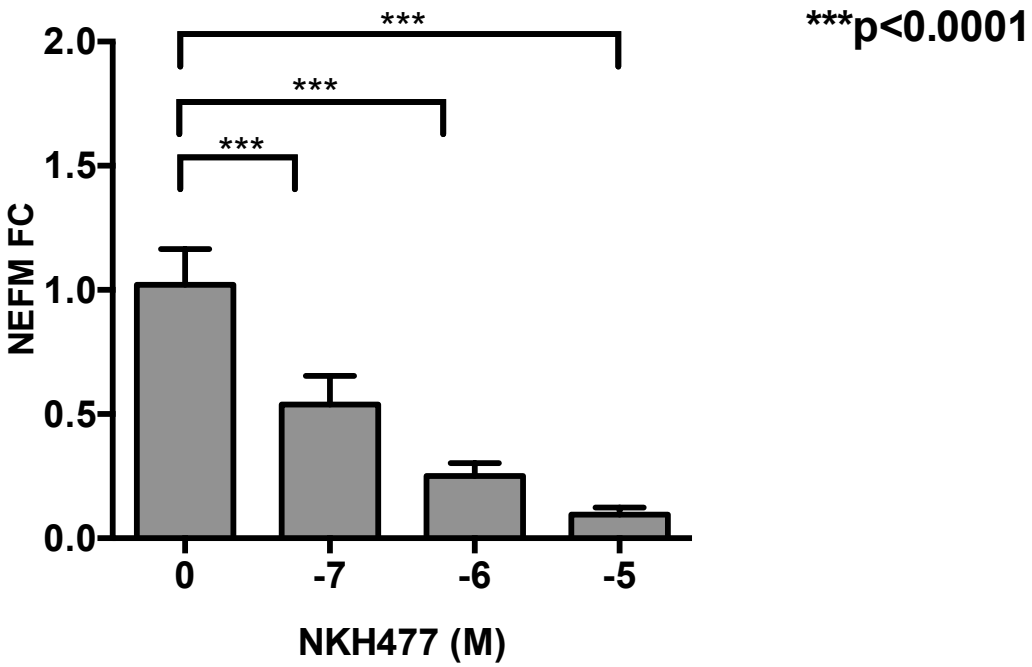

Figure 3.29: H295R treated with forskolin analogue NKH477 for 24 hours decreased *NEFM* mRNA expression by 50, 75 and 95% at 10^{-7}M, 10^{-6}M, and 10^{-5} M, respectively (P<0.001). Results are expressed as geometric mean values with SEM and compared using the 2-sided Student t test vs 0 M. The significance level of P<0.05 was considered to indicate statistical significance. M stands for mol/L.

These results suggest that cyclic AMP-independent mechanism for D1-like receptor signaling are likely to be involved in *NEFM* gene expression regulation as part of the desensitization to D1R stimulation.

3.5.14 *KCNJ5* mutations cause a down-regulation of *NEFM* expression in both H295R and primary ZG-like cells

The transcriptome comparison of the two APA subtypes found that *NEFM* is almost four-fold downregulated in *KCNJ5* mutant ZF-like vs *KCNJ5* wild-type, ZG-like APAs (-3.96 Fold-Change, p= 4.35^{-03}).

We have hypothesized that the down-regulation of *NEFM* expression was a direct effect of *KCNJ5* mutations. To verify the effects of the *KCNJ5*

mutations on *NEFM* expression, we overexpressed *KCNJ5* in H295R adrenal cell line by transfection with pcDNA3.1/*KCNJ5*^{WT}, pcDNA3.1/ *KCNJ5*T^{158A}, pcDNA3.1/*KCNJ5*^{I157Del}, or empty vector. After 48 hours, cells were harvested in 400 ul of Trizol and RNA extracted, cDNA synthetized and qPCR performed for *NEFM* and *18s* mRNA (as housekeeping gene), as described in the first chapter. Whole cell lysate in RIPA buffer was used for western blotting.

NEFM mRNA level decreased by 34% with *KCNJ5*^{I157Del} and by 59% with *KCNJ5*T^{158A}, in comparison to wild-type (Figure 3.30, panel A, N=8, P<0.05). Similar results were obtained at protein level (Figure 3.30, panel B).
To strengthen our hypothesis of a causal correlation between *KCNJ5* genotype and down-regulation of *NEFM* expression (a signature of ZF-like APAs), and aware of the difficulties of isolating a pure ZG cells population from normal adrenal cortex, we have transfected primary cells from a ZG-like APA with the same plasmids from the previous experiment. Since the transfection efficiency rate is low in primary cells, we have not performed qPCR but immunofluorescent staining for *NEFM* and taken pictures of transfected single cells (Figure 3.31).

Similarly to what found in H295R cells, we have observed that *NEFM* (in red), highly expressed in ZG-like APAs and the derived primary cells, is highly expressed in cells transfected with pcDNA3.1 and pcDNA3.1/*KCNJ5*^{WT}, but it disappeared in cells transfected with the two mutations (pcDNA3.1/*KCNJ5*T^{158A} and pcDNA3.1/*KCNJ5*^{I157Del}).

We have then concluded that very low or null levels of *NEFM* expression could be considered part the “ZF-like signature”, the phenotypical changes of APAs carrying *KCNJ5* mutations.

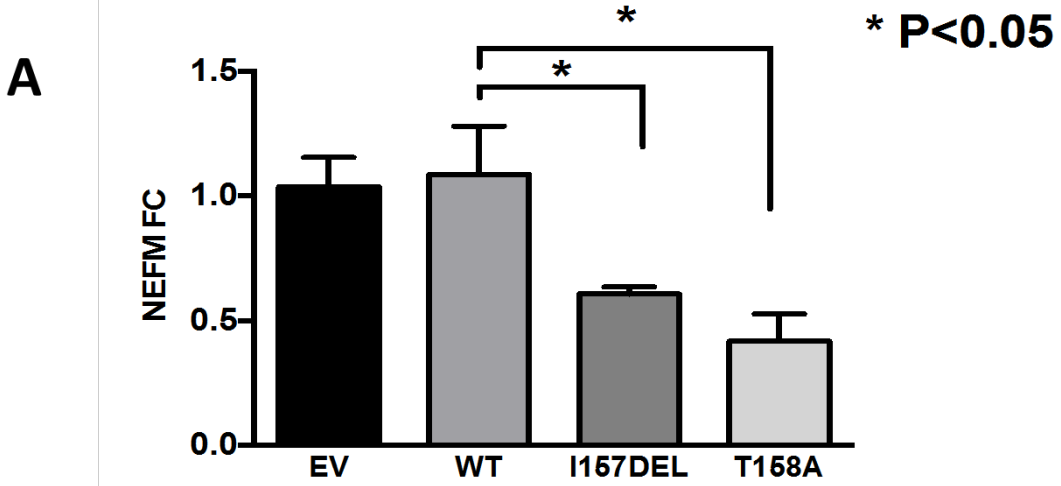

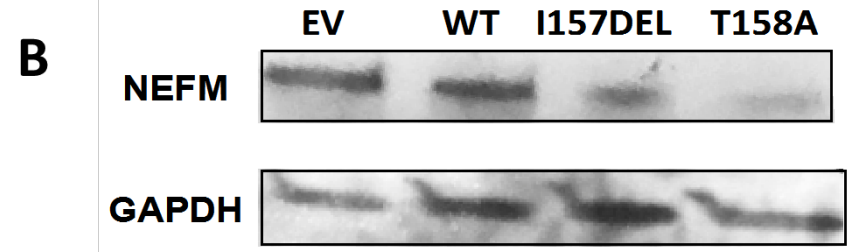

Figure 3.30: Effect of the transfection of *KCNJ5* mutations on *NEFM* mRNA (panel A) and protein (panel B) levels in H295R cells. In comparison to wild-type, pcDNA3.1/*KCNJ5*^{I157Del} and pcDNA3.1/*KCNJ5*T^{158A} caused a decrease of *NEFM* mRNA level by 34% and 59%, respectively (panel A, P<0.05). Similar results were obtained at protein level (panel B)

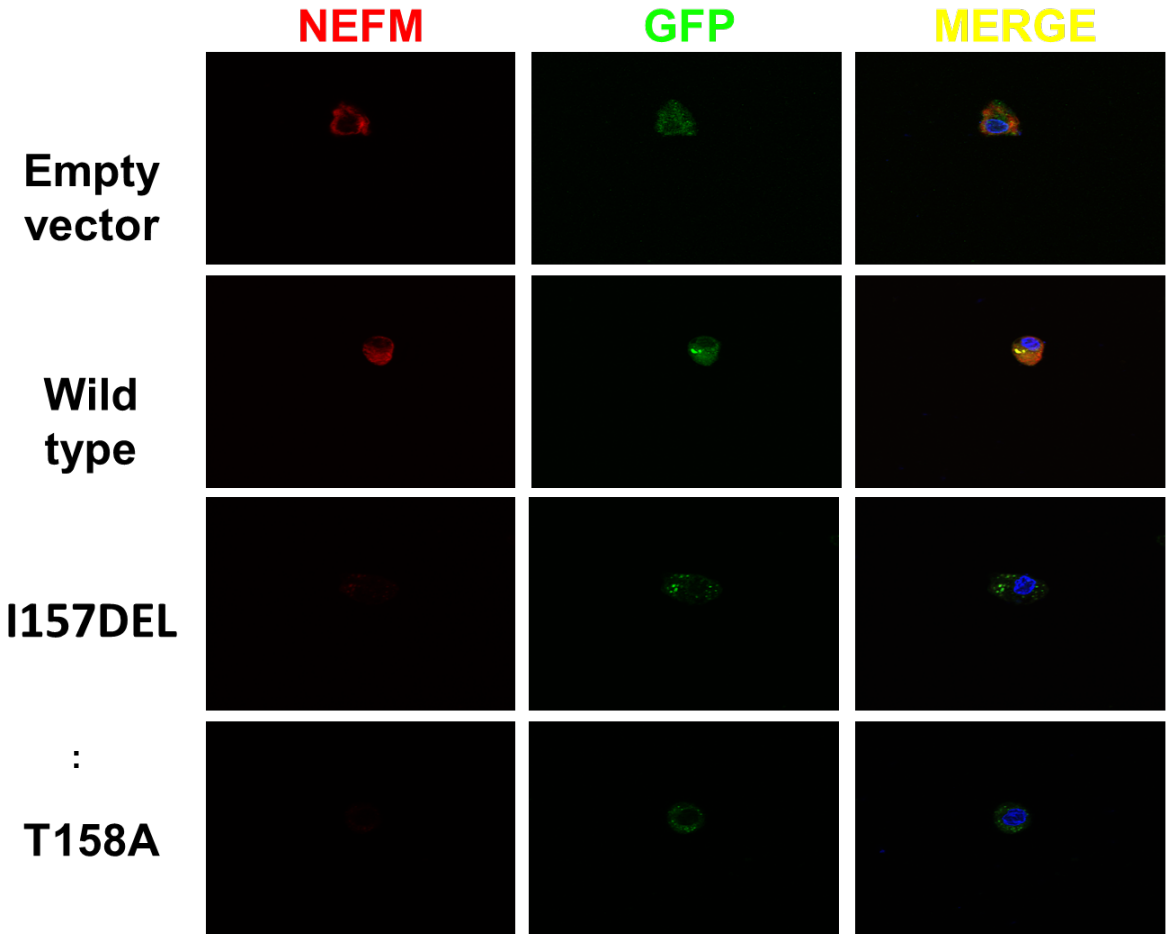

Figure 3.31: Immunofluorescence staining for NEFM (in red), in primary cells from a ZG-like APAs and transfected with *KCNJ5* mutations. NEFM disappeared in cells transfected with the two mutations (pcDNA3.1/*KCNJ5*T^{158A} and pcDNA3.1/*KCNJ5*^{I157Del}).

3.5.15 *NEFM* knock-down causes D1R localisation in the cell plasma membrane of H295R cells

In view of the pharmacological and IHC results, we hypothesized that, *NEFM* silencing causes D1R permanence at plasma membrane thus impairing its trafficking into cytoplasm.
We then decided to transfect H295R cells with GFP expressing shRNA and perform immunocytochemistry with a D1R antibody. For limited number of colour channels at the fluorescence microscope we have decided not to use WGA as a plasma membrane marker.

At immunofluorescence microscopy, *NEFM* knock-down by shRNA increased D1R localization at plasma membrane in transfected (GFP positive) H295R cells. In untransfected cells, the red staining was mainly cytoplasmic (Figure 3.32). Therefore, we concluded that the pharmacological response to D1R agonist or antagonist in *NEFM* silenced cells was due to a reduced D1R trafficking into the cytoplasm and possibly prolonged permanence at the plasma membrane level.

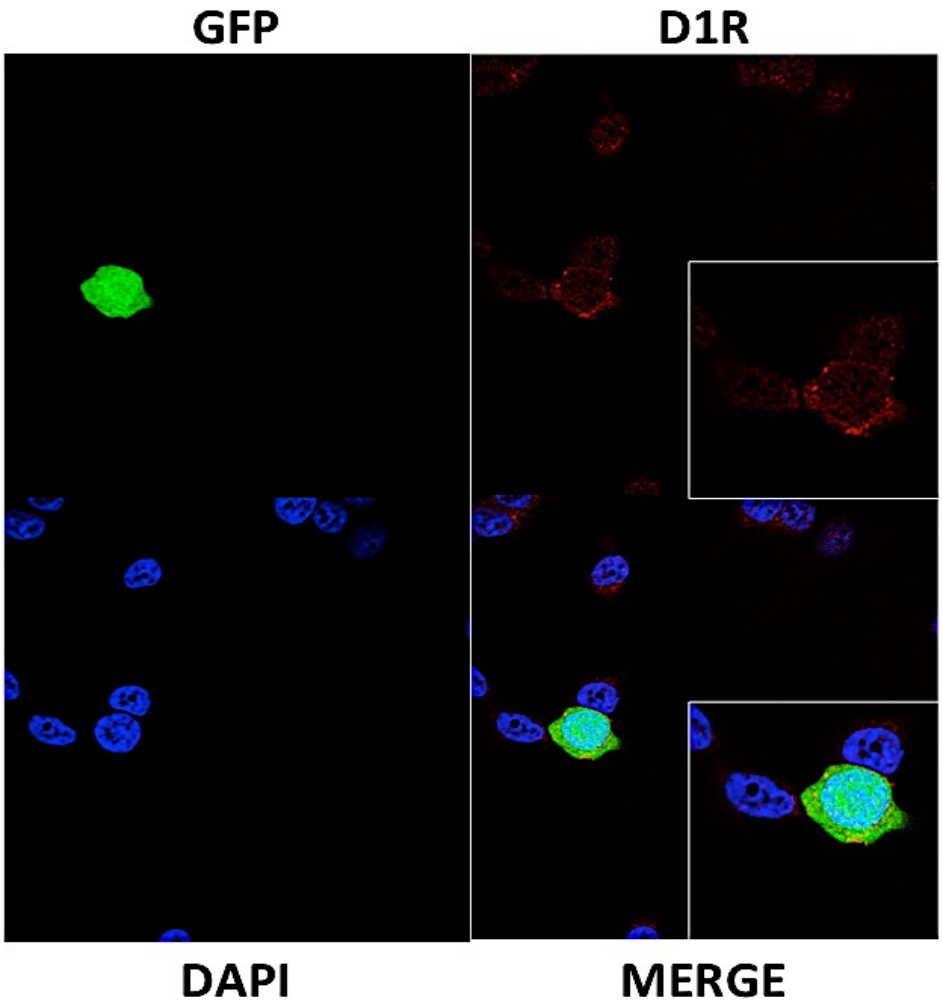

Figure 3.32: Immunofluorescence staining for D1R in H295R cells transfected with GFP-expressing shRNA plasmid. Green=GFP. Red=D1R. Blue=DAPI nuclear staining.
***NEFM* knock-down by shRNA increased D1R localization at plasma membrane in transfected (GFP positive) H295R cells. In untransfected cells, the red staining was mainly cytoplasmic.**

3.6 Discussion

Neurofilament medium (NEFM) was the fourth of the 183 genes up-regulated in ZG vs ZF by at least >10-fold *(LGR5, VSNL1, ANO4, NEFM, VCAN, DACH1,* and *NR4A2*).
NEFM mRNA expression was 14-fold higher in ZG vs ZF. Moreover, *NEFM* resulted to be 4-fold downregulated in ZF-like vs ZG-Like APAs.
Microarray data were confirmed by qPCR performed on the LCM samples. Consistently, IHC demonstrated that NEFM protein was highly and selectively expressed in human ZG and ZG-like APAs. NEFM expression was mainly cytoplasmic and not organized in filaments as in neurons.

NEFM is one of the subunits of NF, the type IV intermediate filament expressed in the nervous systems. Other subunits are Neurofilament light (NEFL) and Neurofilament heavy (NEFH), named after their molecular weight, plus alpha-internexin in the central nervous system or peripherin in peripheral nervous system.

Herein we report the functional studies on NEFM, which is known to be a D1R-interacting protein in synapsis, but it has also been reported to be epigenetically silenced in different cancer types and related to tumour progression (Dubrowinskaja et al. 2014; Calmon et al. 2015; Wang et al. 2016). NEFM and other NF subunits are epigenetically silenced (by microRNA or hypermethylation) in cancers of both neuronal and non-neuronal origin such as neuroblastoma and breast cancer. Their expression levels are also inversely correlated to the aggressiveness and staging of the tumours.

Our functional studies, using H295R as a model of aldosterone producing cells, found that NEFM plays a role in steroidogenesis and that silencing endogenous *NEFM* increases aldosterone secretion.
The increase was not due to an increased synthesis of aldosterone, as we have observed a parallel decrease in *CYP11B2* transcription, but other

mechanisms could explain this divergence. It is likely that the driver to aldosterone secretion was post-transcriptional. One further finding needs comment, namely the reduction in *CYP11B2* expression associated with the increased aldosterone secretion consequent on silencing of *NEFM*. We have noted aldosterone secretion and synthesis to change in opposite directions in previous experiments, and infer that this could be explained by regulatory influences downstream of transcription, for instance on cholesterol uptake into the inner mitochondrial membrane via the steroidogenic acute regulatory (STAR) protein. Although in recent years the emphasis in pathways to aldosterone secretion has been via stimuli to *CYP11B2* transcription, earlier literature showed that many effects, including those of dopamine, occur within minutes – namely too fast for a transcriptional response (Edwards et al. 1980).

Moreover, silencing *NEFM* caused a marked increase in cell proliferation, as demonstrated by two different silencing methods (siRNA and shRNA) and by two different proliferation assays (live cell imaging and colony forming assay).

One of the possible mechanisms unifying both increased aldosterone secretion and proliferation could be an altered mitochondrial function. ShRNA transfected cells showed a more intense MitoTracker Orange CMTMRos staining. The intensity of this dye staining is proportionate to mitochondrial membrane potential, which could be responsible of both increased aldosterone synthesis and cell proliferation.

Overall, these experiments have demonstrated that *NEFM*, similarly to our previously described ZG-selective up regulated genes (*LGR5*, *DACH1*), inhibits rather than stimulates aldosterone and cell proliferation (Shaikh et al. 2015; Zhou et al. 2015).

Since *NEFM* is 4-fold downregulated in large *KCNJ5* mutant, ZF-like APAs that are usually larger than *KCNJ5* wild-type, ZG-like APAs we could

speculate that *NEFM* down-regulation plays a role in the hyperplasia of *KCNJ5* mutant APAs.

Of note, NEFM inhibits not only basal aldosterone secretion but plays a role in regulating dopamine inhibition.
The physiological actions of dopamine are mediated by five G protein-coupled receptors (GPCRs) that are divided into two major groups: the D1 and D2 classes of dopamine receptors. This classification is generally based on the observations that dopamine is able to modulate adenylyl cyclase (AC) activity. The D1-like receptors (D1R and D5R) activate the $G_{\alpha s/olf}$ family that stimulate cAMP production by AC. The D2-like receptors (D2R, D3R, and D4R) couple to the $G_{i/o}$ Family of G proteins and induce inhibition of AC.

Dopamine is known to exert maximal tonic dopaminergic inhibition of aldosterone secretion, and its action seems to be mediated by D2R. In fact, dopaminergic antagonists such as metoclopramide but not dopamine agonists, such as bromocriptine, increase aldosterone without affecting cortisol (Pivonello et al. 2004).

Dopamine-binding sites in the human adrenal cortex are concentrated in the ZG and they are mainly D2R. D1R is also expressed in the adrenal cortex, specifically ZG, of several mammalian species as demonstrated by IHC and autoradiographic or binding studies in rat or bovine adrenal cortex.
In human adrenal cortex autoradiographic or binding studies did not identify any specific [^{3}H] SCH 23390 binding sites (Amenta et al., 1994).

NEFM is involved in the agonist-induced D1R desensitization in the post-synaptic densities, where it binds endosomes formed after internalization of D1R following agonist binding. D1R is retained in an internal pool within the synapsis and ready to be trafficked on the membrane. This mechanism would balance desensitization to D1R stimulation. In fact, in *NEFM* knock out mice, the absence of this anchoring action causes hypersensitivity to D1R agonists

(Yuan et al., 2015) .

We have hypothesized an analogue action of NEFM in the normal ZG. D1R protein expression pattern differ between ZG and ZF. In ZG, which expresses high *NEFM* levels, D1R staining was mainly cytoplasmic, in ZF membranous. The cytoplasmic subcellular localization of D1R could therefore correlate to *NEFM* expression levels.

In support to our hypothesis, D1R staining differs in ZG-like and ZF-like APAs. In ZF-like APAs, characterized by low *NEFM* expression levels, D1R staining was mainly membranous, whereas in ZG-like APAs, which show intense NEFM protein staining, D1R staining was mainly cytoplasmic.

In addition to these histological observations, we have evaluated aldosterone secretion response to increasing doses of D1R agonist fenoldopam in primary cells from the two APAs subtypes. Consistently, cells from ZF-like APAs have a bigger aldosterone response in comparison to those from ZG-like APAs, suggesting that D1R is more sensitive to the agonist because not internalized but recycled to the plasma membrane.

In support to these observations in primary cells and at IHC, we have performed drug experiments in H295R cells after silencing *NEFM*.
NEFM knockout attenuates dopamine-induced inhibition on aldosterone secretion, and amplifies both stimulatory and inhibitory effects on aldosterone secretion of D1R agonist and antagonist, respectively, thus suggesting a direct D1R/NEFM interaction. This was confirmed by co-immunoprecipitation.

Of note, Immunofluorescence staining for D1R in H295R cells after shRNA transfection showed that *NEFM* knock-down increased D1R localization at plasma membrane. In untransfected cells, the red staining was mainly cytoplasmic.

Interestingly, *NEFM* is up regulated in H295R cells treated with D1R agonist fenoldopam, thus supporting the evidence that it is involved in agonist-induced D1R desensitisation.
D2R signalling was not affected by *NEFM* knock-out, as aldosterone stimulation by its antagonist metoclopramide did not differ from controls.

We concluded that *NEFM* is involved in regulating aldosterone inhibition by dopamine, since it internalizes the adenyl-cyclase (AC) stimulating dopamine D1R.
The high *NEFM* levels in ZG could explain why D1R binding sites were not detectable in human adrenal as observed by others.

The disappearance of NEFM protein not only in H295R cells but especially in primary, ZG-like, APA cells transfected with mutant *KCNJ5* suggests that *KCNJ5* genotype is directly correlated to the down-regulation of *NEFM* in common ZF-like APAs.
This observation could suggest that even though ZF-like APAs share phenotypical features with normal cortisol-producing ZF, they are likely to arise from ZG cells with mutant *KCNJ5*.

NEFM and other genes encoding for NF subunits are methylated in several types of cancers and we could speculate that *NEFM* is downregulated in ZF and ZF-like APAs and in *KCNJ5* transfected cells through this epigenetic mechanism, but we did not investigate it experimentally (Calmon et al., 2015; Shen et al., 2016).

As mentioned before, *CYP11B2* positive cell clusters (APCCs) carry mutations in *ATP1A1* and *CACNA1D* but not in *KCNJ5* gene, even though the latter are the most common in sporadic APAs.
NEFM staining was diffuse all over ZG and did not present a patchy pattern as *CYP11B2*, thus suggesting that NEFM is not a marker of APCC, nor co-localized with *CYP11B2*, but can rather be considered a marker of normal or

adenomatous ZG cells, and its disappearance a signature of *KCNJ5* mutant, ZF-like, APAs arising from ZG.

Although this study presents a within-patient comparison of ZG, ZF, and APA transcriptomes, its design leaves some limitations. One is that this study for obvious ethical reasons does not include completely normal adrenals but reflects current indications for adrenalectomy in our hospital.
Secondly, the immortalised adrenal cell line, H295R, is not a perfect model for native ZG cells. These results support our current hypothesis that the human ZG highly expresses genes, which inhibit rather than stimulate aldosterone secretion and cell proliferation.

Because the primary focus of our investigation was *NEFM*, we have concentrated on the D1R, in whose regulation *NEFM* was previously implicated. The D2R function and expression in normal ZG and APAs and its correlation with the cellular composition relies mainly on previous literature. Our experiment using metoclopramide showed that D2R blockade unmasks a net stimulatory effect of dopamine on aldosterone secretion, but future studies on the relationship between APA genotype and D2R function may be required. We used immunostaining rather than autoradiography, to show probable surface expression of D1R in ZF-like APAs and *NEFM*- silenced adrenocortical cells. However, D1R agonist and antagonist modulated aldosterone secretion in H295R cells and, more importantly, in primary cells from APAs, suggested that they express functional receptors.

In conclusion, we confirmed the ZG selective expression of NEFM. Functional analysis of *NEFM* in H295R cells supports *NEFM* role in adrenal steroidogenesis, and although *NEFM* was a “ZG gene” it inhibited aldosterone production.
This suggests that “ZG-specific” genes may be more involved with cell machinery that inhibits rather than stimulates hormone secretion.

We also found that *NEFM* plays a role in dopamine inhibition of aldosterone since it prevents dopamine activation of aldosterone secretagogue signalling by D1R.

This is evident in both normal ZG and in ZG-like APAs. In ZF-like, mutant APA, D1R is membranous and primary cells from this APA subtype secrete significantly more aldosterone in response to D1R agonist.

Disappearance of *NEFM* in *KCNJ5* mutant cells could suggest that ZF-like APAs may originate from ZG cells rather than ZF-cells.

Chapter 4. Role of an anoctamin family member, ANO4, in human adrenal cells

4.1 Abstract

Somatic mutations in *ATP1A1* and *CACNA1D* genes are more common in small, ZG-like APAs, whereas *KCNJ5* mutations are more frequently found in larger ZF-like tumours. These two subtypes differ also in terms of gene expression profile, thus raising the question about the cell origin of APAs and the possible existence of ZG markers. To answer this question, we have performed a microarray analysis comparing the transcriptome of adjacent ZG and ZF and tumour (T) of 14 APA and 7 phaeochromocytoma patients. We found that 28 genes were at least 5-fold over-expressed in ZG vs ZF.

The third most ZG-selective gene was *ANO4*, a member of the anoctamin family that also includes Ca^{2+}-activated chloride channels (CaCCs).

Immunohistochemistry confirmed ZG-selective expression of ANO4 protein. The staining pattern was prevalently cytoplasmic and was also confirmed at immunofluorescence in transfected HEK293 and H295R cells.

ANO4 overexpression in H295R cells increased aldosterone secretion and *CYP11B2* mRNA expression, and in the presence of Ionomycin or AngII, aldosterone production was reduced in comparison to controls.

Yellow fluorescent protein assay was performed to investigate ANO4 activity as a CaCC in comparison with other anoctamins in HEK293 cell and found that when exposed to calcium ionophores, ANO4 generated only small chloride currents.

In conclusion *ANO4* is one of the most highly expressed genes in ZG vs ZF. When overexpressed in an in vitro model of hyperaldosteronism and in presences of calcium agonists and aldosterone secretagogues, it negatively regulates aldosterone synthesis and secretion. Although belonging to a family of CaCCs, it does not generate significant chloride currents.

4.2 Introduction

Chloride (Cl^-) channel family regulates both physiological housekeeping functions such as pH and cell volume regulation, and more specialized physiological functions such as transepithelial electrolyte/fluid transport in epithelia, contraction and excitability. These functions are maintained by various types of Cl^- channels, generally classified in four groups according to the mechanisms of activation: cAMP-regulated chloride channels, ligand-gated chloride channels, voltage-activated chloride channels, and calcium-activated chloride channels (CaCCs).

Three different laboratories have identified the first gene encoding for a CaCC in 2008 (Caputo et al. 2008; Schroeder et al. 2008; Yang et al. 2008), about thirty years after the first description of these currents.

Two genes definitely encoding CaCCs, *ANO1* and *ANO2*, belong to a family that includes eight more genes (ANO1-10). All the members share a common unique structure, eight trans-membrane segments while both N- and C-termini extending in the cytoplasm. The putative trans-membrane domains are highly conserved, while the sequences identity is more divergent in other regions (20–60%).

ANO1 and ANO2 protein sequences are closer than the other members, more evolutionary distant. ANO1 is widely expressed in secretory epithelia, smooth muscle cells and other tissues, poorly expressed in the nervous system. In contrast, ANO2 is exclusively expressed in neurons (Pifferi et al. 2009; Stöhr et al. 2009). The functional meaning of this differential expression relies in their different $[Ca^{2+}]_i$ sensitivity (~10-fold lower in ANO2 vs ANO1).) While ANO1 seems to be constitutively open in epithelial cells with continuous transport activity, ANO2 could be specifically tailored for transient and rapid signals with $[Ca^{2+}]$i peaks and spikes which are more relevant in neurons.

4.2.1 ANO1

The prototype of anoctamins is the widely expressed ANO1, which was reported as CaCC in 2008. When heterologously expressed, it behaves as a CaCC, showing the typical electrophysiological properties: it preferentially

permeates large anions, its voltage/current relationship is dependent on $[Ca^{2+}]i$ concentration as at low concentrations, it is characterized by reversible voltage-dependent activation and time-dependent outward rectification.
ANO1-mediated currents are activated by any physiological or experimental increase of $[Ca^{2+}]i$.
Alternative splicing in different tissues and organs generates different isoforms of ANO1 and is responsible for the different electrophysiological properties of CaCCs in different cell types.

ANO1 is expressed robustly in vascular smooth muscle cells, and knockout mice for ANO1 show a cystic fibrosis phenotype with impaired muco-ciliary clearance and accumulation of mucus in the airways, tracheomalacia and collapsed airways (Rock et al. 2008; Rock & Harfe 2008).

ANO1 plays a role in arteriolar and capillary blood flow and can play a role in the cardiovascular system too as mice lacking vascular ANO1 had lower systemic blood pressure and a decreased hypertensive response following vasoconstrictor stimuli (Heinze et al. 2014).

ANO1 is also up regulated in some tumours like gastrointestinal stromal cancers, oral and neck carcinoma. In vitro, overexpression of ANO1 stimulates cell movement, while pharmacological blocking or silencing of ANO1 decreases cell migration (Ayoub et al. 2010).

So far, there is no convincing evidence that anoctamins other than ANO1 and ANO2 behave as ion channels.
Recent studies gave contrasting results. Only one demonstrated that, in principle, all examined anoctamins are able to generate CaCCs, when overexpressed and activated through the P2Y2 purinergic receptor or with ionomycin which increases $[Ca^{2+}]i$, although less quickly activated than ANO1 (Y Tian et al. 2012).

On the other hand, more than one study showed that expression of ANO3-7 in HEK293 cells did not generate currents. In particular, one of these showed that only ANO1 and ANO2 traffic to the plasma membrane when expressed heterologously, while the other intracellular anoctamins may rather localise to the endoplasmic reticulum, the poor cell membrane trafficking and subcellular localisation being responsible of the absence of currents (Duran et al. 2012).

The different results from these experiments could be due to the use of different cell lines as expression models or to different ways of causing activation of Ca^{2+} signalling. It is also possible that anoctamins need heterodimerization with other paralogues to work as a CaCC, thus single gene overexpression gave negative results.

4.2.2 ANO6

ANO6 recently came to attention as it has been found to be defective in patients suffering from a rare bleeding disorder, the Scott syndrome.
As an ion channel, ANO6 has been described mainly as an outwardly rectifying, Ca^{2+}-dependent and volume regulated Cl- channel, but also as a Ca^{2+} regulated non-selective cation channel permeable to Ca^{2+} and Na^{+}. Beside these ion channel properties, it is pathophysiological relevant as it was found to play a central role in Ca^{2+}-mediated scrambling of membrane phospholipids (PS), and in cell blebbing.

ANO6 has been identified as a scramblase (Suzuki et al. 2010), and missense mutations had been identified in patients with a rare congenital defect in coagulation named Scott syndrome. Their bleeding phenotype is due to an impaired scrambling activity of PS in platelets, as the lack of pro-coagulant phosphatidylserine expose in response to increases of $[Ca^{2+}]i$ prevents the activation of coagulation factors.
The two leaflets of the plasma membrane of quiescent cells have an asymmetric composition in PS, mainly sphingomyelin and phosphatidylcholine in the outer layer, phosphatidylserine and phosphatidylethanolamine in the

inner one. Once established, the PS distribution is not easily disrupted. Flippases maintain the asymmetry of the plasma membrane in an ATP-dependent manner, scramblases mediate Ca^{2+}-dependent but ATP independent movement of all PS in both directions. The asymmetry is lost during physiological functions such as platelets activation and apoptosis.

It is still unclear how the scramblase activity of ANO6 could be related to its ion channel properties. Martins et al. found that whole-cell currents mediated by ANO6, as outwardly rectifying chloride channel (ORCC), are only activated by massive increases of $[Ca^{2+}]_i$ induced by ionomycin, and by apoptotic stimuli (Martins et al. 2011).
On the other hand, activation of the intrinsic or mitochondrial apoptosis with minimal or no increases of $[Ca^{2+}]_i$ stimulated scrambling of PS without generating Cl^- currents. Pharmacological interventions such as inhibitors of Cl^- channels do not affect PS scrambling activity, while they do on ANO6 CaCC activity. These currents were not observed in Scott patients' lymphocytes, either exposed to Fas ligand or to Ca^{2+}ionophores.

Taken together, these observations support not only the hypothesis of two different pathways for PS exposure, one dependent and one independent from Ca^{2+}, but also the speculation that the ANO6 activities as a CaCC and as scramblase are not related.
At least two studies showed that ANO6 could generate cation currents alongside Cl^- currents (Grubb et al. 2013; Kmit et al. 2013). These currents (described as nonselective cation currents, as conducted both Na^+ and Ca^{2+}) were clearly present in wild type lymphocytes, but absent in lymphocytes from Scott patients. Similarly, ANO1 was described to change its anion permeability with increasing Ca^{2+} concentrations (Tian et al. 2012).

It was proposed that ANO6 mediates also Ca^{2+} influx required to increase $[Ca^{2+}]_i$ as, when heterologously expressed, its currents showed prominent outward rectification even at high $[Ca^{2+}]_i$, unlike CaCCs which are typically

characterized by a linear current-voltage (I-V) relationship at saturating $[Ca^{2+}]_i$ thus suggesting that ANO6 does not behave as a CaCC. Moreover, it was permeable to divalent cations, but rather as small-conductance Ca^{2+}-activated nonselective cation channel more permeable to Ca^{2+} than monovalent cations, with synergistic gating by Ca^{2+} and voltage (Yang et al. 2012).

4.2.3 Scramblase activity of other anoctamins

In this scenario of contrasting evidences, Suzuki et al. analysed scrambling and ion channel activities of all anoctamins by expressing them in a mouse lymphocyte cell line with an inactivated allele in the ANO6 gene. They found that ANO6, but also ANO3, 4, 7, and 9 behave as scramblases, but with different preference to lipid substrates.

ANO6 and ANO4 are the paralogues with the stronger ability to enhance the PS exposure in comparison to ANO7 or ANO10. Cells expressing ANO4 have a stronger scramblase activity than ANO6, as they constitutively internalized marked phosphatydicoline a gal-Ceramide (as endogenous levels of Ca^{2+} are sufficient to activate it), and this internalization was strongly enhanced after exposure to ionomycin. No or very weak PS exposure was found in cells expressing ANO1, ANO2, ANO3, ANO5, ANO8, and ANO9. The authors also showed that at patch clamp analysis in 293T cells ANO1 and ANO2, but not other family members, generate currents as CaCC.

These results suggested that ANO3, 4, 6, 7, and 10 scramble various phospholipids and glycosphingolipids with some different substrate preference (Suzuki et al. 2013).

4.2.4 Chloride channels in the adrenal gland

Chorvatova et al. described a Ras-dependent transient chloride current activated by ACTH at very low concentrations in bovine ZG cells through activation of Ras by beta gamma subunits. These currents can have a functional role in aldosterone production at physiological ACTH

concentrations where cAMP production is very low (Chorvatova et al. 1998; Chorvátová et al. 2000).
This was the only study describing a Cl^- current in the ZG cell. No significant Cl^- currents were detected in early studies. Spat et al. examined Cl^- currents with the patch-clamp technique in rat ZG cells. With the application of nearly symmetrical Cl^- concentration, and after inhibiting K+ currents, they did not find any significant channel activity. However, in a significant fraction of the cells, the slow activation of a tiny inward current could be observed at strongly negative voltages. This was significantly accentuated by reducing extracellular pH. Both the kinetic and pharmacological characteristics of this inwardly rectifying current suggest that it passes through ClC-2Cl channels (Spät & Hunyady 2004; Chorvatova et al. 1999).
In synthesis, the functional meaning of Cl^- currents in adrenal cells is still to be determined. Up to now, none of the described channels are CaCCs.

4.2.5 ANO4: previous literature

Controversial data have been published about ANO3–10 members. Duran et al. described that ANO3-7 as intracellular proteins which did not conduct Ca^{2+}-activated Cl^- currents (Duran et al. 2012).
On the other hand, another group have previously showed that most anoctamins overexpressed in the same cell line, HEK293, were expressed on cell membrane (Schreiber et al. 2010).

In particular for ANO4, it has previously been reported that, when co-expressed with purinergic receptor P2Y2, it can conduct currents of variable magnitudes activated by ATP or by ionomycin. Stimulation of purinergic receptors, through an increase of $[Ca^{2+}]i$, depolarized membrane voltages in all anoctamins transfected cells except ANO4, which hyperpolarized the cells. Overexpressed in HEK293, ANO4 localized at plasma membrane level (Y Tian et al. 2012).

ANO4 shares about 40.7% identity with the scramblase ANO6. Suzuki et al

showed that ANO4 constitutively behaves as a scramblase, and its activity is even stronger than ANO6 with specific affinity for some phospholipids. No CaCC activity was found when they measured whole cell current in transfected HEK293 cells.

Duran et al. found the same result in the same cell system, where ANO4 does not localise on the plasma membrane, but its localisation is intracellular. This subcellular distribution of ANO4 is consistent with the lack of finding of chloride currents (Suzuki et al. 2013; Duran et al. 2012).

4.3 Methods and Study design

In order to investigate the role of *ANO4* in the adrenal, we have characterized its protein expression in human adrenals. We also investigated the function of *ANO4* on adrenal steroidogenesis and its effect on the cell proliferation. Chloride currents were measures at YFP assay.

4.3.1 Expression plasmids

P-receiver M29 containing N terminus eGFP-tagged human *ANO4* (encoding 955 amino acids) was purchased from Genecopoeia and shared with Dr Louis Galietta, Gaslini Institute Genoa, Italy.

P-receiver M29 vector control plasmid was generated from this plasmid. The DACH1 (706aa) plasmid was first digested by the restriction enzymes BamHI and HindIII (New England BioLabs Inc, UK) according to the manufacturer's instructions to remove *ANO4* sequence. Then the DNA fragments left were blunted by DNA polymerase I, Large (Klenow) Fragment (New England BioLabs Inc, UK) to remove the 3' overhangs. After blunting, the products were purified by electrophoresis and DNA purification kit (Wizard® SV Gel and PCR Clean-Up System, Promega, USA). Finally, the purified products were ligated together by T4 DNA ligase (New England BioLabs Inc, UK) according to the manufacturer's instructions.

The plasmids were transformed into One Shot® TOP10 Chemically Competent E. coli (Invitrogen, USA) according to the manufacturer's instructions and maxiprepped using EndoFree Plasmid Kits (Qiagen, UK) as

described in Chapter 1. All the above plasmids were sequenced at the end of each step to make sure their sequences were correct.

4.3.3 Transient transfections

For small interfering RNA (siRNA) experiments, H295R cells were seeded at 1.0×10^5/well in 24-well plates in antibiotic-free complete culture medium. After 12 hours the medium was replaced by 500 µl of transfection medium with a final concentration of 50 nM of On-target plus human *ANO4* siRNA-smart pool or On-target plus human non-targeting siRNA (Dharmacon, USA). The cells were then incubated at 37°C in 5% CO_2 for 48 h, then the supernatant was harvested for aldosterone measurement and the cells were harvested for mRNA expression and protein assay.

For over-expression experiments, H295R cells were seeded at 1.0×10^5/well in 24-well plates in antibiotic-free complete culture medium. After 12 hours the medium was replaced by 500 µl of nil media to starve the cells. After at least 6 hours, the transfection was carried out according to the manufacturer instructions for Lipofectamine 3000. The ratio of Lipofectamine 3000 to plasmid was 2:1 per well. Before transfection, the mixture was incubated at room temperature for 15 min. After incubation for 48 h at 37°C in 5% CO_2, cells were harvested for analysis of mRNA expression and protein assay while the supernatant were harvested for aldosterone measurement. Transfection efficiency was monitored by immunofluorescence.

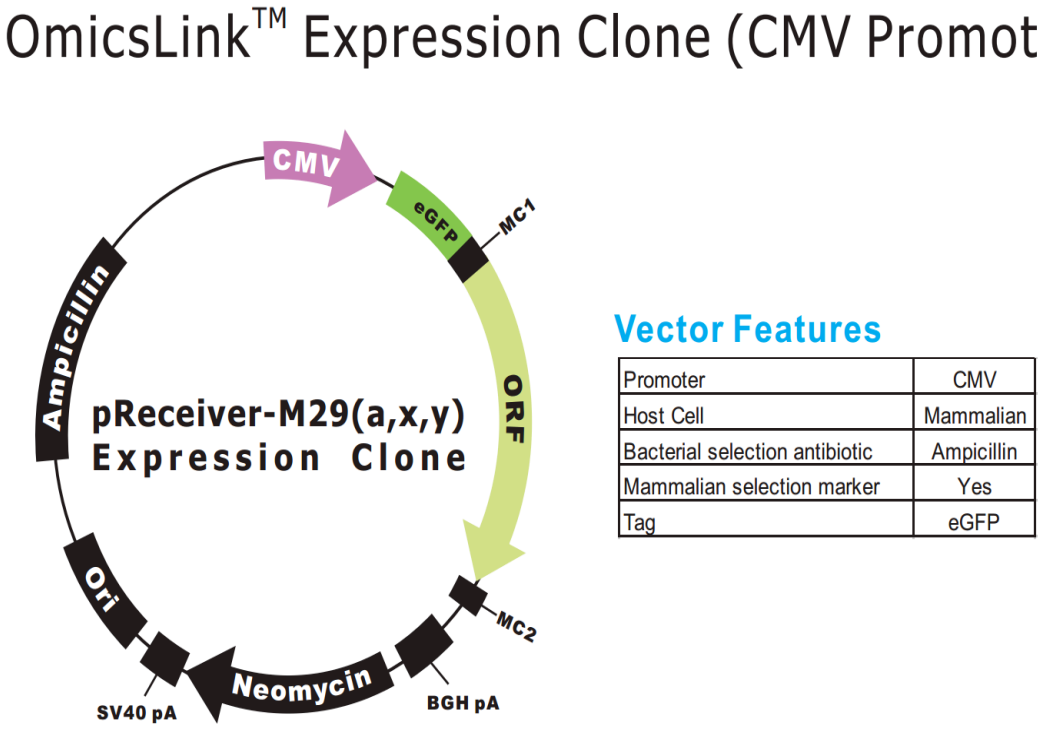

Figure 4.1: schematic representation of the plasmid used for *ANO4* over-expression (From the Genecopoeia website).

4.3.4 CaCC currents measurement by YFP assay

YFP assay is a cell-based assay with an engineered halide-sensitive molecule yellow fluorescent protein originally developed by Galietta and Verkman (Galietta et al. 2001).

This assay detects the iodide (I^-) influx. Cells expressing HS-YFP and CaCCs are exposed to I^--rich solution and a Calcium agonist such as ionomycin at different concentrations. The resulting I^- influx conducted by CaCCs causes a rapid quenching of HS-YFP fluorescence. Hence, the rate of fluorescence quenching is proportional to CaCC activity (Figure 4.2).

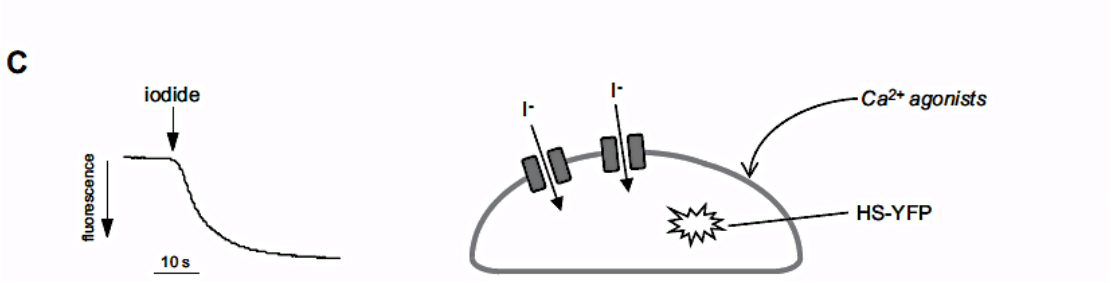

Figure 4.2: Influx detection with the halide-sensitive yellow fluorescent protein (HS-YFP). Cells expressing HS-YFP and CaCCs are exposed to a solution with high I^- concentration and a Ca^{2+} agonist. The resulting I^- influx through CaCCs causes a rapid quenching of HS-YFP fluorescence. The rate of fluorescence quenching is proportional to CaCC activity (modified from Pedemonte &Galietta 2014).

HEK-293 cells were seeded in 96-well microplates (25,000 cells/well) in 100 µl of antibiotic-free culture medium. After 6 h, cells were co-transfected with plasmids carrying the coding sequence for anoctamin constructs and the YFP. After 24 h, the fresh culture medium plus antibiotics replaced transfection media. The HS-YFP functional assay was performed 48 h after transfection. Cells were washed two times with PBS and incubated for 30 min with 60 µl of PBS. After incubation cells were transferred to a microplate's reader (FluoStar Galaxy; BMG Labtech, Ortenberg, Germany) for CaCC activity determination. The plate reader was equipped with high-quality excitation (ET500/20 ×) and emission (ET535/30 m) filters for YFP (Chroma Technology Corp., Brattleboro, VT, USA). Each assay consisted of a continuous 14 s fluorescence reading with 2 s before and 12 s after injection of 165 µl of modified PBS (Cl^- replaced by I^- with final concentration 100 mM) also containing 1 or 10 µM ionomycin. Data were normalized to the initial, background-subtracted, fluorescence. To determine fluorescence quenching

rate (QR) associated with I^- influx, the final 11 s of the data for each well were fitted with an exponential function to extrapolate the initial slope (dF/dt).

4.3.5 XTT assay

XTT is a new tetrazolium dye used in apoptosis, cell proliferation and cytotoxicity tests. XTT is a colourless compound: its reduction causes the breaking apart the positively charged quaternary tetrazole ring and the generation of a soluble, bright orange coloured formazan derivative.

The usage of an intermediate electron carrier, PMS (N-methyl dibenzopyrazine methyl sulphate), as activation reagent increases the sensitivity of the assay as it drives XTT reduction and formation of its derivative**.** XTT dye reduction occurs at the cell surface. PMS mediates electrons transfer at the cell surface from the mitochondrial oxidoreductases.

In brief, the cells were grown in a 96-well plate at a density of 10^5 cells/well in 100 µL of culture medium and transfected with Lipofectamine. After 48 hours from transfection the assay was performed: 25 µL of XTT/PMS solution were added directly to each well containing 100 µL cell culture. The solution was made as described: 4 mg of XTT were dissolved in 4 mL of warm culture media. 10 µL of the PMS solution (10 mM PMS solution in PBS) were added to the 4 mL.

Cells were incubated for 2 hours at 37°C in a CO_2 incubator. The plate was read at 450 nm in a plate reader.

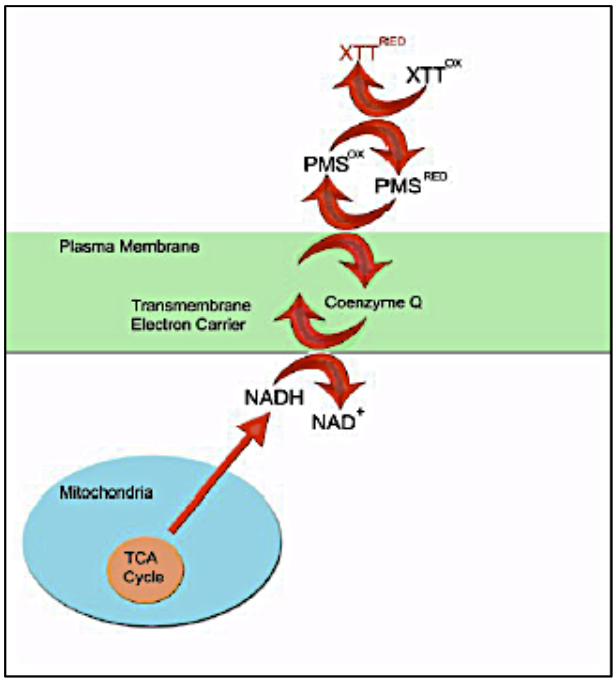

Figure 4.3: The Colorimetric Reduction of XTT by Cellular Enzymes (from XTT Cell Proliferation Assay Kit ATCC instruction manual).

4.4 Results

4.4.1 Microarray

Microarray comparison of ZG vs ZF from 21 human adrenals found that *ANO4* was the third most up-regulated gene (19.9-fold higher, $P=6.6x10^{-24}$, Figure 4.4). *ANO4* expression in most APAs was almost as low as in ZF, regardless of genotype.

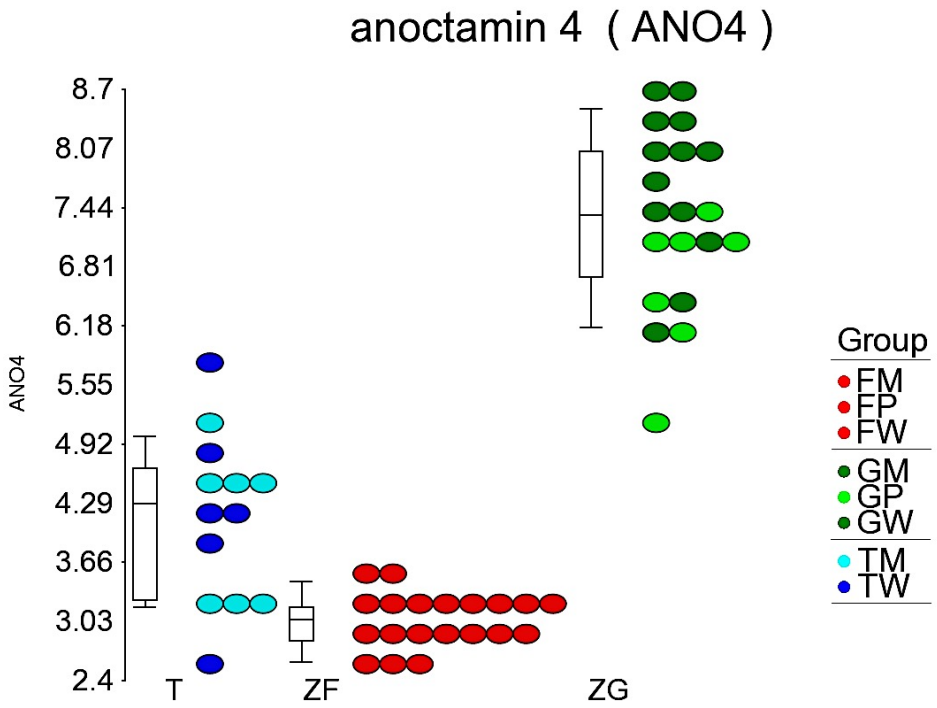

Figure 4.4: Figure 3.1: Representative RMA values of *ANO4* automatically clustered ZF, ZG and APA separately. RMA: Robust Multichip Average. T: Tumor (Aldosterone-Producing Adenoma). ZF: Zona Fasciculata. ZG: Zona Glomerulosa. Group legend: FM: ZF-Mutant KCNJ5. FP: ZF-Phaeocromocytoma. FW: ZF- wild-type KCNJ5. GM: ZG-Mutant KCNJ5. GP: ZG-Phaeocromocytoma. GW: ZG-KCNJ5 wild-type. TM: Tumor -mutant KCNJ5. TW: Tumor- Wild-type KCNJ5.

The microarray results were validated and confirmed by qPCR performed on LCM samples (Figure 4.5).

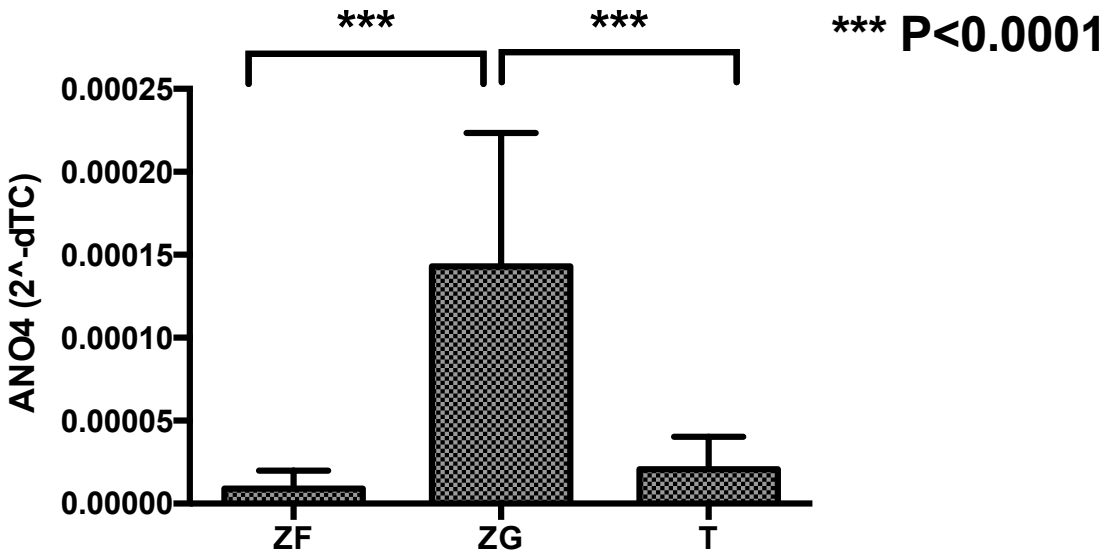

Figure 4.5: *ANO4* qPCR validation of microarray findings performed on LCM samples from ZG, ZF and APAs of 7 patients with phaeocromocytoma, 7 patients with *KCNJ5* mutant, and 7 patients with *KCNJ5* wild-type APAs. Results are expressed as Mean and S.E.M of $2^{-dCT.}$ ZF: Zona Fasciculata. ZG: Zona Glomerulosa. T: Tumor (Aldosterone-Producing Adenoma). Multiple t-tests were applied.

4.4.2 ANO4 protein expression in AAG and APAs

ANO4 protein was selectively expressed in the ZG of adjacent adrenal glands (AAG) next to an APA or AAG next to a Phaeocromocytoma (Figure 4.7). In the positive control sections (human kidney sections), ANO4 stain was observed in the renal tubules and fainter in the glomeruli (Figure 4.6). In the adrenal ZG the staining was cytoplasmic.

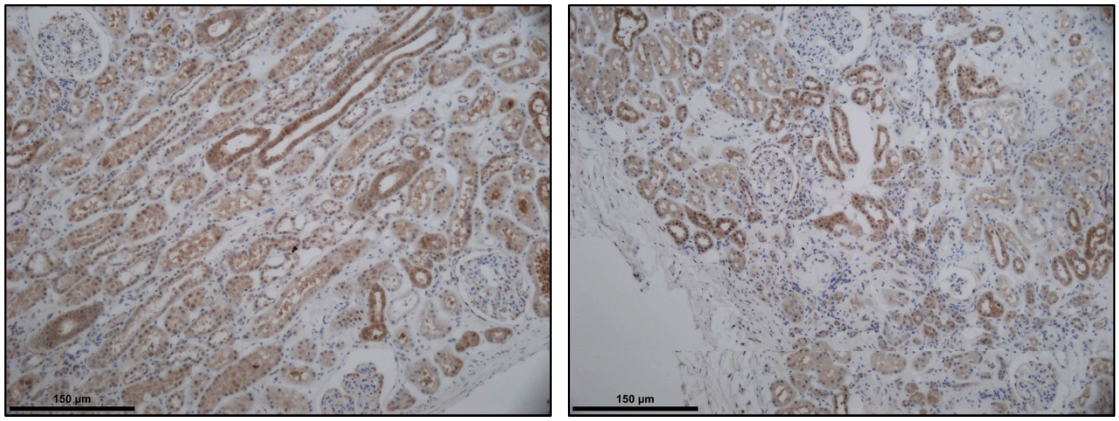

Figure 4.6: IHC of ANO4 in human kidney sections. The staining was mainly tubular and less intense in glomeruli.

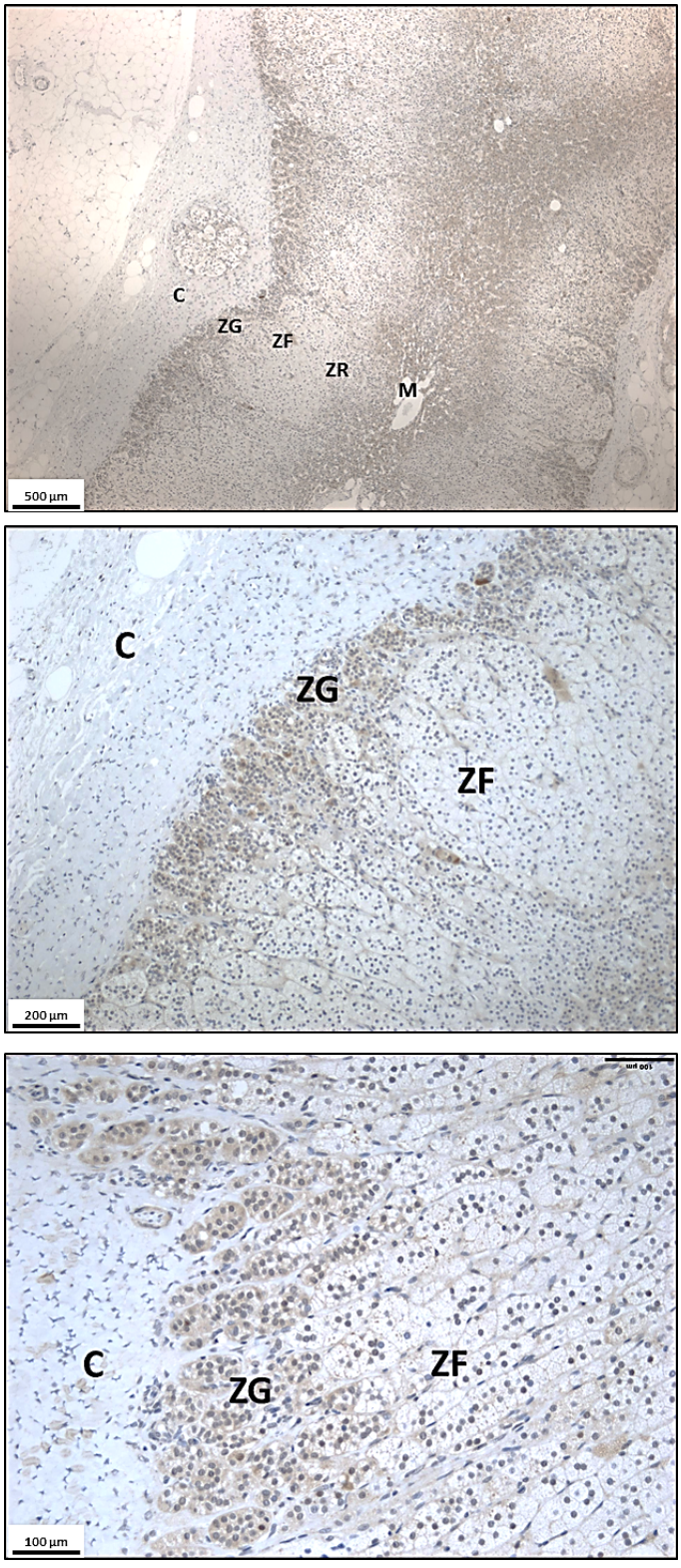

Figure 4.7: IHC of ANO4 in the normal adrenal cortex adjacent to a phaeocromocytoma. The staining was selective for ZG and appeared to be mainly cytoplasmic (C=capsule).

4.4.3 ANO4 protein expression in H295R and HEK293 cells: Immunofluorescent staining in transfected cells

We evaluated ANO4 protein expression pattern in transfected H295R and HEK293 cells by confocal microscopy. We have used two plasmids with different tags as probes, N-terminus eGFP for H295R and C-3xHA-tag for HEK293 cells. The experiments were performed independently in Genoa (for HEK293 cells) and Cambridge (H295R cells).

The cells were counter stained with nuclear staining DAPI and, in case of H295R cells, plasma membrane marker WGA.
In both HEK293T and H295R cells and independently from the tag, the staining for ANO4 in both the cell lines was cytoplasmic (Figure 4.8 and 4.9).
However the caveat for these experiments is that *ANO4* has been overexpressed and its protein products includes tags.

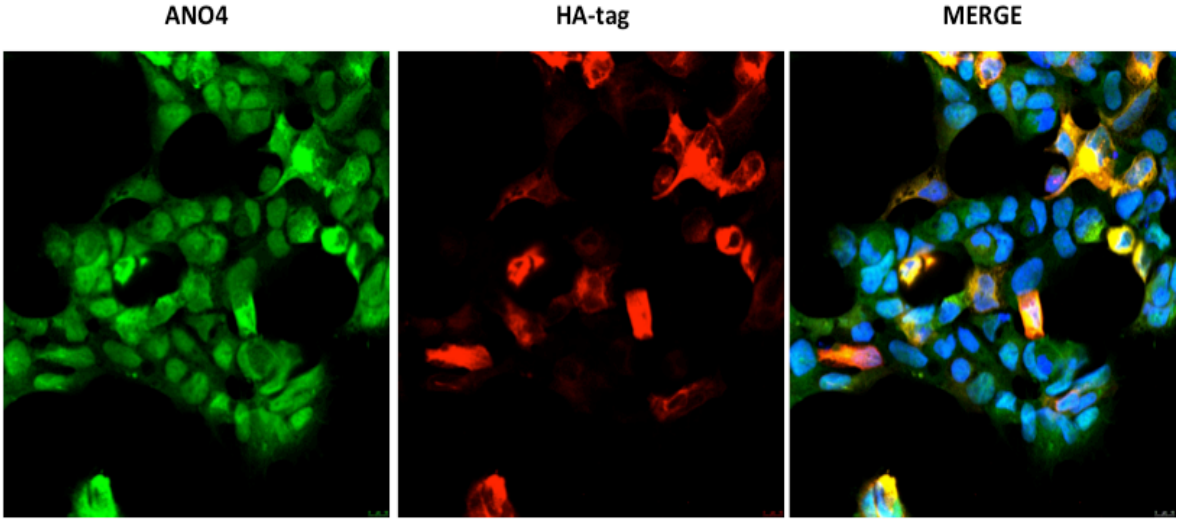

Figure 4.8: Immunofluorescent detection of ANO4 in transfected HEK293 cells. Blue staining corresponds to nuclei, green fluorescence to ANO4. Red staining corresponds to the HA-tag of transfected ANO4. Merge images show cytoplasmic localisation of ANO4 (Courtesy of Dr Paolo Scudery, Genoa).

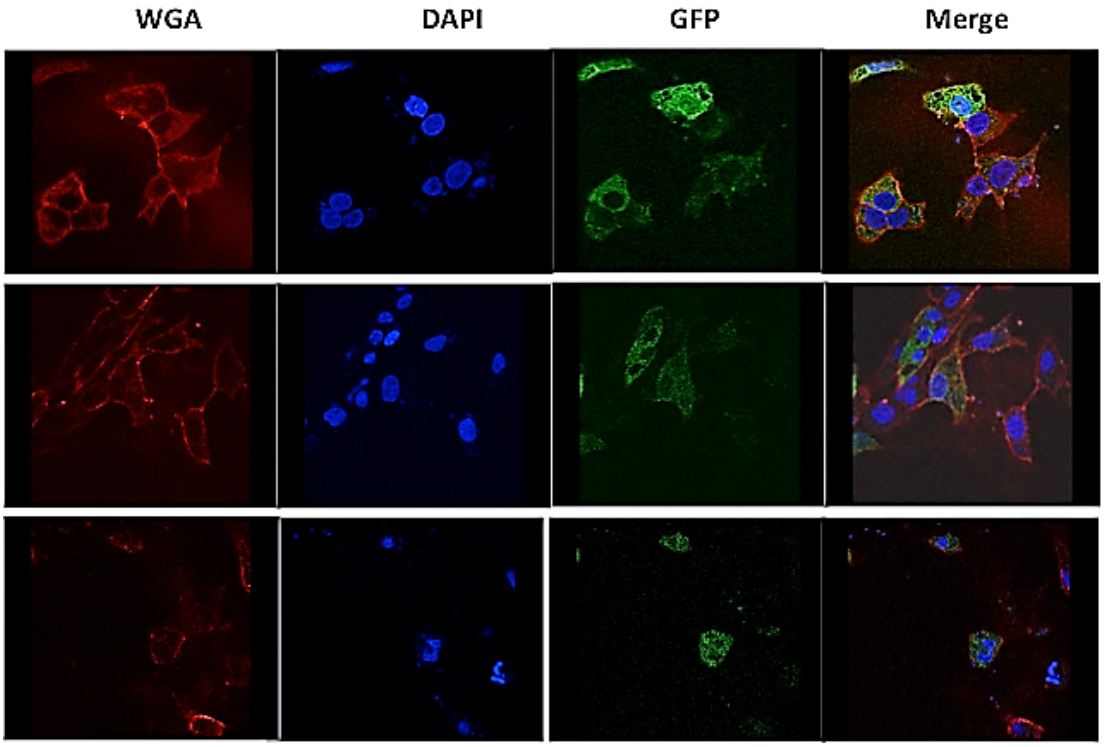

Figure 4.9: Confocal microscopic images of immunofluorescent staining showed transfected ANO4 staining (green-GFP), plasma membrane (red-WGA), nuclei (blue-DAPI) and the overlay of them in the same sight field in H295R cells. ANO4 staining is mainly cytoplasmic. Pictures are representative of three fields.

4.4.4 Effects of *ANO4* overexpression in H295R cells

To evaluate the effects of *ANO4* on aldosterone production, we transfected the adrenocortical cell line H295R with a plasmid expressing N-terminus eGFP tagged *ANO4* and used Lipofectamine 3000 according to the manufacturer's instruction. The cells were harvested at 48 hours from transfection for RNA extraction or protein concentration measurement and media collected for HTRF aldosterone assay.

Comparing to controls, *ANO4* mRNA increased by 12.6 fold in transfected cells (N=12, P< 0.0013; Figure 4.10). This change resulted in a significant 4.3 fold increase in *CYP11B2* mRNA (N=12, P<0.05, Figure 4.11).

Similarly, *ANO4* overexpression stimulated aldosterone synthase transcription factor *NR4A2*. Comparing to control vector, overexpression of *ANO4* significantly stimulated *NR4A2* mRNA expression by 2.4 fold (N=12, P<0.05, Figure 4.12).

However, aldosterone changes induced by *ANO4* overexpression were not significant, although a trend to aldosterone increase was observed (N=12, ns, Figure 4.13).

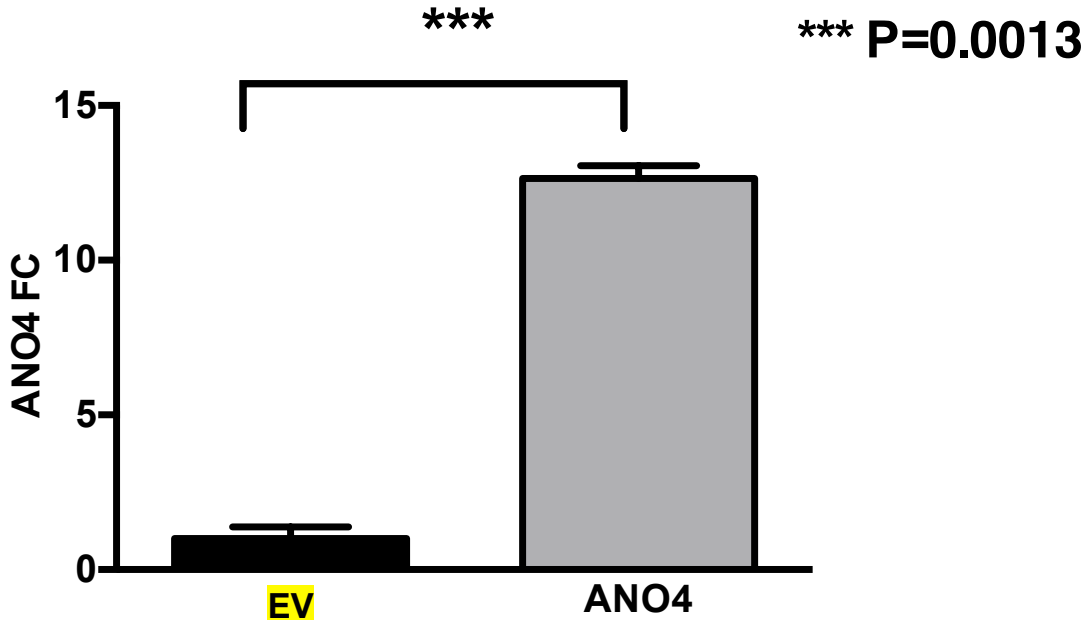

Figure 4.10: Effect of *ANO4* overexpression on *ANO4* mRNA in H295R cells. At 48 hours from transfection *ANO4* mRNA expression increased by 12 fold, comparing to empty vector (EV) (*P=0.001). Data are shown in geometric mean values + S.E.M. Results are expressed as geometric mean values with SEM and compared using the 2-sided Student t test. The significance level of P<0.05 was considered to indicate statistical significance.

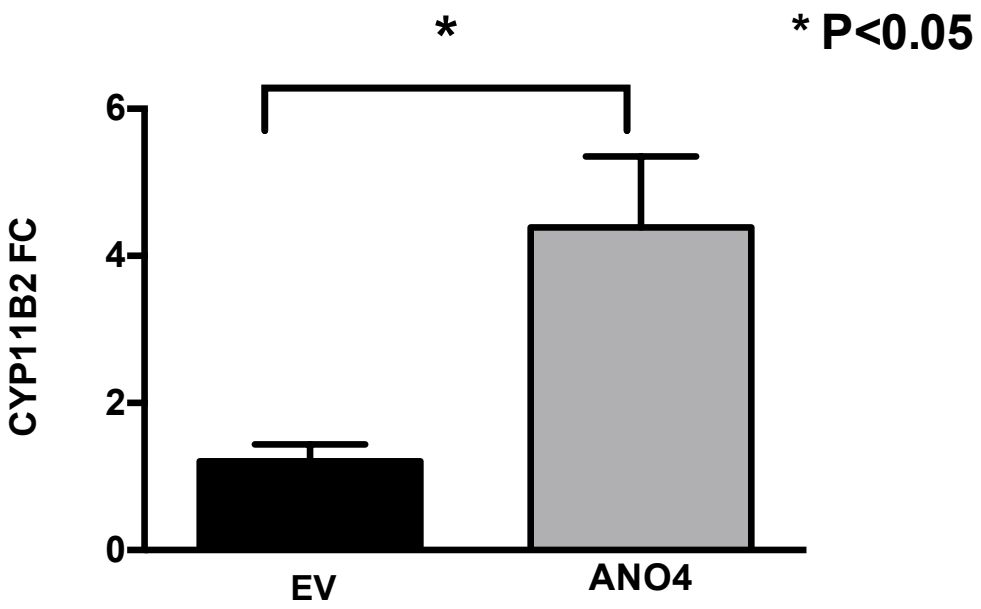

Figure 4.11: Effect of *ANO4* overexpression on *CYP11B2* mRNA in H295R cells. At 48 hours from transfection *CYP11B2* mRNA expression increased by 4.4 fold, comparing to empty vector (EV) (*P<0.05). Results are expressed as geometric mean values with SEM and compared using the 2-sided Student t test. The significance level of P<0.05 was considered to indicate statistical significance.

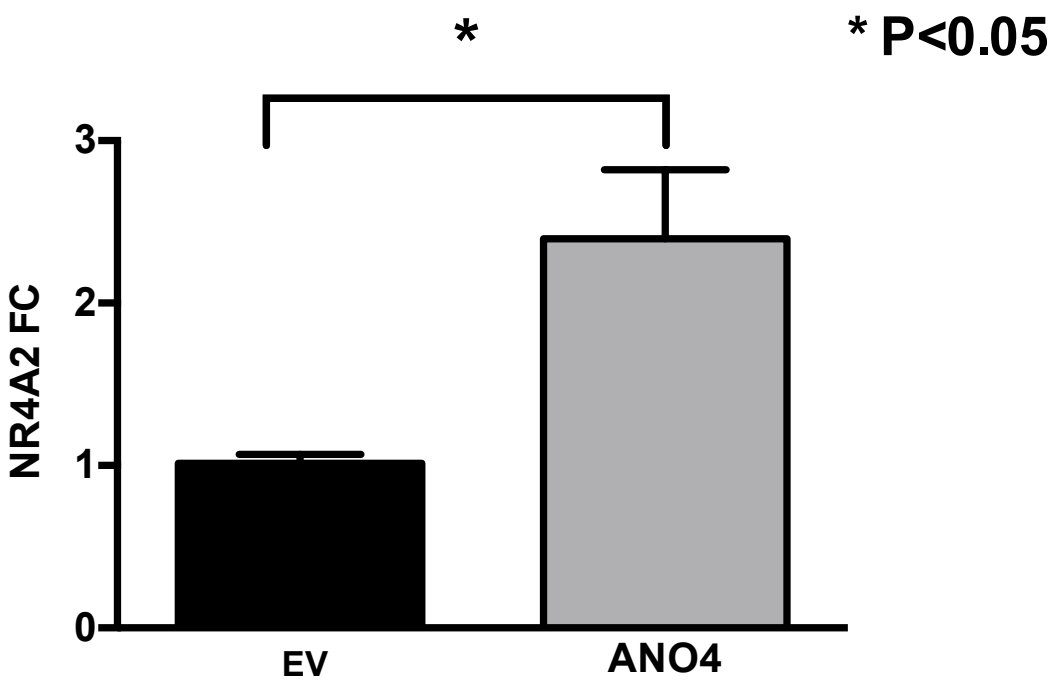

Figure 4.12: Effect of *ANO4* overexpression on *NR4A2* mRNA in H295R cells. At 48 hours from transfection *CYP11B2* mRNA expression increased by 2.4 fold, comparing to empty vector (EV) (*P<0.05). Results are expressed as geometric mean values with SEM and compared using the 2-sided Student t test. The significance level of P<0.05 was considered to indicate statistical significance.

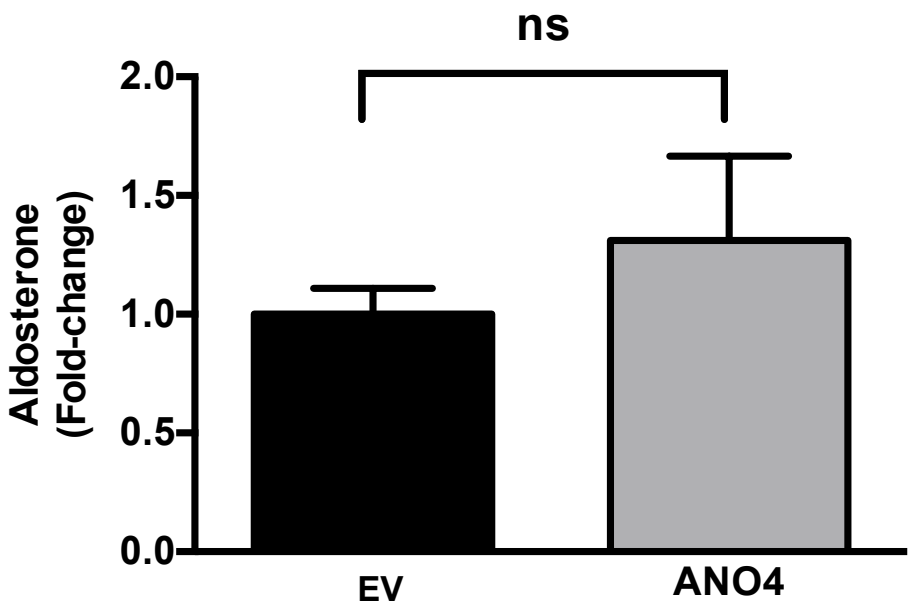

Figure 4.13: Aldosterone secretion in response to the overexpression of ANO4 in H295R cells. There was a trend toward a stimulation of basal aldosterone secretion but it was statistically non-significant. Results are expressed as mean values with SEM and compared using the 2-sided Student t test. The significance level of P<0.05 was considered to indicate statistical significance.

4.4.5 Effects of *ANO4* silencing in H295R cells

Silencing *ANO4* significantly reduced its protein levels at 48 hours (Figure 4.14).

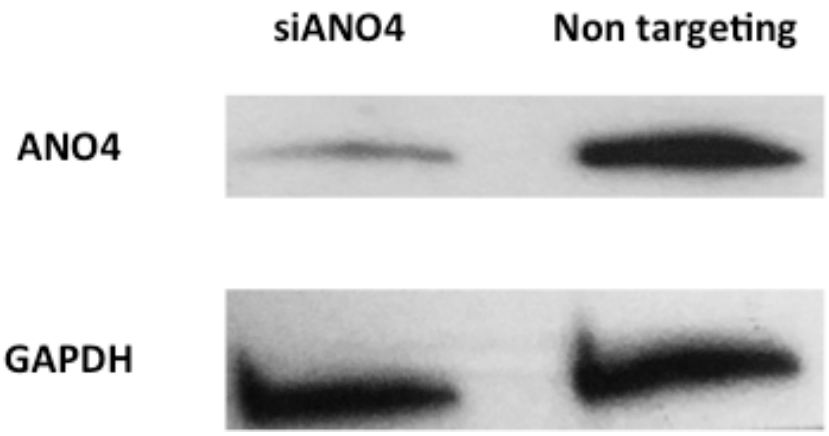

Figure 4.14: Western blot figures showing ANO4 and GAPDH control in H295R cells at 48 hours from silencing ANO4.

Silencing *ANO4* for 48 hours affected *CYP11B2* and *NR4A2* mRNA expression levels, without changing aldosterone secretion.

Silencing *ANO4* for 48 hours induced 37% down-regulation of *CYP11B2* mRNA (N=6, P<0.05, Figure 4.15) and a 35% down-regulation of *NR4A2* mRNA (N=6, P<0.05, Figure 4.16).

Similar to overexpression, silencing *ANO4* did not significantly affect aldosterone secretion although a trend to reduction was observed (N=6, ns, Figure 4.17).

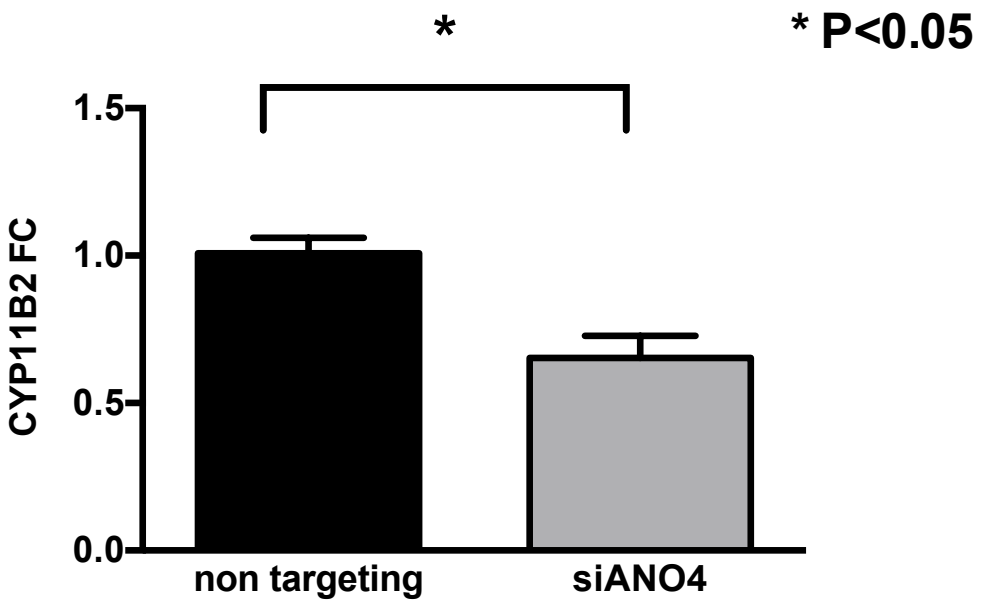

Figure 4.15: Effect of silencing *ANO4* on *CYP11B2* mRNA in H295R cells. At 48 hours from silencing *CYP11B2* mRNA expression decreased by 37%, comparing to non-targeting (*P<0.05). Results are expressed as geometric mean values with SEM and compared using the 2-sided Student t test. The significance level of P<0.05 was considered to indicate statistical significance.

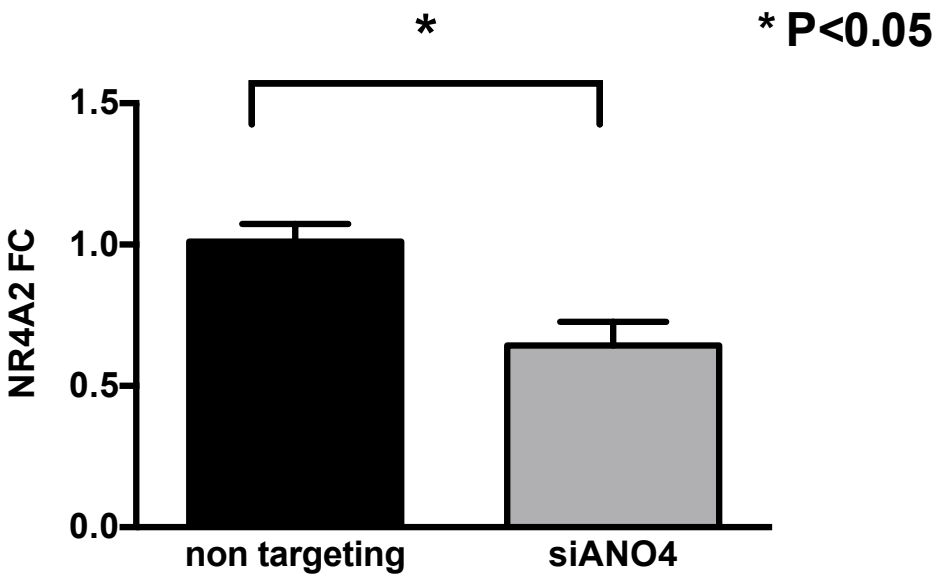

Figure 4.16: Effect of silencing *ANO4* on *NR4A2* mRNA in H295R cells. At 48 hours from silencing *NR4A2* mRNA expression decreased by 35%, comparing to non-targeting (*P<0.05). Results are expressed as geometric mean values with SEM and compared using the 2-sided Student t test. The significance level of P<0.05 was considered to indicate statistical significance.

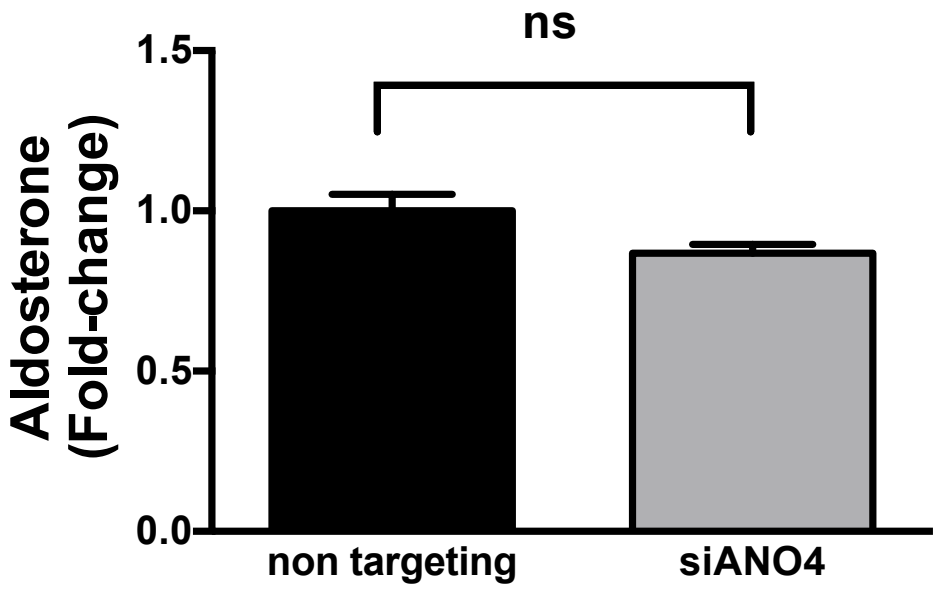

Figure 4.17: Aldosterone secretion in response to *ANO4* silencing in H295R cells. There was a trend toward a downregulation of basal aldosterone secretion but it was statistically non-significant. Results are expressed as mean values with SEM and compared using the 2-sided Student t test. The significance level of P<0.05 was considered to indicate statistical significance.

4.4.6 Effect of *ANO4* on stimulated aldosterone secretion

As *ANO4* overexpression or silencing did not affect basal aldosterone secretion in H295R cells, we measured aldosterone response to secretagogues in transfected cells.

Among all aldosterone secretagogues we have chosen Ang II, Ionomycin and ATP as they increase intracellular calcium concentration, the trigger to activate CaCCs, via different pathways.

The experiment design was similar to the transfection described so far, although at 36 hours we have replaced the media with starving medium for six hours and then treated the cells with different drugs (AngII at 10^{-8} M, Ionomycin 1 μM and ATP 10^{-6}M) for 24 hours. Aldosterone was measured by HTRF assay and normalized by protein concentration measures by BCA assay.

After stimulation with AngII (10^{-8} M for 24 hours), aldosterone secretion increased by 3.5 fold in controls, whereas the increase in *ANO4* transfected cells was smaller, 2.25 fold in comparison to basal concentration (N=6, $P<0.05$, Figure 4.18).

In a similar experiment, the cells were treated with Ionomycin (1 μM for 24 hours). Ionomycin is a calcium ionophore that increases intracellular calcium concentration by stimulating its release from the endoplasmic reticulum storages. Calcium signalling is a known stimulator of aldosterone secretion.

Ionomycin, increased aldosterone by 2.7-fold in controls, whereas in *ANO4* transfected cells the increase was significantly smaller, 1.2-fold (N=6, $P<0.05$, Figure 4.19).

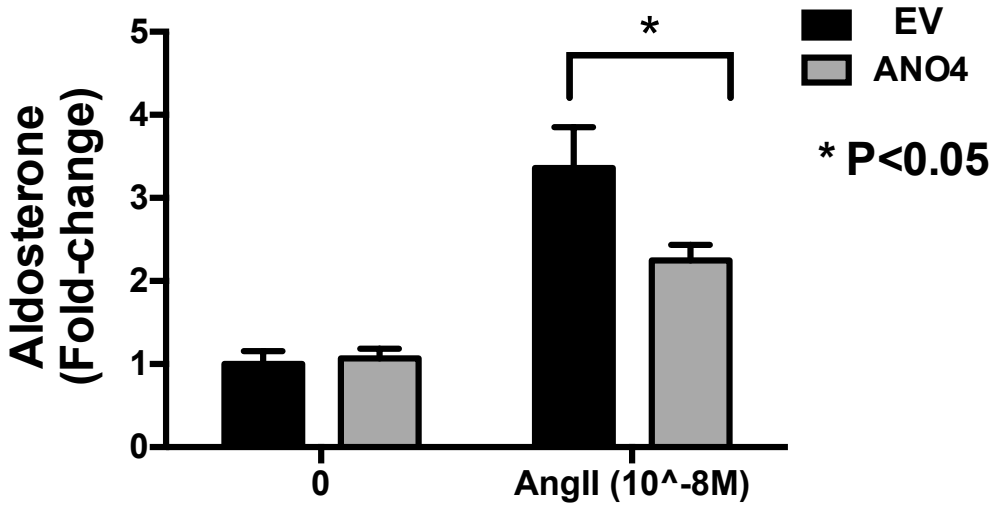

Figure 4.18: Effect of *ANO4* overexpression in H295R on AngII stimulated aldosterone secretion. Aldosterone secretion increased by 4 fold (vs basal aldosterone) in controls, and only 2.25 fold in *ANO4* transfected cells (*P<0.05). Results are expressed as geometric mean values with SEM and compared using one-way ANOVA. The significance level of P<0.05 was considered to indicate statistical significance.

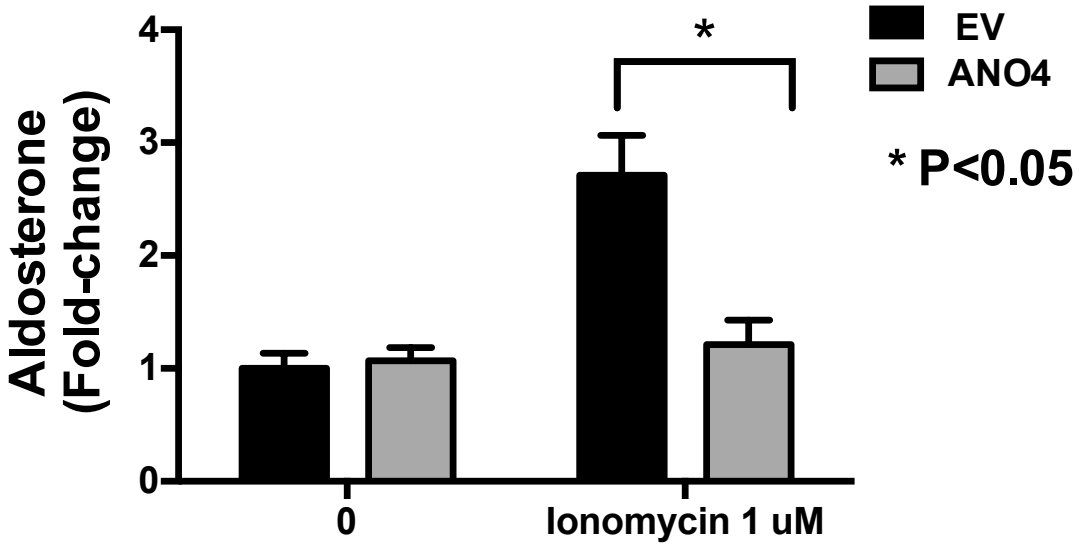

Figure 4.19: Effect of *ANO4* overexpression in H295R on Ionomycin stimulated aldosterone secretion. Aldosterone secretion increased by 2.7 fold (vs basal aldosterone) in controls, and only 1.2 fold in *ANO4* transfected cells (* P<0.05). Results are expressed as geometric mean values with SEM and compared using one-way ANOVA. The significance level of P<0.05 was considered to indicate statistical significance.

Another calcium agonist was tested. Nucleotide ATP is known to activate purinergic signalling via P2Y receptors and activates calcium signalling in H295R cells (Nishi et al. 2013).

ATP treatment for 24 hours increased aldosterone secretion by 1.5 fold in controls but did not affect aldosterone secretion in *ANO4* transfected cells (N=6, P<0.05, Figure 4.20).

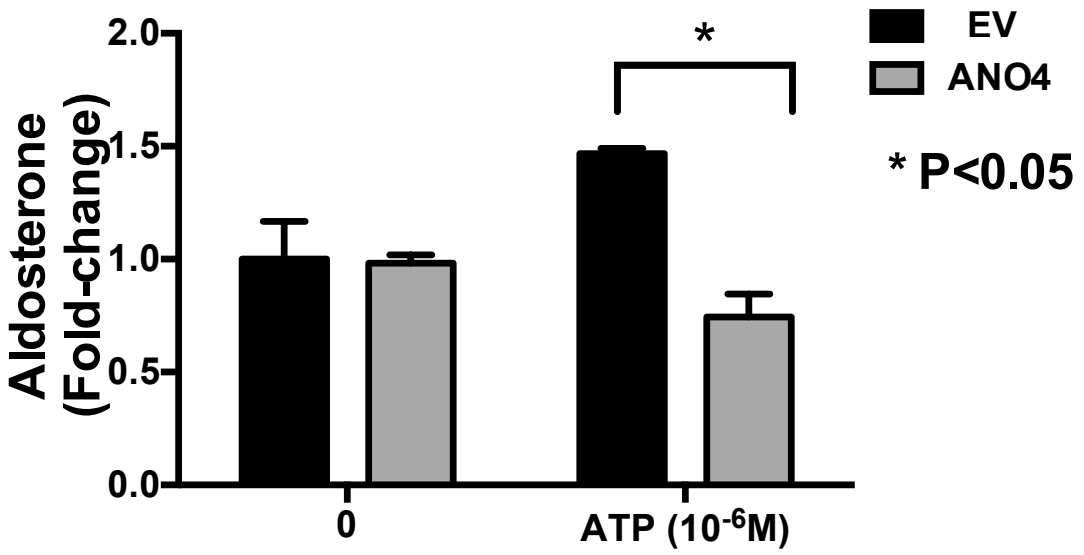

Figure 4.20: Effect of *ANO4* overexpression in H295R on ATP stimulated aldosterone secretion. ATP increased aldosterone secretion by 1.5 fold (vs basal aldosterone) in controls, and reduced it by 0.25 fold in *ANO4* transfected cells (*P<0.05). Results are expressed as geometric mean values with SEM and compared using one-way ANOVA. The significance level of P<0.05 was considered to indicate statistical significance.

4.4.7 Comparison with other anoctamins

We compared the effects of *ANO4* overexpression in H295R cells with those of two other anoctamin family members, ANO1 and ANO6: the former is a plasma membrane protein with Ca^{2+}-dependent Cl^- channel function, the latter has been reported as a scramblase (Caputo et al. 2008; Suzuki et al. 2010).

The outcome was basal and stimulated aldosterone secretion and cell proliferation. We have also evaluated the effects of different anoctamins on iodide currents as evaluated at YFP assay, and compared those generated by ANO4, ANO1 and ANO2, two CaCCs with different sensitivity to $[Ca^{2+}]_i$ and an intracellular anoctamin, ANO5. The latter was chosen mainly for its expression pattern, as ANO4 is expressed as an intracellular protein in human adrenal cells and in H295R and HEK293 cell lines.

4.4.7.1 Aldosterone secretion and synthesis

We evaluated aldosterone secretion and *CYP11B2* mRNA expression in basal or stimulated conditions (with AngII 10^{-8}M for 24 hours) in H295R transfected with empty vector (EV), *ANO1, ANO4 or ANO6*.

We found that, compared to basal aldosterone in controls, basal aldosterone secretion was 2 fold higher, 1.3 fold and 1.1 higher in ANO1, *ANO4* and *ANO6* transfected cells, respectively. Aldosterone response to AngII was 2.6, 3.7, 2.2 and 2.7 fold higher in comparison to basal controls in *EV*, *ANO1, ANO4 and ANO6* transfected cell, respectively. No significant differences were found in both conditions between the three anoctamins (N=6, ns, Figure 4.21).

CYP11B2 mRNA in basal conditions was 2, 2.7 and 2 fold higher in ANO1, ANO4 and ANO6, respectively. *CYP11B2* mRNA expression in response to AngII was 14.6, 20.7, 37.7 and 18.9 fold higher in comparison to basal controls in *EV, ANO1, ANO4 and ANO6* transfected cell, respectively. Ang

II stimulated *CYP11B2* mRNA expression was significantly higher in ANO1 and ANO4 vs stimulated VE (N=6, P<0.05, Figure 4.22).

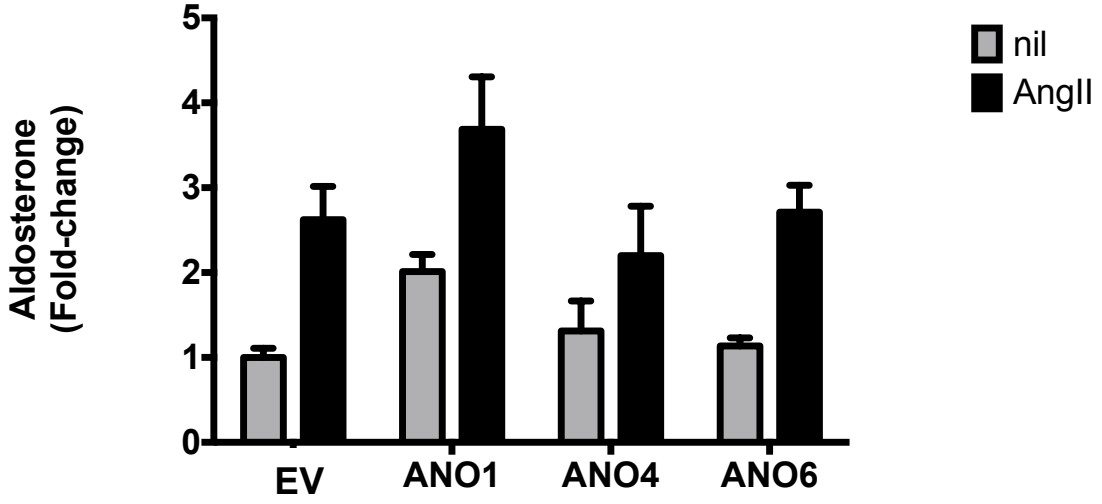

Figure 4.21: Effect of *ANO1, ANO4* and *ANO6* overexpression in H295R on AngII stimulated aldosterone secretion. Aldosterone secretion increased by 2.6, 3.7, 2.2 and 2.7 fold higher in comparison to basal controls in *EV, ANO1, ANO4* and *ANO6* transfected cell, respectively. No significant differences were found in both conditions between the three anoctamins.

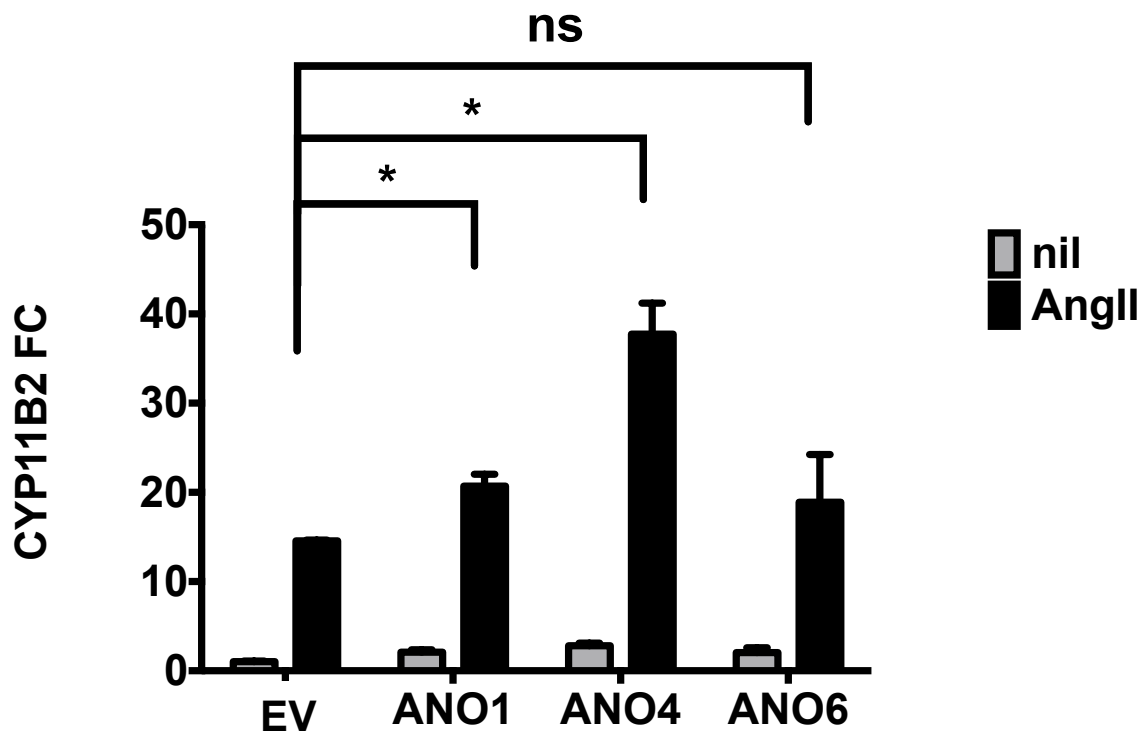

Figure 4.22: Effect of *ANO1*, *ANO4* and *ANO6* overexpression in H295R on AngII stimulated *CYP11B2* mRNA expression. *CYP11B2* mRNA in basal conditions was 2, 2.7 and 2 fold higher vs controls in *ANO1*, *ANO4* and *ANO6*, respectively. *CYP11B2* mRNA expression in response to AngII was 14.6, 20.7, 37.7 and 18.9 fold higher in comparison to basal controls in *EV*, *ANO1*, *ANO4* and *ANO6* transfected cell, respectively. Ang II stimulated *CYP11B2* mRNA expression was significantly higher in *ANO1* and *ANO4* vs stimulated VE (* P<0.05). Results are expressed as geometric mean values with SEM and compared using one-way ANOVA. The significance level of P<0.05 was considered to indicate statistical significance.

4.4.7.2 YFP Assay

To evaluate the activity of ANO4 as CaCC, we performed an YFP assay in collaboration with Dr Galietta's group.

YFP is a quantitative screening procedure for analysis of halide cellular transport. Transfected cell expressing anoctamins together with a yellow fluorescent protein (YFP)-based halide sensor were used.

CaCC function was assayed from the time course of cell fluorescence in response to extracellular addition of I^- (100 mM) followed by Ionomycin, resulting in decreased YFP fluorescence due to CaCC-mediated I^- entry. As shown in Figure 4.24, $[Ca^{2+}]_i$ elevation triggered by ionomycin caused a very large flow of iodide in cells expressing ANO1 and ANO2 which are CaCCs. ANO4's activity is much lower although significantly higher than that of ANO5, which is a protein with prevalent intracellular localization (Duran, Qu, Osunkoya, Cui, & Hartzell, 2012) ($n = 12–15$ experiments, $P< 0.05$ vs ANO1, Figure 4.23).

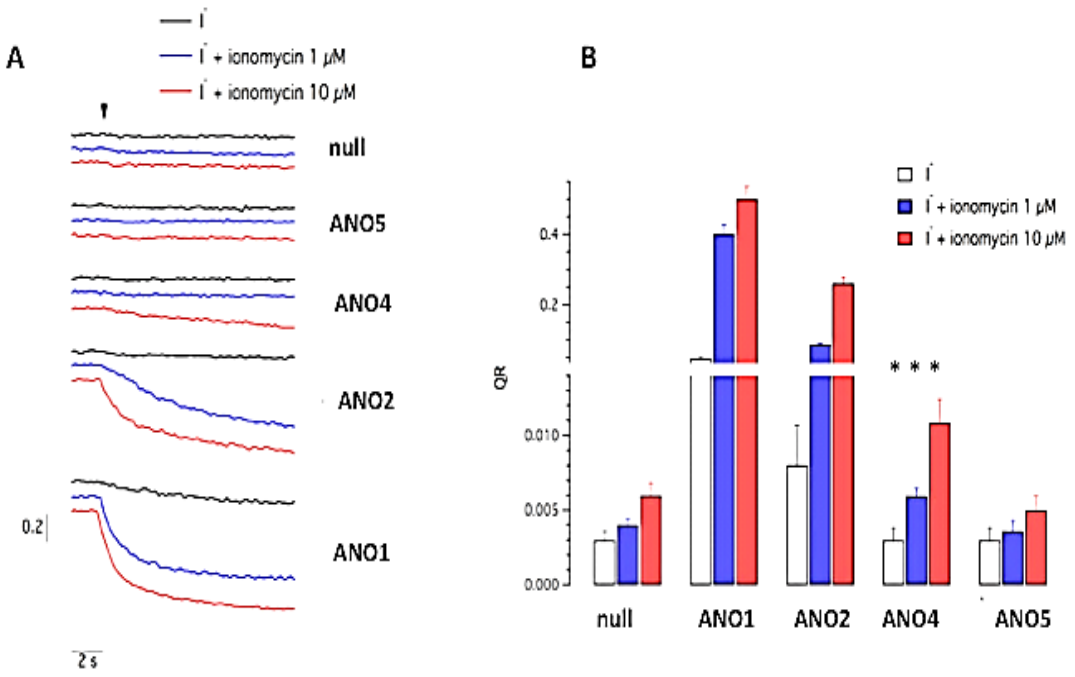

Figure 4.23: Functional evaluation of ANO4 with the halide-sensitive (HS)- yellow fluorescent protein (YFP) assay.
A: Representative traces of HS-YFP experiments. B: Anion transport measured with the HS-YFP assay in HEK-293 cells transfected with the indicated constructs. Data are shown as quenching rate (QR) calculated by fitting the fluorescence decay caused by extracellular I^- addition. White bars: anion transport without intracellular Ca^{2+} elevation. Blue bars: anion transport in cells stimulated with 1 μM ionomycin. Red bars: anion transport in cells stimulated with Ionomycin 10μM (*P< 0.05 vs ANO1). Experiments performed at Dr Galietta's laboratory.

4.4.7.3 XTT assay

Because of the discrepancy between aldosterone and *CYP11B2* mRNA results, and because of the previous literature describing an association between CaCCs and cell proliferation, we decided to evaluate the proliferation of cells transfected with *ANO1*, *ANO4* and *ANO6* plasmids, in basal or stimulated conditions, at XTT assay.

The cells were seeded in 96-well plate at a density of $4x10^5$ cells/well in 100 µL of culture medium and transfected with Lipofectamine. At 48 hours from transfection the assay was performed: cells were incubated for 2 hours at 37°C in a CO2 incubator. The plate was read at 450 nm in a plate reader and absorbance date showed as Relative Units (RU).

At 48 hours from transfection, cell viability increased in all anoctamins, and the 450 nm absorbance increased from 0.28 of controls to 0.47, 0.41 and 0.42 RU in ANO1, ANO4 and ANO6 (N=9, *P<0.05, Figure 4.24).

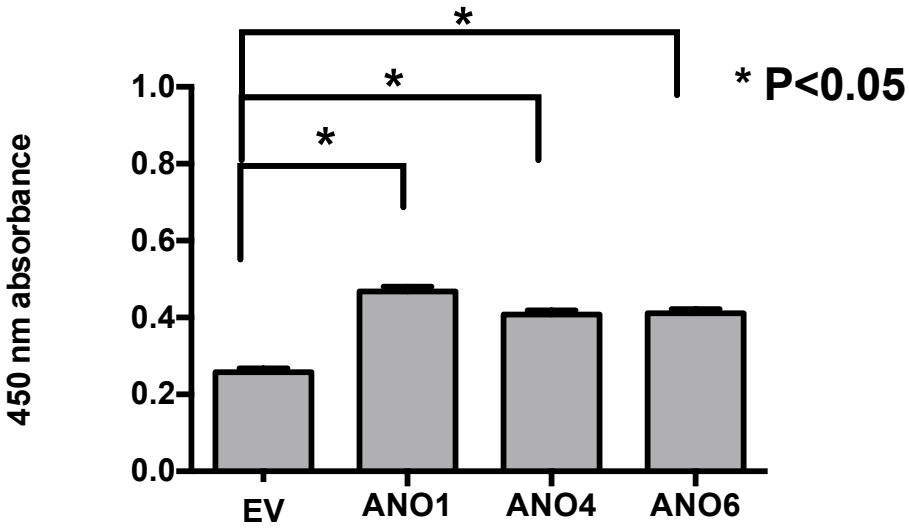

Figure 4.24: Effects of Anoctamins overexpression on the viability of H295R cells. All three anoctamins caused an increase of cell viability compared to empty vector (EV). (*P<0.05). Results are expressed as mean values with SEM and compared using multiple t-test. The significance level of P<0.05 was considered to indicate statistical significance.

Similarly, we have found the same increase of viability in response to AngII was bigger in *ANO1*, *ANO4* and *ANO6* in comparison to stimulated controls

as the 450 nm absorbance increased from 0.32 of controls to 0.57, 0.47 and 0.45 RU in *ANO1*, *ANO4* and *ANO6*, respectively (N=9, P<0.05, Figure 4.25).

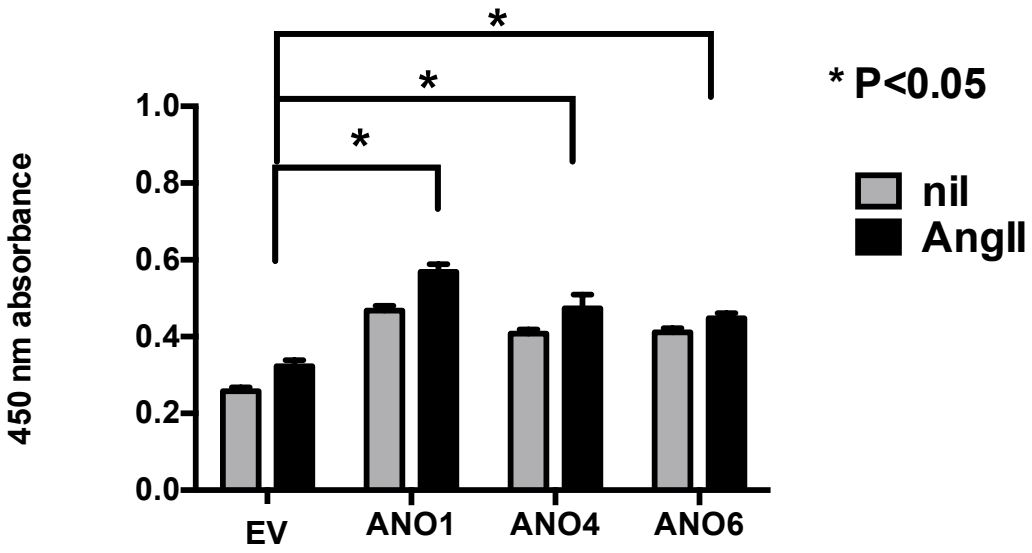

Figure 4.25: Effects of ANO1, ANO4 and ANO6 overexpression on cell viability at baseline and in response to Ang II in H295R cells, evaluated at XTT assay. The increase of viability in response to AngII was bigger in ANO1, ANO4 and ANO6 in comparison to stimulated controls as the 450 nm absorbance increased from 0.32 of controls to 0.57, 0.47 and 0.45 RU in ANO1, ANO4 and ANO6, respectively (*P<0.05). Results are expressed as mean values with SEM and compared using multiple t-test. The significance level of P<0.05 was considered to indicate statistical significance.

We have also tested the effects of Ionomycin 1 μM and observed that viability of H295R cells increases significantly only in ANO1 transfected cells in comparison to treated controls, whereas it was not affected in ANO1 and ANO6 transfected cells (N=9, P<0.05, Figure 4.26).

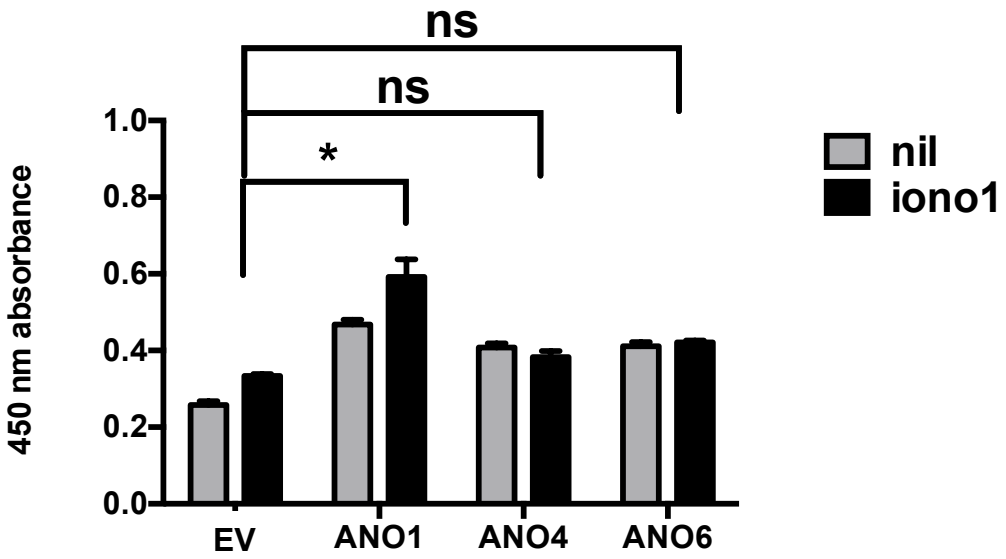

Figure 4.26: Effect of ANO1, ANO4 and ANO6 overexpression in H295R on cell viability at baseline and in response to Ionomycin, as evaluated at XTT assay. The viability increases significantly only in ANO1 transfected cells in comparison to treated controls, whereas it was not affected in ANO1 and ANO6 transfected cells (*P<0.05). Results are expressed as mean values with SEM and compared using multiple t-test. The significance level of P<0.05 was considered to indicate statistical significance.

Overall, the results from the comparison of ANO4 with ANO1 and ANO6 on their effects on aldosterone secretion and synthesis and cell proliferation in H295R cells in basal and stimulated conditions are synthesized in Table 4.1.

	Aldo	Aldo (AngII)	Proliferation (basal)	Proliferation (AngII)	Proliferation (Ionomycin)	YFP Assay
ANO1	↑	↑	↑	↑	↑	CaCC
ANO4	ns	↓	↑	↑	ns	no currents
ANO6	ns	ns	↑	↑	ns	NA

Table 4.1: Summary of the results of the comparison of Anoctamin overexpression effects on H295R cells, including a summary of the results from YFP assay. Aldo: aldosterone. Proliferation is referred to the XTT results. NA: not available.

From our experiments we can conclude that:

1) ANO1, ANO4 and ANO6 stimulate cell proliferation in basal and AngII stimulated condition, although intracellular calcium increase triggered by the Ionomycin stimulates cell proliferation in ANO1 transfected cells only.
2) Aldosterone secretion tends to increase in basal condition in ANO1 and ANO4 only. In stimulated conditions, ANO1 tends to stimulate aldosterone secretion while ANO4 counteract the secretagogue action.
3) *CYP11B2* mRNA expression increases was significantly higher in ANO1 and ANO4 in baseline and AngII stimulated conditions.
4) Only ANO1 and ANO2 generate CaCC mediated currents. ANO4 cannot be considered a CaCC as only at high concentrations of Ionomycin generates a small I^- flux.
These results suggest that ANO4 is not a CaCC. It generates small iodide currents in transfected HEK293 cells at YFP assay only at very high concentrations of Ionomycin but the fluorescence quenching curve does do not resemble that of classical CaCCs such as ANO1 and ANO2.

However, some biological effects (mainly on AngII stimulated aldosterone secretion and synthesis) are similar to those of ANO1.

4.5 Discussion

ANO4 was the third of the 7 genes up regulated in ZG vs ZF by at least >10-fold (*LGR5, VSNL1, ANO4, NEFM, VCAN, DACH1,* and *NR4A2*).

ANO4 mRNA expression was 19.9-fold higher in ZG vs ZF. Moreover, ANO4 resulted to be 9.3 -fold downregulated in APAs vs ZG.

Microarray data were confirmed by qPCR performed on the LCM samples. Accordingly, IHC demonstrated that ANO4 protein was highly and selectively expressed in human ZG. Its expression was mainly cytoplasmic.

ANO4 is one of the members of anoctamin family, which includes 10 proteins. Among them, only ANO1 and ANO2 have been confirmed to be CaCC and contrasting data exist for the other members.
ANO1 has a ubiquitously expression pattern, ANO2 expression appears to be selective for the nervous system. They also differ in terms of sensitivity for $[Ca^{2+}]_{i,}$ as the response threshold to its increases is higher for ANO2 than ANO1.

CaCCs conducted currents have been observed in almost all tissues, with different physiological functions. CaCCs mediate the Cl^- secretion in secretory epithelia, such as gastrointestinal, airways, salivary glands, and pancreatic ducts cells.
CaCC currents have been recorded in excitable cells such as neurons, smooth muscles, and cardiac muscles. CaCCs are activated by $[Ca^{2+}]_i$, have an outwardly rectifying current voltage relationship and show greater current amplitude in a depolarization state than at hyperpolarization.

ANO1 plays a role not only in the aforementioned cells in the exocrine function, but it regulates cell proliferation in normal tissues and tumours.

ANO2 is mainly expressed in neuronal cells and can play a role in the synapses of olfactory cells and in hippocampus.
ANO3 is expresses in neurons involved in nociception (Huang et al. 2013).
ANO5 is mainly found in muscles and bones. It is not localized in the plasma membrane and is not a channel. Mutations in ANO5 have been found in gnathodiaphyseal dysplasia and muscular dystrophy (Bolduc et al. 2010).
ANO6 is a Fas ligand-activated Cl^- channel and a Ca^{2+} dependent scramblase that transports phospholipids bi-directionally between the two leaflets. A mutation of ANO6 that truncates the ANO6 protein is associated with a rare bleeding disease, the Scott syndrome.

Controversial data have been published about ANO3–10 members. Some authors found that ANO3-7 are intracellular proteins with no activity as CaCC (Duran et al. 2012).
On the other hand, another group has previously showed that most anoctamins overexpressed in the same cell line, HEK293, were expressed on cell membrane (Schreiber et al. 2010).

It has previously been reported that ANO4, overexpressed in HEK293, localized at plasma membrane level and, when co-expressed with purinergic receptor P2Y2, it can conduct currents activated by ATP or by ionomycin. In particular stimulation of purinergic receptors, through an increase of $[Ca^{2+}]i$, depolarized membrane voltages in all anoctamins transfected cells except ANO4, which hyperpolarized the cells. (Y Tian et al. 2012).

Suzuki et al showed that ANO4 constitutively behaves as a scramblase, and its activity is even stronger than ANO6 with specific affinity for some phospholipids. No CaCC activity was found when they measured whole cell current in transfected HEK293 cells.
Duran et al. found the same result in the same cell system, where ANO4 does not localise on the plasma membrane, but its localisation is intracellular. This

subcellular distribution of ANO4 is consistent with the lack of finding of chloride currents (Suzuki et al. 2013; Duran et al. 2012).

Herein we report some functional studies on *ANO4*, which has never been associated to adrenal cortex endocrine function before.

Functional analyses, using H295R as a model of aldosterone producing cells, showed that *ANO4* plays a role in steroidogenesis as its overexpression and silencing modulate *CYP11B2* mRNA levels although not accompanied to any change in aldosterone secretion.

Stimulated aldosterone secretion by AngII or calcium agonists was instead affected by *ANO4* overexpression as we have observed that the degree of aldosterone secretion in response to these drugs is lower than controls.

As mentioned before, anoctamin family includes both CaCCs (such as ANO1 and ANO2) and scramblase (such as ANO6). In order to understand whether ANO4 behaves as one of the other members of its family, we have compared the effects of ANO1, ANO4 and ANO6 on aldosterone secretion, both basal and AngII stimulated.

Overall, from the comparison of ANO4 with ANO1 and ANO6 we can conclude that the three anoctamins stimulate cell proliferation in basal and AngII stimulated condition, although calcium ionophore ionomycin stimulates cell proliferation only in ANO1 transfected cells.
Aldosterone secretion tends to increase in basal condition in ANO1 and ANO4 only. In stimulated conditions, ANO1 tends to stimulate aldosterone secretion while ANO4 counteract the secretagogue action. ANO6 did not affect aldosterone production.
CYP11B2 mRNA expression increases was significantly higher in ANO1 and ANO4 in baseline and AngII stimulated conditions.

YFP assay showed that only ANO1 and ANO2 generate CaCC mediated currents. ANO4 cannot be considered a CaCC as only at high concentrations of Ionomycin generates a small I^- flux.
These results suggest that ANO4 is unlikely to be a CaCC. It generates small iodide currents in transfected HEK293 cells at YFP assay only at very high concentrations of Ionomycin but the fluorescence quenching curve does not resemble that of classical CaCCs such as ANO1 and ANO2.
However, some biological effects (mainly on AngII stimulated aldosterone secretion and synthesis) are similar to those of ANO1.

Consistent with the IHC findings in human ZG and kidney, immunofluorescence staining of ANO4-transfected cells (both HEK293 and H295R) showed cytoplasmic staining. This expression pattern may suggest that ANO4 is unlikely to be an ion channel. It is worth to mention that the chloride currents recorded before in the adrenocortical cells are different from CaCCs.

Overall, these experiments have demonstrated that *ANO4*, similarly to our previously described ZG-selective up regulated genes (*NEFM*, *LGR5*, and *DACH1*), inhibits rather than stimulates aldosterone secretion in a condition of $[Ca^{2+}]_i$ increase.

We have used a screening assay in HEK293 cells and did not manage to prove that ANO4 is a CaCC. There are some caveats about these conclusions: first of all, we did not use the gold standard technique for detection of ion channel function, the patch-clamp.

The second consideration is that the YFP assay was performed in HEK293 cell line whose electrophysiological properties (in terms of channels expression and physiological membrane potential) differ from those of the cell line used for the functional experiments, H295R cells.

The third caveat regards the co-expression of *ANO4* with receptors (such as

AngII or purinergic receptors) or other anoctamins, which may be necessary for a functional ANO4.
Further experiments to investigate the function of ANO4 as scramblase in the H295R or primary cells have to be considered.

In conclusion, we found that *ANO4* is a novel selective ZG gene which negatively regulates stimulated aldosterone secretion and synthesis and a positively affects cell viability. It was not possible to conclusively establish a possible function of ANO4 in the adrenocortical cells, as we just excluded its function as a CaCC but did not manage to investigate other possible currents conducted nor scramblase activity.

Chapter 5: Overall discussion and perspectives

The physiological function of aldosterone played a role in the evolutionary passage from aquatic to terrestrial life. The development of aldosterone/mineralocorticoid receptor system was necessary and functional to the adaptation to land life in a little salt and water environment if compared to the seawater (Williams 2005).

Nowadays, excessive salt intake (9-12 g/day), a feature of the diet in most countries, is linked to elevated blood pressure and cardiovascular diseases.

As a feature of our species, *CYP11B2* expression ZG shows a patchy expression in human adult adrenal. Only few cell clusters, the APCCs, are positive for *CYP11B2*, thus suggesting that the human ZG tends to produce less aldosterone. Similar IHC studies in the rodent adrenal have showed that aldosterone synthase is expressed all over the ZG and its expression increases in salt-deprived conditions (Nishimoto et al., 2014).

In our study, we have differentiated ZG from ZF cells by using cresyl violet and collected the RNA from the two layers by LCM. Therefore, most of the ZG RNA was from non-APCCs cells.

The transcriptome comparison of ZG vs ZF discovered several up regulated ZG genes.

We have found that two of the top hit ZG genes, *ANO4* and *NEFM*, inhibited rather than stimulate aldosterone production, *ANO4* in response to secretagogues, *NEFM* by regulating dopamine suppression.

Similarly, *LGR5* and *DACH1*, the first and sixth “ZG genes” in our microarray assay, also inhibited aldosterone production (Shaikh et al. 2015; Zhou et al. 2015).

These results support our hypothesis that the adult human adrenal tries to reduce aldosterone secretion and its mineralocorticoid action as a result of chronic exposure to high salt from the diet. However, the effects of chronic salt exposure on human ZG gene expression profile will require further investigation.

Of interest, one of the top hit ZG genes investigated in this study, *NEFM* is 4-fold down-regulated in ZF-like APAs carrying *KCNJ5* mutations. *NEFM* expression levels directly correlate with *KCNJ5* mutational status, as demonstrated by transfection of mutant *KCNJ5* in adrenocortical cell line H295R and in primary cells from ZG-like APAs highly expressing *NEFM*.
These results suggest that the down-regulation of some of the ZG genes such as *NEFM* could be not only a signature of ZF-like APAs but one of the events necessary for the tumorigenesis of this APA subtype and give more hints about their cell origin.

Paradoxically, *KCNJ5* mutant APAs histologically and biochemically resemble cortisol producing ZF but, rather than from a mutant ZF cell, they are more likely to arise from ZG cells harbouring a mutation in *KCNJ5* affecting the cell phenotype and gene expression profile.
On the other hand, APCCs cells have the same mutations in *CACNA1D* or *ATP1A1* genes as the small ZG-like APAs, and this observation could suggest that *CYP11B2* positive cells in the ZG may be pre-tumorous lesions.

Further investigation in terms of single cell RNA seq of *KCNJ5* mutant transfected cells is required.

In the attempt to identify the functional role of *NEFM* in the adrenal, we have observed that *NEFM* silencing significantly amplified aldosterone response to dopamine D1R agonists and antagonist.
Dopamine is one of the main inhibitors of aldosterone secretion. It action is mediated by D2R activation, with final cAMP synthesis inhibition. D2R antagonist metoclopramide in fact stimulates aldosterone secretion.
Interestingly, high sodium intake reduces aldosterone response to metoclopramide, and stimulates urinary dopamine excretion in normal individuals.
While rat adrenal ZG expresses both D1R and D2R at mRNA and protein level, and is positive for specific binding sites for both receptors, the human ZG expresses D1-like and D2-like receptors at mRNA level (Pivonello et al. 2004), but autoradiographic studies have identified only D2R binding sites

(Amenta et al. 1994).
Here we have showed that *NEFM*, highly expressed in ZG, is responsible of the intracellular redistribution of D1R whose activation by dopamine could cause a stimulation rather than inhibition of aldosterone secretion. For this reason, D1R is expressed but internalized, not available for dopamine binding, and not traceable at autoradiographic studies.

Similarly to normal glomerulosa cells, small ZG-like *KCNJ5* wild-type APAs highly expressed *NEFM*, as a preserved ZG feature, whereas it was 4-fold downregulated in *KCNJ5* mutant APAs.
This different expression levels were also correlated to different D1R staining pattern and different response to D1R activation: ZG-like APA cells retained D1R at cytoplasmic level, and fenoldopam stimulation of aldosterone in primary cells from this subtype was smaller than in those from *KCNJ5* mutant APAs with membranous expression of D1R.

This diversity has potential clinical implications: the measurement, in either peripheral or adrenal vein plasma, of aldosterone secretion in response to pharmacological D1R activation or blockade could be used as a diagnostic test to differentiate or predict the two APA subtypes.

On the other hand, different responses to dopaminergic drugs have already been described in APAs. Before the discovery of somatic mutations in APAs, differences in cellular composition had been correlated to different responses to D2R antagonist metoclopramide.
Wu et al. in 1995 described that the increase of aldosterone after metoclopramide is inversely correlated with the percentage of ZF cells in APA. In other words, ZF-like APAs aldosterone secretion in response to metoclopramide is minor than in ZG-like APAs, thus suggesting a lower degree of dopaminergic inhibition (Wu et al. 1995).
The same group found that D2R and D4R are expressed at mRNA level in normal ZG and that their expression in APA is inversely proportional to the percentage of ZF-cells (Wu et al. 2001).

The two APA subgroups patients present also different responses of aldosterone secretion to metoclopramide on changes of salt intake: a subgroup with less dopaminergic inhibition and less urinary dopamine excretion and greater BP elevation on high salt diet (Wu et al. 2002).

Here we postulate that *KCNJ5* mutant ZF-like APAs have a D1R/D2R imbalance, due not only to the previously reported D2R down-regulation but also to the D1R localisation at plasma membrane level.
The consequences of different mutations are not only on the cellular composition but also on responsiveness to dopaminergic drugs.

ANO4 was the second gene subject of this PhD. A member of anoctamin family, *ANO4* is a novel selective ZG gene. It differs from *NEFM* as its expression in APAs does not differ from ZF and is not affected by APA genotype and subtype.
We found that *ANO4* negatively regulates stimulated aldosterone secretion and regulates cell proliferation. An intracellular protein, it did not conduct currents at YFP thus excluding a function as CaCC.
It generates small iodide currents, and only at very high concentrations of Ionomycin, in transfected HEK293 cells as detected by YFP assay, but the fluorescence quenching curve does do not resemble that of classical CaCCs such as ANO1 and ANO2.
The comparison of *ANO4* with *ANO1* and *ANO6* effects on basal and stimulated aldosterone secretion and cell proliferation found that all of them stimulate cell proliferation in basal conditions and following AngII stimulation.
Aldosterone secretion tends to increase in basal condition in ANO1 and *ANO4* only. In stimulated conditions, *ANO1* tends to stimulate aldosterone secretion while *ANO4* counteract the secretagogue action.
These results suggest that *ANO4* is unlikely to be a CaCC. However, some biological effects (mainly on AngII stimulated aldosterone secretion and synthesis) are similar to those of ANO1.

Although we did not manage to conclusively determine its function in the adrenocortical cells, *ANO4* negative regulation of steroidogenesis is

consistent with that found for other ZG selective genes, including *NEFM*, found at our microarray study (Shaikh et al., 2015; Zhou et al., 2015).

Our studies present several limitations. First of all, the adrenal samples used for the collection of RNA do not include completely normal adrenals, but are from APAs and Phaeocromocytoma patients, the latter included as they in a sense represent the opposite spectrum to PA patients in terms of sodium balance.

Second, the immortalized adrenal cell line, H295R, is not a perfect model for native ZG cells. H295R cells were derived from a human adrenal carcinoma and secrete androgens and cortisol besides aldosterone (Wang et al. 2012). We have therefore for selected experiments supported the cell line data with data from primary human adrenal cells from ZG and ZF-like APAs.
Future improvements to the study could be done by culturing separately ZG and ZF cells or from an immortalized cell line derived from these layers to be used to silence or overexpress genes in primary cells. The absence of an animal model of APA affects the choice of models to be used to investigate these genes.

In summary, two novel genes appeared to be up-regulated in ZG vs ZF as the result of a whole transcriptome comparison of pathological (APAs) and physiological (adjacent ZG) sites for aldosterone production and of ZG with paired cortisol producing ZF.

In addition, we have found that *ANO4* and *NEFM*, genes highly up-regulated in human ZG, inhibit aldosterone secretion, the first in response to secretagogues, the second as part of dopamine inhibition, since it affects dopamine receptor D1R trafficking in human ZG and in ZG-like APAs.

The two APA subtypes' heterogeneity can be explained by genotype, biochemical and transcriptome differences. *NEFM* downregulation in *KCNJ5* mutant APAs is an example of this diversity, which has potential clinical, translational consequences.

The inhibitory effects of ZG up-regulated genes on aldosterone production may represent an attempt to respond to chronic high salt intake action on the cardiovascular and renal system.

List of publications and conference papers following my work during the PhD

In *Italics* the publications I am co-author of, but which are not part of my PhD projects.

- Neurofilament Medium Polypeptide (NEFM), a marker for Zona Glomerulosa Cells in Human Adrenal, Inhibits Dopamine Receptor (D1) Mediated Secretion of Aldosterone Maniero C, Garg S, Zhao W, Johnson TI, Zhou J, Gurnell M, Brown MJ. Hypertension. 2017 Aug;70(2):357-364.
- *Regulation of aldosterone secretion by Cav1.3. Xie CB, Haris Shaikh L, Garg S, Tanriver G, Teo AE, Zhou J, Maniero C, Zhao W, Kang S, Silverman RB, Azizan EA, Brown MJ. Sci Rep. 2016 Apr 21;6:24697.*
- *DACH1, a Zona Glomerulosa Selective Gene in the Human Adrenal, Activates Transforming Growth Factor-β Signaling and Suppresses Aldosterone Secretion. Zhou J, Shaikh LH, Neogi SG, McFarlane I, Zhao W, Figg N, Brighton CA, Maniero C, Teo AE, Azizan EA, Brown MJ. Hypertension. 2015 May;65(5):1103-10.*
- Role of ANO4 in regulation of aldosterone secretion in the zona glomerulosa of the human adrenal gland. Maniero C, Zhou J, Shaikh LH, Azizan EA, McFarlane I, Neogi S, Scudieri P, Galietta LJ, Brown MJ. Lancet. 2015 Feb 26;385 Suppl 1:S62.
- *Somatic mutations in ATP1A1 and CACNA1D underlie a common subtype of adrenal hypertension. Azizan EA, Poulsen H, Tuluc P, Zhou J, Clausen MV, Lieb A, Maniero C, Garg S, Bochukova EG, Zhao W, Shaikh LH, Brighton CA, Teo AE, Davenport AP, Dekkers T, Tops B, Küsters B, Ceral J, Yeo GS, Neogi SG, McFarlane I, Rosenfeld N, Marass F, Hadfield J, Margas W, Chaggar K, Solar M, Deinum J, Dolphin AC, Farooqi IS, Striessnig J, Nissen P, Brown MJ. Nat Genet. 2013 Sep;45(9):1055-60.*

References

Åkerström, T. et al., 2012. Comprehensive re-sequencing of adrenal aldosterone producing lesions reveal three somatic mutations near the *KCNJ5* potassium channel selectivity filter. PLoS ONE, 7(7).

Åkerström, T. et al., 2016. Activating mutations in CTNNB1 in aldosterone producing adenomas. Sci Rep, 6, 19546.

Amenta, F. et al., 1994. Pharmacological characterization and autoradiographic localization of dopamine receptors in the human adrenal cortex. Eur J Endocrinol, 131(1), pp.91–96.

Ahmed, A. H., et al. 2011 'Quality of life in patients with bilateral primary aldosteronism before and during treatment with spironolactone and/or amiloride, including a comparison with our previously published results in those with unilateral disease treated surgically', J Clin Endocrinol Metab, 96(9), pp. 2904-11.

Ayoub, C. et al., 2010. ANO1 amplification and expression in HNSCC with a high propensity for future distant metastasis and its functions in HNSCC cell lines. Br J Cancer, 103(5), pp.715–726.

Azizan, E.A. et al., 2012. Microarray, qPCR, and *KCNJ5* Sequencing of Aldosterone-Producing Adenomas Reveal Differences in Genotype and Phenotype between Zona Glomerulosa- and Zona Fasciculata-Like Tumors. Journal of Clinical Endocrinology & Metabolism, 97(5), pp.E819–E829.

Azizan, E.A. et al., 2012. Somatic mutations affecting the selectivity filter of *KCNJ5* are frequent in 2 large unselected collections of adrenal aldosteronomas. Hypertension, 59(3), pp.587–591.

Azizan, E.A. et al., 2013. Somatic mutations in *ATP1A1* and *CACNA1D* underlie a common subtype of adrenal hypertension. Nat Genet, 45(9), pp.1055–1060.

Bassett, M.H. et al, 2004. A role for the NGFI-B family in adrenal zonation and adrenocortical disease. Endocr Res, 30(4), pp.567–574.

Beitner-Johnson, D.et al, 1992. Neurofilament proteins and the mesolimbic dopamine system: common regulation by chronic morphine and chronic cocaine in the rat ventral tegmental area. J Neurosci, 12(6), pp.2165–2176.

Beuschlein, F. et al., 2013. Somatic mutations in *ATP1A1* and *ATP2B3* lead to aldosterone-producing adenomas and secondary hypertension. Nature Genetics, 45(4), pp.440–444.

Bolduc, V. et al., 2010. Recessive Mutations in the Putative Calcium-Activated Chloride Channel Anoctamin 5 Cause Proximal LGMD2L and Distal MMD3 Muscular Dystrophies. American Journal of Human Genetics, 86(2), pp.213–221.

Boulkroun, S. et al., 2012. Prevalence, clinical, and molecular correlates of *KCNJ5* mutations in primary aldosteronism. Hypertension, 59(3), pp.592–598.

Calmon, M.F. et al., 2015. Epigenetic silencing of neurofilament genes promotes an aggressive phenotype in breast cancer. Epigenetics, 10(7), pp.622–632.

Caputo, A. et al., 2008. TMEM16A, a membrane protein associated with calcium-dependent chloride channel activity. Science, 322(5901), pp.590–594.

Carss, K.J. et al., 2011. Further study of chromosome 7p22 to identify the molecular basis of familial hyperaldosteronism type II. Journal of human hypertension, 25(9), pp.560–564.

Charmandari, E. et al., 2012. A Novel Point Mutation in the *KCNJ5* Gene Causing Primary Hyperaldosteronism and Early-Onset Autosomal Dominant Hypertension. The Journal of Clinical Endocrinology & Metabolism, 97(8), pp.E1532–E1539.

Choi, M. et al., 2011. K+ channel mutations in adrenal aldosterone-producing adenomas and hereditary hypertension. Science, 331(6018), pp.768–772.

Chorvatova, A. et al., 1998. Activation by angiotensin II of Ca(2+)-dependent K+ and Cl- currents in zona fasciculata cells of bovine adrenal gland. J Membr Biol, 162(1), pp.39–50.

Chorvatova, A. et al., 1999. Characterization of an ACTH-induced chloride current in rat adrenal zona glomerulosa cells. Endocr Res, 25(2), pp.173–178.

Chorvátová, A. et al., 2000. A Ras-dependent chloride current activated by adrenocorticotropin in rat adrenal zona glomerulosa cells. Endocrinology, 141(2), pp.684–692.

Conn, J.W., 1955. Primary aldosteronism, a new clinical syndrome. The Journal of laboratory and clinical medicine, 45(1), pp.3–17.

Conn, J.W. & Louis, L.H., 1956. Primary Aldosteronism, A New Clinical Entity. Ann Intern Med, 44, pp.1–15.

Davies, L. A. et al., 2008. TASK channel deletion in mice causes primary hyperaldosteronism. Proc Natl Acad Sci U S A, 105(6), 2203-2208.

Delyani, J. A. 2000. Mineralocorticoid receptor antagonists: the evolution of utility and pharmacology. Kidney Int, 57(4), 1408-1411.

Dubrowinskaja, N. et al., 2014. Neurofilament Heavy polypeptide CpG island methylation associates with prognosis of renal cell carcinoma and prediction of antivascular endothelial growth factor therapy response. Cancer medicine, 3(2), pp.300–309.

Duran, C. et al., 2012. ANOs 3-7 in the anoctamin/Tmem16 Cl- channel family are intracellular proteins. Am J Physiol Cell Physiol, 302(3), pp.C482-893.

Edwards, C.R.W. et al., 1980. In vivo and in vitro studies on the effect of metoclopramide on aldosterone secretion. Clinical Endocrinology, 13(1), pp.45–50.

Ehlers, M.D. et al., 1998. Splice variant-specific interaction of the NMDA receptor subunit NR1 with neuronal intermediate filaments. The Journal of neuroscience, 18(2), pp.720–730.

Ehlers, M.D. et al., 1995. Regulated subcellular distribution of the NR1 subunit of the NMDA receptor. Science (New York, N.Y.), 269(5231), pp.1734–1737.

Fallo, F., et al. 2006. Prevalence and characteristics of the metabolic syndrome in primary aldosteronism. The Journal of Clinical Endocrinology & Metabolism; 91(2):454-459.

Fernandes-Rosa, F.L. et al., 2014. Genetic spectrum and clinical correlates of somatic mutations in aldosterone-producing adenoma. Hypertension, 64(2), pp.354–361.

Funder, J.W. et al., 2016. The Management of Primary Aldosteronism: Case Detection, Diagnosis, and Treatment: An Endocrine Society Clinical Practice Guideline. The Journal of clinical endocrinology and metabolism,

101(May), p.jc20154061.

Galietta, L. V, Jayaraman, S. & Verkman, A.S., 2001. Cell-based assay for high-throughput quantitative screening of CFTR chloride transport agonists. Am J Physiol Cell Physiol, 281(5), pp.C1734-42.

Gazdar, A.F. et al., 1990. Establishment and Characterization of a Human Adrenocortical Carcinoma Cell Line That Expresses Multiple Pathways of Steroid Biosynthesis. Cancer Research, 50(17).

Geller, D.S. et al., 2008. A novel form of human mendelian hypertension featuring nonglucocorticoid-remediable aldosteronism. J Clin Endocrinol Metab, 93(8), pp.3117–3123.

Giacchetti, G., et al. 2007. Aldosterone as a key mediator of the cardiometabolic syndrome in primary aldosteronism: an observational study. *J Hypertens, 25*(1), 177-186.

Graham, F.L. et al., 1977. Characteristics of a human cell line transformed by DNA from human adenovirus type 5. Journal of General Virology, 36(1), pp.59–72.

Grubb, S. et al., 2013. TMEM16F (Anoctamin 6), an anion channel of delayed Ca(2+) activation. J Gen Physiol, 141(5), pp.585–600.

Guagliardo, N. A. et al., 2012. TASK-3 channel deletion in mice recapitulates low-renin essential hypertension. Hypertension, 59(5), 999-1005.

Hattangady, N.G. et al., 2012. Acute and chronic regulation of aldosterone production. Mol Cell Endocrinol, 350(2), pp.151–162.

Heinze, C. et al., 2014. Disruption of vascular Ca2+-activated chloride currents lowers blood pressure. The Journal of clinical investigation, 124(2), pp.675–686.

Hiramatsu, K. et al., 1981. A screening test to identify aldosterone-producing adenoma by measuring plasma renin activity. Results in hypertensive patients. Archives of internal medicine, 141(12), pp.1589–1593.

Huang, F. et al., 2013. TMEM16C facilitates Na(+)-activated K+ currents in rat sensory neurons and regulates pain processing. Nat Neurosci, 16(9), pp.1284–1290.

Jung, J. et al., 2012. Variations in the potassium channel genes KCNK3 and KCNK9 in relation to blood pressure and aldosterone production: an exploratory study. J Clin Endocrinol Metab, 97(11), E2160-2167.

Kempers, M.J. et al., 2009. Systematic review: diagnostic procedures to differentiate unilateral from bilateral adrenal abnormality in primary aldosteronism. Ann Intern Med, 151(5), pp.329–337.

Kim, O.-J. et al., 2002. Neurofilament-M interacts with the D1 dopamine receptor to regulate cell surface expression and desensitization. The Journal of neuroscience : the official journal of the Society for Neuroscience, 22(14), pp.5920–5930.

Kmit, A. et al., 2013. Calcium-activated and apoptotic phospholipid scrambling induced by Ano6 can occur independently of Ano6 ion currents. Cell Death Dis, 4, p.e611.

Kovacs, K., et al., 2010. Effect of nicotine and cocaine on neurofilaments and receptors in whole brain tissue and synaptoneurosome preparations. Brain Research Bulletin, 82(1–2), pp.109–117.

Lifton, R. P. et al., 1992. Hereditary hypertension caused by chimaeric gene duplications and ectopic expression of aldosterone synthase. Nat Genet, 2(1), 66-74.

Martins, J.R. et al., 2011. Anoctamin 6 is an essential component of the outwardly rectifying chloride channel. Proc Natl Acad Sci U S A, 108(44), pp.18168–18172.

Mulatero, P. et al., 2012. *KCNJ5* mutations in European families with nonglucocorticoid remediable familial hyperaldosteronism. Hypertension, 59(2), pp.235–240.

Nishi, H. et al., 2013. NCI-H295R, a Human Adrenal Cortex-Derived Cell Line, Expresses Purinergic Receptors Linked to Ca2+-Mobilization/Influx and Cortisol Secretion. PLoS ONE, 8(8).

Nishimoto, K. et al., 2015. Aldosterone-stimulating somatic gene mutations are common in normal adrenal glands. Proceedings of the National Academy of Sciences of the United States of America, 112(33), pp.E4591-4599.

Nishimoto, K. et al., 2014. Sodium deficiency regulates rat adrenal zona glomerulosa gene expression. Endocrinology, 155(4), 1363-1372.

Nunez, L. et al., 2006. Cell proliferation depends on mitochondrial Ca2+ uptake: inhibition by salicylate. J Physiol, 571(Pt 1), 57-73.

Pedemonte, N. et al., 2014. Structure and function of TMEM16 proteins (anoctamins). Physiological reviews, 94(2), pp.419–459.

Peng, G. et al., 2015. miR-25 promotes glioblastoma cell proliferation and invasion by directly targeting NEFL. Molecular and Cellular Biochemistry, 409(1–2), pp.103–111.

Perrot, R. et al., 2008. Review of the multiple aspects of neurofilament functions, and their possible contribution to neurodegeneration. Molecular Neurobiology, 38(1), pp.27–65.

Pifferi, S., Dibattista, M. & Menini, A., 2009. TMEM16B induces chloride currents activated by calcium in mammalian cells. Pflugers Arch, 458(6), pp.1023–1038.

Pivonello, R. et al., 2004. Dopamine receptor expression and function in human normal adrenal gland and adrenal tumors. J Clin Endocrinol Metab, 89(9), pp.4493–4502.

Rock, J.R., Futtner, C.R. & Harfe, B.D., 2008. The transmembrane protein TMEM16A is required for normal development of the murine trachea. Dev Biol, 321(1), pp.141–149.

Rock, J.R. & Harfe, B.D., 2008. Expression of TMEM16 paralogs during murine embryogenesis. Dev Dyn, 237(9), pp.2566–2574.

Rossi, G.P. et al., 2006. A prospective study of the prevalence of primary aldosteronism in 1,125 hypertensive patients. Journal of the American College of Cardiology, 48(11), pp.2293–2300.

Rossi, G. P., 2011. A comprehensive review of the clinical aspects of primary aldosteronism. Nat Rev Endocrinol, 7(8), 485-495.

Scholl, U.I. et al., 2012. Hypertension with or without adrenal hyperplasia due to different inherited mutations in the potassium channel *KCNJ5*. Proceedings of the National Academy of Sciences of the United States of America, 109(7), pp.2533–2538.

Scholl, U.I. et al., 2013. Somatic and germline *CACNA1D* calcium channel mutations in aldosterone-producing adenomas and primary aldosteronism. Nat Genet, 45(9), pp.1050–1054.

Schreiber, R. et al., 2010. Expression and function of epithelial anoctamins. Journal of Biological Chemistry, 285(10), pp.7838–7845.

Schroeder, B.C. et al., 2008. Expression cloning of TMEM16A as a calcium-activated chloride channel subunit. Cell, 134(6), pp.1019–1029.

Seccia, T. M. et al., 2012. Somatic mutations in the KCNJ5 gene raise the lateralization index: implications for the diagnosis of primary aldosteronism by adrenal vein sampling. J Clin Endocrinol Metab, 97(12), E2307-2313.

Shaikh, L.H. et al., 2015. LGR5 Activates Noncanonical Wnt Signaling and Inhibits Aldosterone Production in the Human Adrenal. J Clin Endocrinol Metab, 100(6), pp.E836-844.

Shaw, G., et al., 2002. Preferential transformation of human neuronal cells by human adenoviruses and the origin of HEK 293 cells. The FASEB Journal;16(8):869-871.

Shen, Z. et al., 2016. Methylation of neurofilament light polypeptide promoter is associated with cell invasion and metastasis in NSCLC. Biochemical and Biophysical Research Communications, 470(3), pp.627–634.

Spät, A. & Hunyady, L., 2004. Control of aldosterone secretion: a model for convergence in cellular signaling pathways. Physiol Rev, 84(2), pp.489–539.

Stanwood, G.D., et al., 2005. Anatomical abnormalities in dopaminoceptive regions of the cerebral cortex of dopamine D 1 receptor mutant mice. Journal of Comparative Neurology, 487(3), pp.270–282.

Stöhr, H. et al., 2009. TMEM16B, a novel protein with calcium-dependent chloride channel activity, associates with a presynaptic protein complex in photoreceptor terminals. J Neurosci, 29(21), pp.6809–6818.

Strous, R.D. et al., 2007. Association of the dopamine receptor interacting protein gene, NEF3, with early response to antipsychotic medication. Int J Neuropsychopharmacol , 10(3), pp.321–333.

Suzuki, J. et al., 2013. Calcium-dependent phospholipid scramblase activity of TMEM16 protein family members. J Biol Chem, 288(19), pp.13305–13316.

Suzuki, J. et al., 2010. Calcium-dependent phospholipid scrambling by TMEM16F. Nature, 468(7325), pp.834–838.

Taguchi, R. et al., 2012. Expression and mutations of *KCNJ5* mRNA in Japanese patients with aldosterone-producing adenomas. Journal of Clinical Endocrinology and Metabolism, 97(4), pp.1311–1319.

Teo, A.E.D. et al., 2015. Pregnancy, Primary Aldosteronism, and Adrenal *CTNNB1* Mutations. The New England journal of medicine, 373(15), pp.1429–36.

Terry-Lorenzo, R.T. et al., 2000. Neurofilament-L is a protein phosphatase-1-binding protein associated with neuronal plasma membrane and post-synaptic density. J Biol Chem, 275(4), pp.2439–2446.

Tian, Y., et al., 2012. Anoctamins are a family of Ca2+-activated Cl- channels. J Cell Sci, 125(Pt 21), pp.4991–4998.

Tissier, F. et al., 2005. Mutations of β-Catenin in Adrenocortical Tumors: Activation of the Wnt Signaling Pathway Is a Frequent Event in both Benign and Malignant Adrenocortical Tumors. Cancer Research, 65(17), 7622-7627.

Wang, T. et al., 2012. Comparison of aldosterone production among human adrenocortical cell lines. Hormone and Metabolic Research, 44(3), pp.245–250.

Wang, Z. you et al., 2016. Up-Regulation of microRNA-183 Promotes Cell Proliferation and Invasion in Glioma By Directly Targeting NEFL. Cellular

and Molecular Neurobiology, 36(8), pp.1303–1310.

Wang, Z., et al., 2015. Targeting miR-381-NEFL axis sensitizes glioblastoma cells to temozolomide by regulating stemness factors and multidrug resistance factors. Oncotarget, 6(5), 3147-3164.

Williams, G.H., 2005. Aldosterone biosynthesis, regulation, and classical mechanism of action. Heart Failure Reviews, 10(1), pp.7–13.

Williams, T.A. et al., 2016. Genotype-Specific Steroid Profiles Associated With Aldosterone-Producing Adenomas. Hypertension, 67(1), pp.139–145.

Williams, T.A. et al., 2014. Somatic *ATP1A1*, *ATP2B3*, and *KCNJ5* mutations in aldosterone-producing adenomas. Hypertension, 63(1), pp.188–195.

Williams, T.A. et al., 2012. Visinin-like 1 is upregulated in aldosterone-producing adenomas with *KCNJ5* mutations and protects from calcium-induced apoptosis. Hypertension, 59(4), pp.833–839.

Wu, V. C. et al., 2017. The prevalence of CTNNB1 mutations in primary aldosteronism and consequences for clinical outcomes. *Sci Rep, 7*, 39121.

Wu, K.-D. et al., 2002. Dopaminergic Modulation of Aldosterone in Aldosterone-Producing Adenoma. Am J Hypertens, 7061(2), pp.609–614.

Wu, K.D. et al., 2001. Expression and localization of human dopamine D2 and D4 receptor mRNA in the adrenal gland, aldosterone-producing adenoma, and pheochromocytoma. J Clin Endocrinol Metab, 86(9), pp.4460–4467.

Wu, K.D. et al., 1995. Zona Fasciculata-Like Cells Determine the Response of Plasma Aldosterone to Metoclopramide and Aldosterone Synthase Messenger Ribonucleic Acid Level in Aldosterone-Producing Adenoma*.

The Journal of Clinical Endocrinology & Metabolism, 80(3), pp.783–789.

Yang, H. et al., 2012. TMEM16F forms a Ca2+-activated cation channel required for lipid scrambling in platelets during blood coagulation. Cell, 151(1), pp.111–122.

Yang, Y.D. et al., 2008. TMEM16A confers receptor-activated calcium-dependent chloride conductance. Nature …, 455(7217), pp.1210–1215.

Yuan, A. et al., 2015. Neurofilament subunits are integral components of synapses and modulate neurotransmission and behavior in vivo. Mol Psychiatry, 20(8), pp.986–994.

Yuan, A. & Nixon, R.A., 2016. Specialized roles of neurofilament proteins in synapses: Relevance to neuropsychiatric disorders. Brain Research Bulletin, 126, pp.334–346.

Zennaro, M.C., Boulkroun, S. & Fernandes-Rosa, F., 2015. An update on novel mechanisms of primary aldosteronism. Journal of Endocrinology, 224(2), pp.R63–R77.

Zhou, J. et al., 2015. DACH1, a zona glomerulosa selective gene in the human adrenal, activates transforming growth factor-β signaling and suppresses aldosterone secretion. Hypertension, 65(5), pp.1103–1110.